Properties of Fibrillar Protein Assemblies and their Percolating Networks

Promotor: Prof. dr. E. van der Linden
Hoogleraar in de Fysica en fysische chemie van levensmiddelen, Wageningen Universiteit

Co-promotor: Dr. ir. L. M. C. Sagis
Universitair docent bij de leerstoelgroep Fysica en fysische chemie van levensmiddelen, Wageningen Universiteit

Promotiecommissie: Prof. dr. A. M. Donald (University of Cambridge, UK)
Prof. dr. J. Mellema (Universiteit Twente)
Prof. dr. A. P. Philipse (Universiteit Utrecht)
Prof. dr. M. A. Cohen Stuart (Wageningen Universiteit)

Properties of Fibrillar Protein Assemblies and their Percolating Networks

Cecile Veerman

"All we need to make us happy is something to be enthusiastic about"

Charles Kingsley

C. Veerman (2004)

Properties of Fibrillar Protein Assemblies and their Percolating Networks.

PhD thesis, Wageningen University, The Netherlands

Abstract

The objective of this thesis was to explore the assembly of food proteins into fibrils, and to describe the resulting percolating systems at rest and under shear flow, in terms of mesoscopic fibril properties. The effect of ionic strength on the percolation concentration for three different food proteins, namely β-lactoglobulin, bovine serum albumin and ovalbumin is described. The dependence of ionic strength on the percolation concentration was explained using an adjusted random contact model, in which the percolation concentration is related to the average number of contacts per particle, and the excluded volume of the rod. Also the contour length, persistence length, and bending rigidity for these three protein assemblies were determined, as well as the phase behaviour of β-lactoglobulin at low pH. A new multistep Ca^{2+}-induced cold gelation process is described to prepare β-lactoglobulin gels at very low protein concentrations (0.07%). The behaviour of fibrillar assemblies of ovalbumin under oscillatory shear, close to the critical percolation concentration, was probed with the use of rheo-optical measurements and Fourier transform rheology. Also the effect of shear flow on the critical percolation concentration for solutions of fibrillar protein assemblies was investigated. Results of viscosity measurements were analysed using percolation theory, where the effect of shear flow was taken into account. The experimental results were compared with our theoretical calculations for the percolation concentration versus shear, based on a random contact model for rodlike particles, making use of a shear dependent excluded volume per fibril. In conclusion conditions leading to gel formation, in terms of mesoscopic fibril properties, under non-flow conditions have been discussed. The observed critical gelation concentration was explained in terms of an excluded volume per fibril (at zero shear). The influence of shear flow on this critical gelation concentration was also described. Here, the critical percolation concentration versus shear flow could again be expressed in terms of an excluded volume per fibril, in this case as a function of shear.

Table of contents

1

Introduction

1.1 Background and aim of this thesis

The relation between macroscopic properties of complex systems and molecular properties of their ingredients has received considerable attention in recent years. To bridge the gap between properties at these two length scales, it is important to focus on the intermediate mesoscopic level (10 – 1000 nm). The description of complex systems at this intermediate length scale offers challenges from a fundamental and applied point of view.

The objective of this thesis was to explore the assembly of food proteins into fibrils, and to describe the resulting percolating systems at rest and under shear flow, in terms of mesoscopic fibril properties.

Protein fibrils are interesting structures, which can serve as model systems to study the behaviour of semiflexible polymers, and can be used for structuring at minimal weight fractions of material, a major issue in foods. For example, the food protein β-lactoglobulin (β-lg) can form a network consisting of long semiflexible fibrils. Neither the formation of this type of meso-structures, nor their resulting mesoscopic properties have been fully investigated. For industrial applications the effect of shear flow of fibrillar structures is important. A better understanding of this effect allows a more accurate prediction of behaviour of fibrillar structures in the processing of materials. A detailed exploration of the formation and properties of these fibril-based meso-structures will yield novel fundamental understanding as well as novel product concepts.

1.2 Fibrillar protein assemblies

Fibrillar protein assemblies were obtained from three different globular food proteins, namely β-lg, bovine serum albumin (BSA) and ovalbumin. β-lg and BSA are both whey proteins, which are by-products of cheese manufacturing.[1,2] About 60% of the whey proteins consist of β-lg, whereas 8% consist of BSA.[1-3] Serum albumins are also found in animal blood plasma, animal tissue, bodily secretions and excrements.[4] Ovalbumin belongs to a family of more than 20 homologous proteins, the serpins, found in animals, plants and viruses.[5] Ovalbumin is also a major globular protein component in egg white.[6,7]

All three proteins are often used as ingredients in foods because of their unique functional properties. An important property is their contribution to the

consistency of foods by the formation of heat-induced gels.[3,6-10] The gel properties depend on protein concentration, ionic strength, pH, and heating procedure.[3,11]

The formation of heat-induced gels from globular proteins takes place in three steps: denaturation, aggregation, and the formation of a gel network. In the denaturation process, a change from the native protein conformation to a more unfolded conformation takes place.[2,12-14] Some of the hydrophobic areas that have been hidden within the interior of the globular molecule are exposed to the exterior surface.[2,3,6,13] The exposure of these groups results in hydrophobic interactions which play a role in the aggregation process.[9,14]

After denaturation, physical and/or chemical bonds between heat-denatured monomers are formed, when the protein concentration is high enough. This aggregation process is governed by a balance between attractive hydrophobic and repulsive electrostatic interactions.[13-17] Repulsive forces are induced by the net surface charge of the protein, and the attractive forces originate from the various functional groups exposed by the thermal unfolding of the protein.[18] At pH values far from the iso-electric point and at low ionic strength, electrostatic repulsive forces hinder the formation of random aggregates, and linear fibrils are formed. At high ionic strength, and a pH near the iso-electric point, random aggregates are formed because of a weaker electrostatic repulsion (Figure 1.1).[11,14,19-23]

The final step in the gelation process is the gel formation. When the protein concentration is high enough, a well ordered network can be formed.[13,14,17,19,22,24-26]
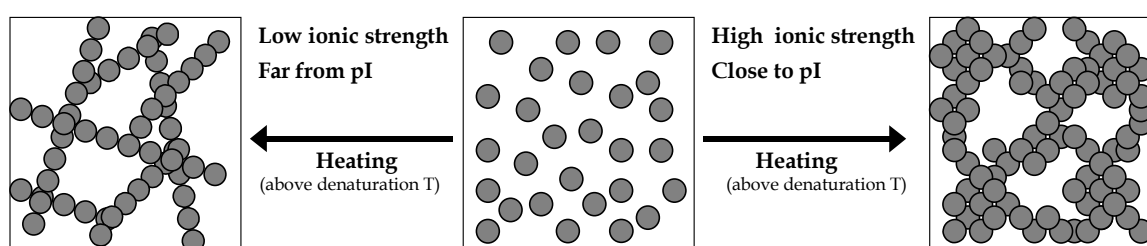
Figure 1.1 Schematic picture of heat-induced gelation at various conditions, for a protein concentration above the critical gelation concentration.

The procedure of making gels described above is called heat-induced gelation. The heat-induced gelation method consists of heating the protein solution and subsequent cooling, during which gelation takes place.[16,19,27-31] It is also possible to make gels via a cold-set gelation method. To obtain gels via the cold-set gelation

method, it is necessary to prepare a heat-denatured *solution*, with a protein concentration below the critical gelation concentration. The *gelation* is induced at low temperatures by the addition of mono- or polyvalent cations (Figure 1.2).[3,32-38] Cold-set gelation can lead to new uses for whey proteins, in a variety of foods.[39]

Heating

(above denaturation T)

+ Salt
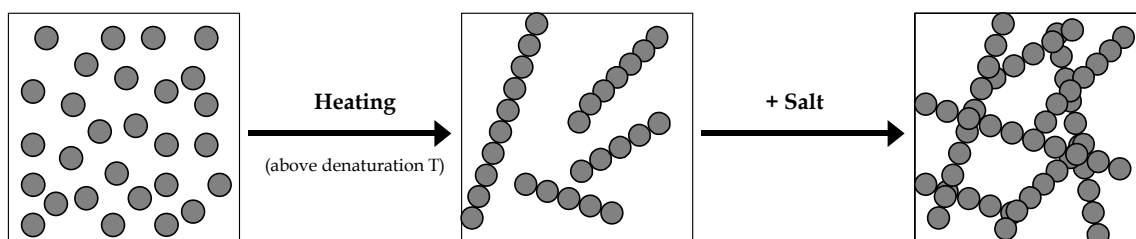
Figure 1.2 Schematic picture of the cold-set gelation method.

1.3 Structures under shear flow

In the absence of an external field, fibrillar structures in solution are usually isotropically, i.e. randomly, distributed. When an external field (e.g. shear, electric, magnetic) is applied, the fibrils tend to align in the direction of the field, leading to a more anisotropic system (Figure 1.3).

Under shear flow, a preferred average orientation of non-absorbing, anisotropic particles generally leads to a difference in polarizability of a particle segment perpendicular and parallel to the flow field.[40-43] The resulting refractive index tensor, $\mathbf{n} = \mathbf{n'} - i\mathbf{n''}$, is complex with a real part inducing a phase shift in transmitted light and an imaginary part causing attenuation.[44] Both real and imaginary part may be anisotropic, and birefringence ($\Delta n'$) and dichroism ($\Delta n''$) are defined as the difference in the principal eigenvalues of $\mathbf{n'}$ and $\mathbf{n''}$ respectively.[43,44] Birefringence and dichroism can be measured with the use of rheo-optics. This technique analyses the interaction of polarized light with a material subject to flow, and is a method to probe the mesoscopic structural response.[40,44]

The effect of a flow field on systems containing anisotropic particles will also result in a non-linear material response, due to the fact that the applied deformation causes a change in microstructure of the system.[45,46] A method to investigate the non-linear stress response is Fourier transform rheology.[45-48] With the use of this method the intensity of higher harmonics in the stress response as a function of strain can be measured.[45,47,48]
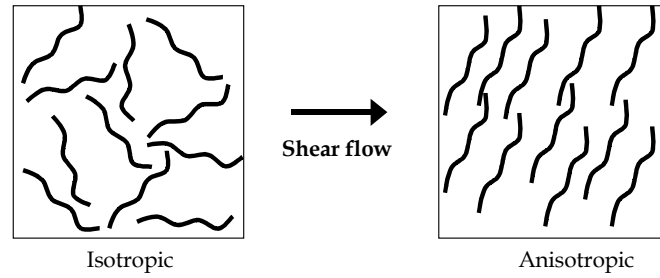
Figure 1.3 Schematic picture of the effect of shear flow on fibrillar particles.

1.4 Percolating networks

The behaviour of materials close to the sol-gel transition can be described e.g. by percolation theory.[49-51] Many different approaches have been undertaken. The basic idea is illustrated as follows. Consider a periodic lattice, where each site is randomly occupied with probability p or empty with probability $(1 - p)$.[49,50] A group of occupied sites connected by nearest-neighbour distances is called a cluster. The radius of a cluster signifies the correlation length, or spatial length of the connectivity function, equal to the probability that two particles at distance r belong to the same cluster.[49,50] The size of the clusters depends on the distance from the sol-gel transition. In general there is a sharp transition at some critical point $p = p_c$, where one infinite cluster starts to appear. The value of p_c depends on the nature of the lattice.[52] Below the sol-gel transition small clusters are formed, $p < p_c$, and no percolating network exists, whereas at $p > p_c$ a gel is formed and one percolating network occurs (Figure 1.4).[49,50]

Universal scaling laws, which are valid close to the percolation concentration, have been predicted for e.g. the viscosity of the sol, η, and the elasticity of the gel, G'.[50] These parameters diverge or vanish respectively at the gel point:

$$\eta \sim (p_c - p)^{-k} \qquad\qquad (p < p_c) \qquad\qquad\qquad (1.1)$$

$$G' \sim (p - p_c)^t \qquad\qquad (p > p_c) \qquad\qquad\qquad (1.2)$$

De Gennes proposed a critical exponent t equal to 11/6 for percolation in three dimensions.[51] This scaling relation is based on an analogy between the electrical conductivity and the elastic modulus.[51] This analogy applied to viscous solutions gives a value for k of about 0.7 in three dimensions.[50]
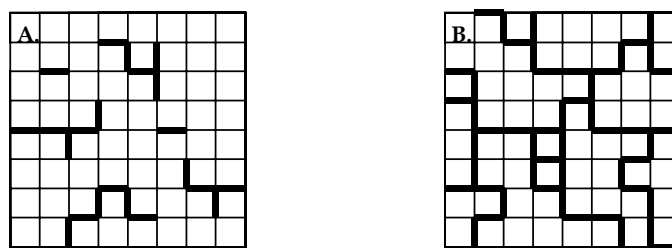
Figure 1.4 Schematic picture of percolation on a lattice, illustrating (A.) $p < p_c$, and (B.) $p > p_c$.

1.5 Outline of this thesis

The central theme of this thesis is to explore the assembly of food proteins into fibrils, and to describe the resulting percolating systems at rest and under shear flow, in terms of mesoscopic fibril properties.

In chapters 2 to 4 the effect of ionic strength on the percolation concentration for three different food proteins, namely β-lg, BSA and ovalbumin is described. The dependence of ionic strength on the percolation concentration was explained using an adjusted random contact model, in which the percolation concentration is related to the average number of contacts per particle, and the excluded volume of the rod (chapter 2). This model was also applicable for BSA (chapter 3) and ovalbumin (chapter 4). Reversibility of fibril assembly of BSA and ovalbumin was also addressed in chapters 3 and 4 respectively.

Chapter 5 summarizes the results obtained in chapters 2 to 4, and gives a further characterization of the fibrillar properties of the three protein assemblies, and also describes the phase behaviour of β-lg at low pH.

In chapter 6 a new process is described to prepare β-lg gels at very low protein concentrations, making use of the fundamental knowledge obtained in chapters 2 – 4. In summary, these chapters all discuss conditions leading to gel formation, and critical percolation concentrations in terms of mesoscopic fibril properties, under static, i.e. non-flow conditions.

Chapters 7 and 8 refer to the influence of shear flow on the critical percolation concentration. Those investigations have been performed on ovalbumin fibril solutions. The behaviour of fibrillar protein assemblies under oscillatory shear, close to the percolation concentration was investigated in chapter 7. In chapter 8 results of viscosity measurements were analysed using percolation theory, where the effect of shear flow was taken into account. The experimental results were

compared with our theoretical calculations for the percolation concentration versus shear, based on a random contact model for rodlike particles, making use of a shear dependent excluded volume per fibril.

References

1. Kinsella, J.E.; Whitehead, D.M. In *Proteins in whey: chemical, physical, and functional properties* **1989**, 343-367.

2. Mulvihill, D.M.; Donovan, M. *Ir. J. Food Sci. Technol.* **1987**, *11*, 43-75.

3. Bryant, C.M.; McClements, D.J. *Trends Food Sci. Technol.* **1998**, *9*, 143-151.

4. Giancola, C.; Sena de, C.; Fessas, D.; Graziano, G.; Barone, G. *Int. J. Biol. Macromolecules* **1997**, *20*, 193-204.

5. Stein, P.E.; Leslie, A.G.W.; Finch, J.T.; Carrell, R.W. *J. Mol. Biol.* **1991**, *221*, 941-959.

6. Nemoto, N.; Koike, A.; Osaki, K.; Koseki, T.; Doi, E. *Biopolymers* **1993**, *33*, 551-559.

7. Mine, Y. *J. Agric. Food Chem.* **1996**, *44*, 2086-2090.

8. Paulsson, M.; Dejmek, P.; Vliet van, T. *J. Dairy Sci.* **1990**, *73*, 45-53.

9. Boye, J.I.; Alli, I.; Ismail, A.A. *J. Agric. Food Chem.* **1996**, *44*, 996-1004.

10. Hagolle, N.; Relkin, P.; Dalgleish, D.G.; Launay, B. *Food Hydrocolloids* **1997**, *11*, 311-317.

11. Doi, E. *Trends Food Sci. Technol.* **1993**, *4*, 1-5.

12. Kleef van, F.S.M. *Biopolymers* **1986**, *25*, 31-59.

13. Hatta, H.; Kitabatake, N.; Doi, E. *Agric. Biol. Chem.* **1986**, *50*, 2083-2089.

14. Lefebvre, J.; Renard, D.; Sachez-Gimeno, A.C. *Rheol. Acta* **1998**, *37*, 346-357.

15. Harwalkar, V.R.; Kalab, M. *Milchwissenschaft* **1985**, *40*, 65-68.

16. Koseki, T.; Kitabatake, N.; Doi, E. *Food Hydrocolloids* **1989**, *3*, 123-134.

17. Egelandsdal, B. *J. Food Sci.* **1980**, *45*, 570-573.

18. Yasuda, K.; Nakamura, R.; Hayakawa, S. *J. Food Sci.* **1986**, *51*, 1289-1292.

19. Doi, E.; Kitabatake, N. *Food Hydrocolloids* **1989**, *3*, 327-337.

20. Kitabatake, N.; Kinekawa, Y.I. *Food Chem.* **1995**, *54*, 201-203.

21. Nakamura, R.; Sugiyama, H.; Sato, Y. *Agric. Biol. Chem.* **1978**, *42*, 819-824.

22. Clark, A.H. In *Functional properties of food macromolecules* Hill, S.E.; Ledward, D.A.; Mitchell, J.R. (Eds.) **1998**, Aspen Publishers: Great Britain, 77-142.

23. Tobitani, A.; Ross-Murphy, S.B. *Macromolecules* **1997**, *30*, 4845-4854.

24.   Arntfield, S.D.; Murray, E.D.; Ismond, M.A.H.; Bernatsky, A.M. *J. Food Sci.* **1989**, *54,* 1624-1631.

25.   Sugiyama, M.; Nakamura, A.; Hiramatsu, N.; Annaka, M.; Kuwajima, S.; Hara, K. *Biomacromolecules* **2001**, *2,* 1071-1073.

26.   Kavanagh, G.M.; Clark, A.H.; Ross-Murphy S.B. *Int. J. Biol. Macromolecules* **2000**, *28,* 41-50.

27.   Koseki, T.; Fukuda, T.; Kitabatake, N.; Doi, E. *Food Hydrocolloids* **1989**, *3,* 135-148.

28.   Matsudomi, N.; Rector, D.; Kinsella, J.E. *Food Chem.* **1991**, *40,* 55-69.

29.   Murata, M.; Tani, F.; Higasa, T.; Kitabatake, N.; Doi, E. *Biosci. Biotechnol. Biochem.* **1993**, *57,* 43-46.

30.   Stading, M.; Hermansson, A.-M. *Food Hydrocolloids* **1990**, *4,* 121-135.

31.   Langton, M.; Hermansson, A.-M. *Food Hydrocolloids* **1992**, *5,* 523-539.

32.   Barbut, S. *Lebensm. -Wiss. Technol.* **1997**, *29,* 590-593.

33.   Hongsprabhas, P. *Lebensm. -Wiss. Technol.* **1999**, *32,* 196-202.

34.   Ju, Z.Y.; Kilara, A. *J. Agric. Food Chem.* **1998**, *46,* 3604-3608.

35.   Hongsprabhas, P.; Barbut, S. *J. Food Sci.* **1997**, *62,* 382-385.

36.   Bryant, C.M.; McClements, D.J. *J. Food Sci.* **2000**, *65,* 259-263.

37.   Bryant, C.M.; McClements, D.J. *J. Food Sci.* **2000**, *65,* 801-804.

38.   Hongsprabhas, P.; Barbut, S. *Int. Dairy J.* **1997**, *7,* 827-834.

39.   Hongsprabhas, P.; Barbut, S. *Food Res. Int.* **1996**, *29,* 135-139.

40.   Fuller, G.G. *Ann. Rev. Fluid Mech.* **1990**, *22,* 387-417.

41.   Kulicke, W.-M.; Arendt, O. *Applied Rheol.* **1997**, *7,* 12-18.

42.   Clasen, C.; Kulicke, W.-M. *Progress in Polymer Sci.* **2001**, *26,* 1839-1919.

43.   Johnson, S.J.; Frattini, P.L.; Fuller, G.G. *J. Coll. Interf. Sci.* **1985**, *104,* 440-455.

44.   Fuller, G.G.; Mikkelsen, K.J. *J. Rheol.* **1989**,*33* 761-769.

45.   Wilhelm, M. *Macromol. Mat. Eng.* **2002**, *287,* 83-105.

46.   Sagis, L.M.C.; Ramaekers, M.; Linden van der, E. *Phys. Rev. E* **2001**, *63,* 051504:1-8.

47.   Wilhelm, M.; Maring, D.; Spiess, H.-W. *Rheol. Acta* **1998**, *37,* 399-405.

48.   Wilhelm, M.; Reinheimer, P.; Ortseifer, M. *Rheol. Acta* **1999**, *38,* 349-356.

49.   Stauffer, D. *Phys. Rep.* **1979**, *54,* 1-74.

50.   Stauffer, D.; Coniglio, A.; Adam, M. *Adv. Polym. Sci.* **1982**, *44,* 103-158.

51.   Gennes de, P.G. *J. Phys.* **1976**, *37,* L1-L2.

52.   Peyrelasse, J.; Lamarque, J.P.; Habas, J.P.; Bounia, N.E. P*hys. Rev. E* **1996**, *53,* 6126-6133.

2

Effect of Electrostatic Interactions on the Percolation Concentration of Fibrillar β-Lactoglobulin Gels

Abstract

The effect of electrostatic interactions on the critical percolation concentration (c_p) of fibrillar β-lactoglobulin gels at pH 2 was investigated using rheological measurements, transmission electron microscopy (TEM), and performing conversion experiments. A decreasing c_p with increasing ionic strength was found. The fraction non-aggregated β-lactoglobulin was independent of ionic strength in the regime of 0.01 – 0.08 M. TEM experiments showed long fibrils (2 – 7 μm) for ionic strengths between 0.01 and 0.08 M. Since both the conversion of monomers and the contour length of the fibrils were independent of ionic strength (0.01 – 0.08 M), the linear increase of c_p with the Debye length can be attributed purely to an increase of electrostatic repulsion between the fibrils. This increase is explained in terms of an adjusted random contact model which takes into account the charge and semiflexibility of the fibrils.

2.1 Introduction

Whey proteins which contain mainly β-lactoglobulin (β-lg) are often used as ingredients in foods because of their unique functional properties. An important property is their contribution to the consistency of foods by forming thermally induced gels.[1,2]

Heat-induced β-lg gels have been obtained by controlling pH, ionic strength, protein concentration and heating procedure.[1,3] Varying these conditions can result in different structures of aggregates. The formation of gels is primarily governed by the equilibrium between attractive forces among thermally unfolded molecules and repulsive forces resulting from the net charge of the protein.[4] At low pH and low ionic strength the protein is highly charged (+20).[5] The electrostatic repulsion is high and strandlike or fibrillar aggregates are formed. The electrostatic repulsion decreases with increasing pH and ionic strength, and random particle gels are formed.[3]

Light microscopy, scanning electron microscopy (SEM) and transmission electron microscopy (TEM) confirmed the formation of turbid particulate gels in the pH regime of pH 4 – 6.[6] Below and above this regime transparent fine-stranded gels were formed. At pH < 4 stiff short strands were formed, whereas fine-stranded gels formed at pH > 6 had longer and more flexible strands.[6] Differences between fine-stranded gels below and above the iso-electric point were studied on a molecular level using Fourier transform infrared (FTIR) spectroscopy.[7] Differences in hydrogen-bond strengths, number of intermolecular bonds and protein conformation were observed. These factors are believed to be responsible for differences in the properties of the strands formed at pH < 4 and pH > 6.[7]

Aymard et al.[8] performed small-angle neutron scattering (SANS) and X-ray scattering experiments at low pH which showed a strong decrease in persistence length of the fibrils with increasing ionic strength (38 nm for 0.1 M ionic strength and 600 nm for 0.013 M). The large persistence length at low ionic strength cannot be attributed solely to electrostatic interactions along the chain, but could be due to specific binding between the proteins, such as the formation of intermolecular hydrogen-bonding β-sheet structures.[8,9] Kavanagh et al.[10] examined TEM experiments and observed a strong decrease in contour length with increasing ionic strength. They found long linear aggregates at pH 2 in the absence of salt. In the presence of 0.05 M or at higher pH, these long linear fibrils were not formed.[10]

The kinetics of aggregation of β-lg at pH 2 and pH 2.5 is also strongly dependent on ionic strength.[8,11] For constant temperature and protein concentration, the aggregation kinetics is slower at lower ionic strengths.[8,11] After a heating time of about 10 h the conversion of monomers has reached a constant value. This value is lower at lower ionic strengths.[8] Schokker et al.[11] used size exclusion chromatography in combination with multi-angle laser light scattering (SEC-MALLS) to determine the conversion of β-lg monomers at pH 2.5.[11] Besides a strong dependence on ionic strength, the conversion strongly increased with increasing β-lg concentration.[11]

The effect of pH and ionic strength on the critical concentration for gel formation has also been studied. To quantify the effect of pH and ionic strength on the critical gel concentration, Renard et al.[12] proposed a model based on changes in electrostatic and van der Waals free energies. Experimental results showed transparent gels at pH 2 for all measured salt concentrations (0.04 – 0.14 M NaCl). The critical gel concentration, determined visually, decreased with increasing ionic strength (from 70 g/L at 0.04 M to 25 g/L at 0.14 M for pH 2), except near the iso-electric pH where the critical gel concentration remained constant.[12] Kavanagh et al.[13] and Stading et al.[14] performed rheological measurements to observe the β-lg gelation over a range of pH values and protein concentrations at low ionic strength. Differences were observed between the critical gel concentration below and above the iso-electric point which indicates, according to Stading et al.[14], a different network structure below and above the iso-electric point.

Here we define the critical gel concentration as the critical percolation threshold, c_p. Assuming a scaling relation $G' \sim (c - c_p)^t$, c_p and t can be determined by G' measurements as a function of protein concentration.[15] Here G' is the storage modulus, c the concentration of monomers in the system, and t a scaling exponent.

In this study the effect of ionic strength on the percolation concentration of fibrillar β-lg gels at pH 2 was investigated using rheological measurements. In order to eliminate the effect of monomer conversion and fibril length on c_p, conversion experiments and TEM experiments were performed. Our results show that the dependence of the percolation concentration on ionic strength can be explained in terms of an adjusted random contact model.

2.2 Materials and Methods

2.2.1 Sample preparation

β-lg was obtained from Sigma (L-0130) and is a mixture of the genetic variants A and B. The protein was dissolved in a HCl solution of pH 2. To remove traces of calcium ions from the β-lg and to obtain a protein solution with the same pH and ionic strength as the solvent, the protein was diluted repeatedly with HCl solvent and filtered through a 3K filter in an Omegacell™ membrane cell (Filtron) at 4 °C and a maximum pressure of 3 bar. The procedure was stopped when the pH and conductivity of the eluted solution and the solvent were the same. The β-lg solution was centrifuged at 22600g for 30 min. To remove any traces of undissolved protein, the supernatant was filtered through a protein filter (FP 030/2, 0.45 μm, Schleicher & Schuell). A UV spectrophotometer was used to determine the exact β-lg concentration, using a calibration curve of known β-lg concentrations determined at a wavelength of 278 nm. After this procedure the absorption of the dialysed β-lg was measured. The obtained stock protein solution of pH 2 (i.e. ionic strength equal to 0.01 M) was used for all measurements. Ionic strengths higher than 0.01 M were prepared by adding NaCl to this stock solution.

2.2.2 Rheological measurements

A Bohlin VOR strain-controlled rheometer with a concentric cylinder geometry (C14) was used to determine the storage modulus (G') as a function of strain (frequency 1 Hz, temperature 20 °C, strain 0.000206 – 0.206). β-lg samples at pH 2 and varying ionic strengths (0.01 – 0.09 M) were heated at 80 °C for 10 h, and subsequently cooled to 20 °C for 2 h. After this procedure a strain sweep was performed.

2.2.3 Transmission electron microscopy (TEM)

β-lg samples (1.5% (w/w)) at pH 2 and various ionic strength were heated in an oven at 80 °C for 10 h. After cooling, the samples were diluted by a factor 35. The TEM samples were prepared by negative staining. A drop of the diluted solution was deposited onto a carbon support film on a copper grid. The excess was removed after 30 s using a piece of filter paper. A droplet of 2% uranyl acetate, pH 3.8, was added for 15 s, any excess being removed as before. Electron

micrographs were made using a Philips CM 12 transmission electron microscope operating at 80 kV.

2.2.4 Conversion experiments

A series of test tubes with varying β-lg concentrations (0.5, 1, 2, 3, and 4% (w/w)) and various ionic strengths (0.01 – 0.1 M) were heated at 80 °C. After various time periods between 0 and 600 min, tubes were taken out of the water bath and immediately cooled in ice water.

To determine the concentration non-aggregated β-lg, the heated samples were diluted in a 0.1 M citric acid/ phosphate buffer at pH 4.8. After precipitation of the aggregates overnight, the supernatant was centrifuged for 10 min at 20000g. The non-aggregated β-lg concentration present in the supernatant was determined by a UV spectrophotometer at a wavelength of 278 nm.

2.3 Results and Discussion

2.3.1 Rheological measurements

The storage modulus (G') as a function of strain for β-lg at pH 2, 0.01 M ionic strength, and varying protein concentrations, is presented in Figure 2.1. The same experiments were performed for β-lg at pH 2 and ionic strengths of 0.02, 0.03, 0.05, 0.07, and 0.09 M. G' was determined from the linear regime of the curve for each β-lg concentration. These values were used to determine the percolation concentration (c_p) and the scaling exponent t using the method described by van der Linden and Sagis.[15] This method is a graphical method that uses plots of $(G')^{1/t}$ versus c and extrapolates these plots to $(G')^{1/t} = 0$. This procedure makes use of the fact that independent of the value of t the curves must all intersect the concentration axis at the same value. When the assumed value for t is close to the actual value, the plot will be linear. If t is too small or too large the lines are curved. From the plots of $(G')^{1/t}$ versus c for various t we selected those t values that give an approximately straight line. From these plots an average value of c_p was determined. We plotted log G' versus log ($c - c_p$), using the different values for c_p obtained from the estimated t values. For each of the values for c_p we determined the t value and averaged these values. Table 2.1 shows the average values for c_p and t. A decreasing c_p with increasing ionic strength was observed. The value for t was about 2 except

for the value at 0.02 M. This value indicates isotropic force percolation and a homogeneous network.[15] The low value for *t* at 0.02 M may be due to the large scattering in the rheological measurements at this condition.
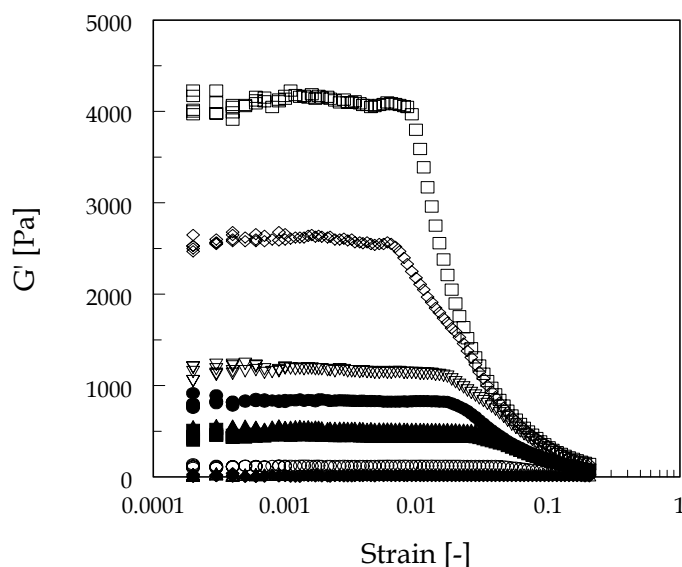
Figure 2.1 *G′* versus strain for various β-lg concentrations at pH 2 and 0.01 M ionic strength. 2.5% (◆); 2.7% (△); 2.9% (○); 3.0% (■); 3.5% (▲); 3.8% (●); 4.5% (▽); 5% (◇); 6% (□).

Kavanagh et al.[13] determined for β-lg at pH 2 and low ionic strength a critical gelation concentration of 6.8% using the branching model and 8.0% using a semi-empirical model derived from a consideration of the critical behaviour near the gel point. A higher critical gelation concentration was observed because a different method was used to determine *G′* and the critical gelation concentration. They continuously monitored the gelation process isothermally at 80 °C using dynamic oscillatory measurements.[13] For 8.2% β-lg at pH 2 and low ionic strength an "infinite time" storage modulus of 134 Pa was estimated by extrapolation. In this paper, the values for *G′* were determined after heating for 10 h at 80 °C and cooling for 2 h *in rest*. For 6% β-lg at pH 2 and low ionic strength a *G′* of 4080 Pa was found. Due to the difference in measuring method, this value was much higher than the value found by Kavanagh et al.[13]

Table 2.1 Values of c_P and t for various ionic strengths.

Ionic strength [M]	c_P [%(w/w)]	t [-]
0.01	2.3 ± 0.1	2.1 ± 0.2
0.02	2.1 ± 0.3	1.6 ± 0.2
0.03	1.6 ± 0.1	2.1 ± 0.2
0.05	1.4 ± 0.1	2.1 ± 0.2
0.07	1.2 ± 0.1	1.9 ± 0.3
0.09	0.3 ± 0.2	2.2 ± 0.3

2.3.2 Transmission electron microscopy (TEM)

Figure 2.2 shows TEM micrographs for β-lg at pH 2 and varying ionic strengths (0.01 – 0.1 M). Fibrils of about 2 – 7 μm were observed for ionic strengths of 0.01 – 0.05 M (Figure 2.2A – E, and versions of these taken with a smaller magnification). Up to an ionic strength of 0.08 M the length of the fibrils decreased slightly (Figure 2.2F – H). Short fibrils were observed for 0.09 and 0.1 M (Figure 2.2I and J).

Aymard et al.[8] investigated β-lg structures at low pH using TEM, SANS and X-ray scattering. Long fibrils were observed for pH 2 and 0.03 M, which is in agreement with our results. Using X-ray scattering and SANS, they estimated persistence lengths of 38, 300, and 600 nm for ionic strengths of 0.1, 0.03, and 0.013 M respectively.[8] Figure 2.2A – E shows persistence lengths of about 1 μm for ionic strengths up to 0.05 M. The persistence length found for 0.1 M (Figure 2.2J) is in the same order of magnitude as described by Aymard et al.[8] The differences between results presented in this paper and that of Aymard et al. can be due to the fact that Aymard et al. used light scattering and fitted the intensity of the scattered light with an expression for wormlike chains.[8] Kavanagh et al.[10] reported, after heating at 80 °C for 6 h, long linear aggregates at pH 2 in the absence of salt. In the presence of 0.05 M or at higher pH, these fibrils were not formed.[10] The samples used for the preparation of TEM micrographs, shown in Figure 2.2, were heated at 80 °C for 10 h which indicates that the length of the fibrils is strongly dependent on the heating time. In contrast to some of the literature reports, the results presented
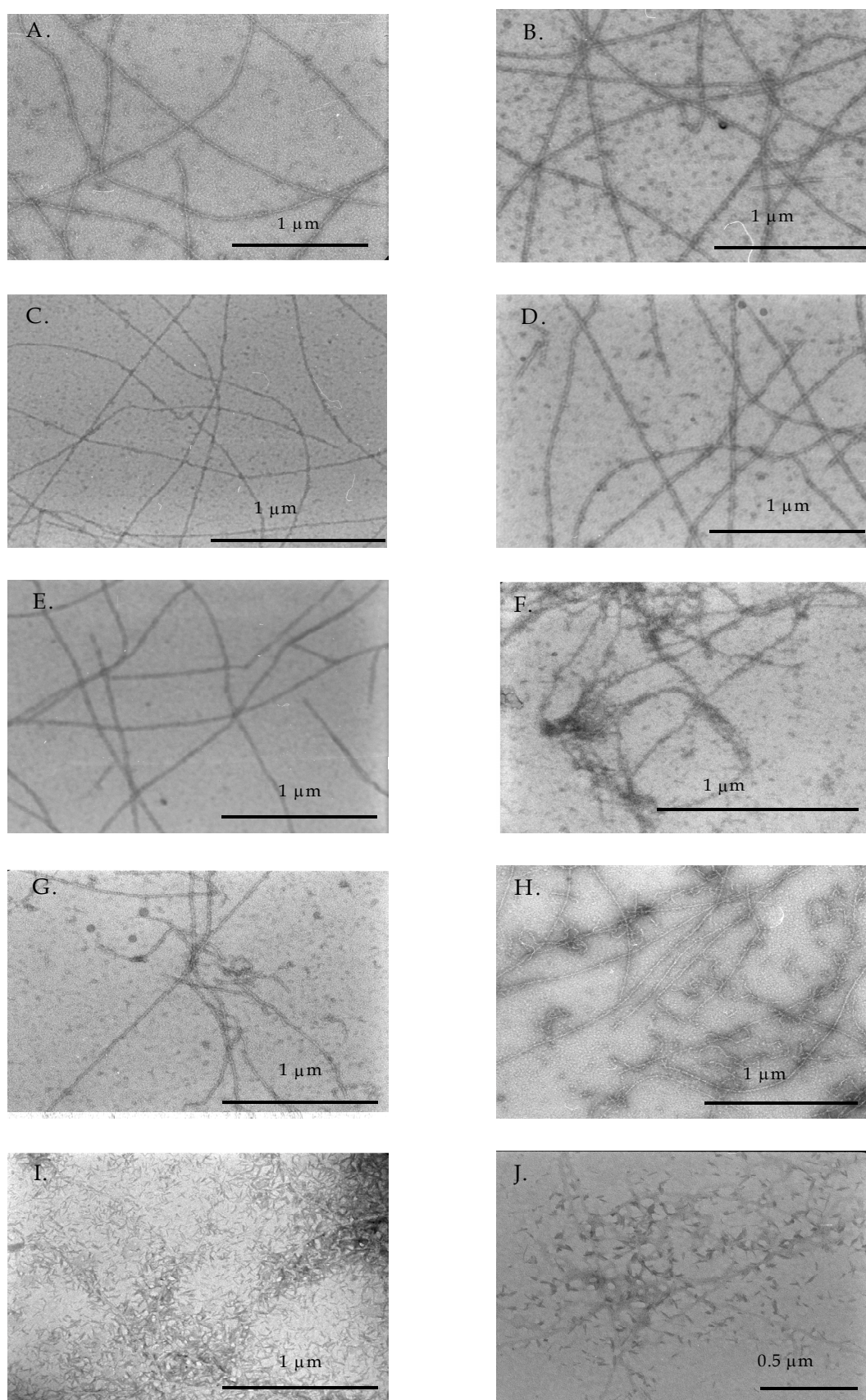
Figure 2.2 TEM micrographs for β-lg at pH 2 and various ionic strengths. (A.) 0.01 M; (B.) 0.02 M; (C.) 0.03 M; (D.) 0.04 M; (E.) 0.05 M; (F.) 0.06 M; (G.) 0.07 M; (H.) 0.08 M; (I.) 0.09 M; (J.) 0.10 M.

in this paper do not show a strong dependence of the length of the fibrils on the ionic strength in the regime of 0.01 to 0.08 M. Comparing TEM micrographs at pH 7 and pH 2, much longer fibrils were observed in fine stranded networks below the iso-electric point.[6,8,10]

2.3.3 Conversion experiments

The fraction non-aggregated β-lg at pH 2 for 0.01 M as a function of heating time was determined for various β-lg concentrations (Figure 2.3). An increasing conversion with increasing protein concentration was observed. For 1% β-lg a small increase in absorption was noticed for short heating times. This effect may be due to measuring inaccuracies which are higher when a small amount of β-lg is converted. Experiments were also performed for ionic strengths up to 0.1 M. The asymptotic values for the fraction non-aggregated β-lg, after 10 h, as a function of ionic strength are presented in Figure 2.4. Below 4% β-lg the conversion is independent of the ionic strength up to 0.08 M. At 4% β-lg the conversion started to increase at 0.05 M.
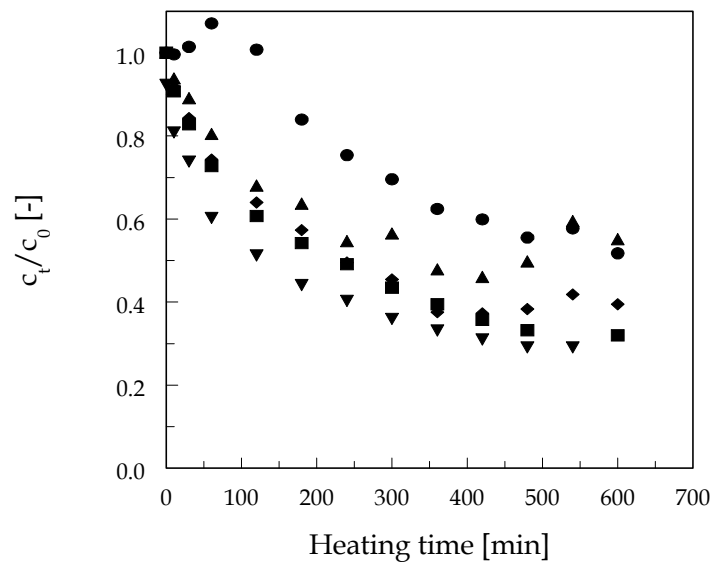
Figure 2.3 Fractional concentration c_t/c_0 versus heating time for various β-lg concentrations at pH 2 and 0.01 M ionic strength. 0.5% (▲); 1% (●); 2% (◆); 3% (■); 4% (▼).

Aymard et al.[8] determined the fraction non-aggregated β-lg as a function of heating time. They observed a decreasing asymptotic value after long heating times for increasing ionic strengths (0.013, 0.1, and 0.2 M). These results are in agreement with the results presented in this paper for the ionic strength regime above 0.08 M. Schokker et al.[11] did conversion experiments for β-lg at pH 2.5. Also an increasing conversion with increasing ionic strength was found (0.1 and 0.2 M).

The reaction order for β-lg aggregation was determined according to the method used in Verheul et al.[16] For all conditions used, a reaction order of 1 was found, i.e. the reaction rate increases proportional with the protein concentration.
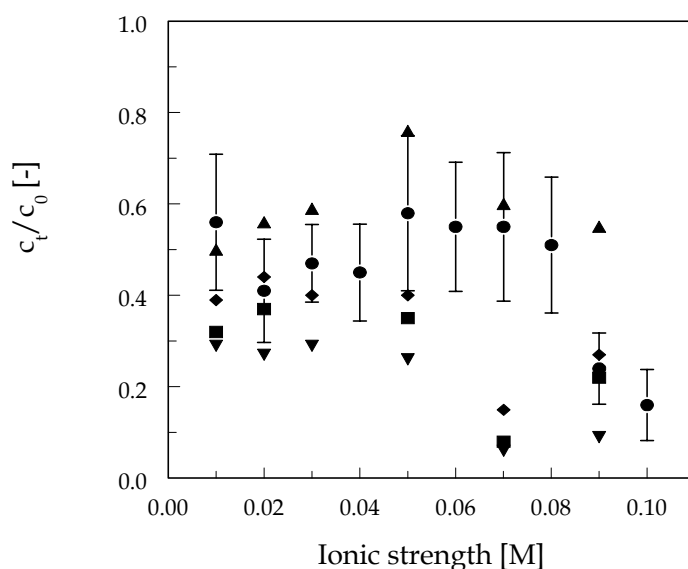
Figure 2.4 Fractional concentration c_t/c_0 as a function of ionic strength for β-lg at pH 2. 0.5% (▲); 1% (●); 2% (◆); 3% (■); 4% (▼).

2.3.4 Electrostatic interactions and percolation concentration

Combining all results, the decreasing percolation concentration with increasing ionic strength can be explained in terms of electrostatics. The TEM micrographs showed that the length of the fibrils was independent of ionic strength in the regime of 0.01 – 0.08 M. A much shorter contour length above 0.08 M was observed. The conversion experiments illustrated that the fraction non-aggregated β-lg was independent of ionic strength for ionic strengths up to 0.08 M. In this regime (0.01 – 0.08 M) the same amount of fibrils of approximately equal length was formed. This result implies that the decreasing percolation concentration with

increasing ionic strength (Table 2.1) is solely due to a change in electrostatic interactions between the chains.

Qualitatively we can explain the increase of percolation concentration with decreasing ionic strength as follows. At low ionic strength the electrostatic repulsion is high. It is difficult to form cross-links between the fibrils, which results in a high percolation concentration. The electrostatic repulsion decreases with increasing ionic strength. Cross-links can be formed more easily resulting in a lower percolation concentration.

A more quantitative analysis is given below. A critical percolation volume fraction (ϕ_p) for hard rigid rods is derived by Philipse[17] as

$$\phi_p = \alpha\,(D_0/L) \qquad\qquad \text{for } (L/D_0) \gg 1 \qquad\qquad (2.1)$$

where D_0 is the diameter of the rods (4 nm for β-lg), L the contour length of the rods, and α the average number of contacts per rod, assumed to be of order 1 at the percolation concentration. α is related to the excluded volume of the rod ($V_{ex,rod} = \frac{1}{2}\pi L^2 D_0$)[18,19] and the number density of the rods ($\rho = \phi_p / V_0$; where V_0 is the volume of a rod), according to a 'mechanical equation of state'[17]

$$\rho = 2\langle\alpha\rangle / V_{ex,rod} \qquad\qquad (2.2)$$

Note that Philipse[17] gives an expression for the critical percolation *volume* fraction while we use a critical percolation *mass* fraction of the fibrils, $\phi_{p,m}$ (equal to $0.6(c_p/100)$, where 0.6 is the conversion factor).

To obtain an expression for the percolation concentration for the β-lg system, we have to adjust the random contact model for rigid hard rods, because a β-lg fibril at pH 2 is not a hard rigid rod, but is highly charged and semiflexible (TEM micrographs Figure 2.2). The semiflexibility introduces an extra lengthscale, the persistence length, and the charge introduces the Debye screening length, κ^{-1} as another important lengthscale. We propose the following random contact model for charged semiflexible fibrils. The excluded volume is in this case given by $V_{ex,rod} = (L/P)\frac{1}{2}\pi P^2 D_{eff}$, where D_{eff} is an effective diameter which incorporates the charge of the rod and the Debye length.[20] P is the persistence length of the fibril, which consists predominantly of the bare persistence length (order 1 μm). The

contribution of the electrostatic persistence length is small (less than 1 nm). Using the 'mechanical equation of state' argument (Eq. (2.2)), we find for the percolation mass fraction of a charged semiflexible system:

$$\phi_{p,m} = \alpha(D_{eff}^2 P / P^2 D_{eff}) = \alpha(D_{eff}/P) \qquad \text{for } (P/D_{eff}) >> 1 \qquad (2.3)$$

The linear dependence of $\phi_{p,m}$ on D_{eff} is confirmed experimentally for ionic strengths of 0.01 – 0.07 M (Figure 2.5). Since the system at 0.09 M contains much shorter rods than 2 µm, we do not expect this particular point (D_{eff} = 4.5 nm) to be part of the straight line as predicted by Eq. (2.3). The vertical dashed line gives the theoretical limit of Eq. (2.3).
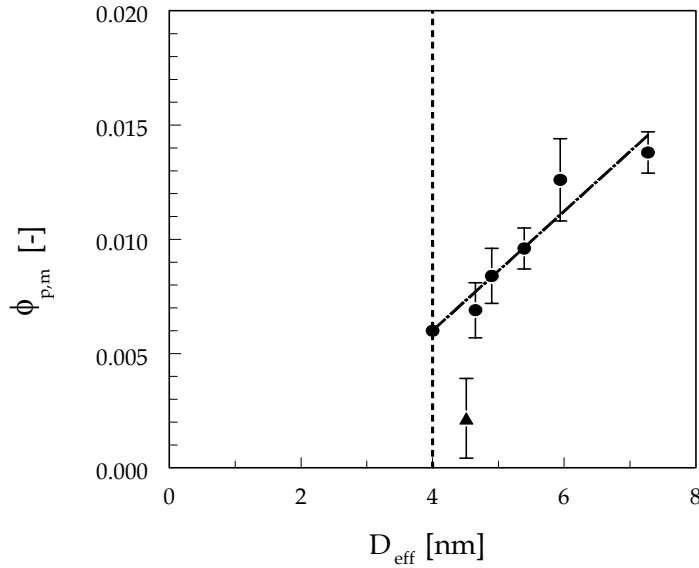
Figure 2.5 $\phi_{p,m}$ as a function of D_{eff} for β-lg at pH 2.

From Figure 2.5 and using P ~ 1 µm (TEM micrographs), we find α ~ O(1) which means that percolation occurs when there are on average a few (order one) contacts per rodlike segment with length P. We note that α ~ O(1) was shown by simulations for percolating hard rods and for the percolation concentration of continuous systems of spherocylinders.[21,22] We conclude that our experimental results for charged semiflexible β-lg fibrils can be explained by an adjusted random contact model which takes into account the charge and semiflexibility of the fibrils.

2.4 Conclusion

Using rheological measurements, a decreasing percolation concentration, c_p, with increasing ionic strength was found. The scaling exponent t was 2 in the regime of 0.01 – 0.09 M ionic strength which corresponds to a homogeneous network. TEM micrographs showed short fibrils in the ionic strength regime of 0.09 and 0.1 M. Long fibrils (2 – 7 μm) were formed for ionic strengths between 0.01 and 0.08 M. The fraction non-aggregated protein was independent of ionic strength in the regime of 0.01 – 0.08 M and β-lg concentrations below 4% (w/w). At 4% β-lg the conversion started to increase at 0.05 M.

The fraction non-aggregated β-lg was independent of ionic strength in the regime of 0.01 – 0.08 M. Also the contour length of the strands was independent of ionic strength in this regime. These results imply that the linear increase of c_p with the Debye screening length can be attributed purely to an increase of electrostatic repulsion between the fibrils. This increase is explained in terms of an adjusted random contact model which takes into account the charge and semiflexibility of the fibrils.

References

1. Bryant, C.M.; McClements, D.J. *Trends Food Sci. Tech.* **1998**, *9*, 143-151.
2. Paulsson, M.; Dejmek, P.; Vliet van, T. *J. Dairy Sci.* **1990**, *73*, 45-53.
3. Doi, E. *Trends Food Sci. Tech.* **1993**, *4*, 1-5.
4. Harwalkar, V.R.; Kalab, M. *Milchwissenschaft* **1985**, *40*, 65-68.
5. Aymard, P.; Durand, D.; Nicolai, T. *Int. J. Biol. Macromolecules* **1996**, *19*, 213-221.
6. Langton, M.; Hermansson, A.-M. *Food Hydrocolloids* **1992**, *5*, 523-539.
7. Lefevre, T.; Subirade, M. *Biopolymers* **2000**, *54*, 578-586.
8. Aymard, P.; Nicolai, T.; Durand, D. *Macromolecules* **1999**, *32*, 2542-2552.
9. Allain, A.-F.; Paquin, P.; Subirade, M. *Int. J. Biol. Macromolecules* **1999**, *26*, 337-344.

10. Kavanagh, G.M.; Clark, A.H.; Ross-Murphy, S.B. *Int. J. Biol. Macromolecules* **2000**, *28*, 41-50.

11. Schokker, E.P.; Singh, H.; Pinder, D.N.; Creamer, L.K. *Int. Dairy J.* **2000**, *10*, 233-240.

12. Renard, D.; Lefebvre, J. *Int. J. Biol. Macromolecules* **1992**, *14*, 287-291.

13. Kavanagh, G.M.; Clark, A.H.; Ross-Murphy, S.B. *Langmuir* **2000**, *16*, 9584-9594.

14. Stading, M.; Hermansson, A.-M. *Food Hydrocolloids* **1990**, *4*, 121-135.

15. Linden van der, E.; Sagis, L.M.C. *Langmuir* **2001**, *17*, 5821-5824.

16. Verheul, M.; Roefs, S.P.F.M.; Kruif de, C.G. *J. Agric. Food Chem.* **1998**, *46*, 896-903.

17. Philipse, A.P. *Langmuir* **1996**, *12*, 1127-1133.

18. Onsager, L. *Ann. N.Y. Acad. Sci.* **1949**, *51*, 627-659.

19. Vroege, G.J.; Lekkerkerker, H.N.W. *Rep. Prog. Phys.* **1992**, *55*, 1241-1309.

20. Stroobants, A.; Lekkerkerker, H.N.W.; Odijk, T. *Macromolecules* **1986**, *19*, 2232-2238.

21. Boissonade, J.; Barreau, F.; Carmona, F. *J. Phys. A.: Math. Gen.* **1983**, *16*, 2777-2787.

22. Balberg, I.; Binnenbaum, N.; Wagner, N. *Phys. Rev. Lett.* **1984**, *52*, 1465-1468.

3

Mesostructure of Fibrillar Bovine Serum Albumin Gels

Abstract

The mesostructure of bovine serum albumin (BSA) at low pH was investigated. Rheological measurements were performed to determine the critical percolation concentration (c_p). A decreasing c_P with increasing ionic strength was found. Fibrils with a contour length of about 100 – 300 nm were found using transmission electron microscopy. The measured conversion of monomers into fibrils was independent of ionic strength (0.20 – 0.30 M). Dilution of BSA samples showed that the aggregation process is reversible and that there exists a critical concentration for the self-assembly of BSA. We explain the decreasing c_P with increasing ionic strength in terms of an adjusted random contact model.

3.1 Introduction

Serum albumins play an important role in various processes. In animal blood plasma 50% of the total amount of plasma protein consists of serum albumins. They are also found in animal tissue, bodily secretions and excrements.[1] In the food industry bovine serum albumin (BSA) is an important protein because of its ability to form heat-induced gels.[2] Whey proteins consist for 10% of BSA. The properties of albumin derived from blood, and serum albumin derived from whey are similar.[3]

BSA is a globular protein with a molecular weight of 66000 Da, consisting of 582 amino acid residues, with 17 disulphide bridges and 1 free thiol group.[1-3] A BSA monomer has an ellipsoidal shape with a diameter of 4 x 14 nm.[4,5] Hydrogen titration curves of BSA in 0.15 M KCl at 25 °C showed a positive charge of about 90 at pH 2.

BSA can form heat-induced gels.[2] The first step in the gelation process is the unfolding of the BSA monomer.[6] The change in conformational structure of a protein is a function of temperature and the duration of heat treatment.[3] Conformational changes, induced by heat, increase the number of hydrophobic residues exposed to the aqueous solvent. The exposure of these groups results in hydrophobic interactions which play a dominant role in the aggregation process.[2,6]

The aggregation process is governed by the balance between attractive and repulsive interactions between denatured protein molecules.[6] Repulsive forces are induced by the surface charge, and the attractive forces originate from the various functional groups exposed by the thermal unfolding of the protein.[7] The structures of the aggregates formed will depend on pH, which controls the net charge of the protein, and on the ionic strength of the solvent, which controls the screening of electrostatic interactions.[6]

Aggregation will lead to the formation of a gel when the protein concentration is larger than a critical value.[6] Network structures consist of assemblies of fine strands of BSA monomers, when the unfolded protein molecules are highly charged, and when electrolyte screening effects are small.[8,9] These conditions will result in a transparent network. Heterogeneous networks are formed around the iso-electric point, when screening effects are large, resulting in a turbid gel.[8,9]

Murata et al.[10] determined the presence and transparency of a gel for a 6% BSA solution, heated at 85 °C for 20 min, as function of pH, in the absence of salt. A

steel ball in a tube indicated whether the BSA was gelled or not. Gels were formed between pH 4.0 and 6.5. Transparent solutions were found at pH < 4 or at pH > 6.[10]

To study the structure of BSA, Murata et al.[10], Boye et al.[11], and Clark et al.[12] performed transmission electron microscopy (TEM) experiments. Murata et al.[10] obtained TEM micrographs of 6% BSA at pH 7.5, heated at 85 °C for 20 min, and showed short rod-like polymers in the absence of NaCl (~ 75 nm). Long linear polymers were formed when 0.01 or 0.02 M NaCl was added (~ 300 nm). With increasing salt concentration, the length of the linear polymers increased and interactions between linear polymers also increased.[10] Boye et al.[11] performed TEM experiments for BSA at pH 3, after heating at 90 °C for 30 min. The gel appeared to be a network of chain-like filamentous strands, which are linked at specific junctions.[11] Clark et al.[12] observed linear aggregates with a thickness of about one native monomer for BSA at pH 7, at low ionic strength, heated at 65 °C for 1 h.[12]

To obtain information on the minimum concentration of gelation, Tobitani et al.[9] performed dynamic oscillatory measurements as a function of time for BSA at pH 7. A minimum concentration of gelation between 5 and 6% (w/w) was found.[9] Tobitani et al.[13] observed a lower critical concentration with increasing ionic strength for BSA at pH 7.[13] In this paper we define the critical gel concentration as the critical percolation threshold, c_P. This c_P can be determined from the storage modulus, G', as a function of protein concentration, c, assuming the scaling relation $G' \sim (c - c_P)^t$, where t is a universal scaling exponent.[14]

Most literature about BSA describes experiments performed with BSA above the iso-electric point. The mechanism of gel formation of BSA can be different on either side of the iso-electric point.[7] The denaturation temperature of BSA in 0.1 M NaCl was 46.8 °C for pH 3.5, while above the iso-electric point, the denaturation temperature was about 60 °C.[15] Alizadeh-Pasdar et al.[16] studied the hydrophobicity of BSA heated at 80 °C for 30 min for varying pH using fluorescent probes. A decrease in hydrophobicity was observed after heating for pH values above the iso-electric point, while no change in hydrophobicity was observed after heating BSA at pH 3.[16]

The objective of this study was to obtain a better insight in the mesostructure of BSA gels at low pH for various ionic strengths and heating times. Turbidity measurements were performed to construct phase diagrams. To obtain information on the size and shape of the structures formed, TEM experiments were performed.

The fraction non-aggregated protein was determined using conversion experiments. Using rheological measurements, the critical percolation concentration was determined for various ionic strengths and heating times. The dependence of the percolation concentration on ionic strength was explained using an adjusted random contact model for charged semiflexible fibrils.[17]

3.2 Materials and Methods

3.2.1 Sample preparation

BSA, obtained from Sigma (A4503, Lot no 89H1270), was dissolved in a HCl solution of pH 2. To remove traces of calcium ions from BSA, and to obtain a protein solution with the same pH and ionic strength as the solvent, the protein was diluted repeatedly with HCl solvent and filtered through a 3K filter in an Omegacell™ membrane cell (Filtron) at 4 °C and a maximum pressure of 3 bar. The procedure was stopped when the pH and conductivity of the eluted solution and the solvent were the same. The BSA solution was centrifuged at 22600g for 30 min. To remove any traces of undissolved protein, the supernatant was filtered through a protein filter (FP 030/2, 1.2 µm, Schleicher & Schuell). A UV spectrophotometer was used to determine the exact BSA concentration, at a wavelength of 278 nm.

3.2.2 Turbidity measurements

1 ml BSA samples with varying protein concentration (1.5 – 8% (w/w)), ionic strength (0.0003 – 0.35 M), heating times (1 – 40 h), and pH (2 – 3.5), were put into turbiscan tubes and heated in a waterbath at 60 °C. The tubes were cooled for 1 h before the transmission was measured in a Turbiscan MA 2000.

3.2.3 Transmission electron microscopy (TEM)

BSA samples, near the percolation concentration, at pH 2, with varying ionic strength, and heating time were heated in a water bath at 60 °C. After cooling, the samples were diluted to a protein concentration of 0.04% (w/w). Directly after dilution, the TEM samples were prepared by negative staining. A drop of the diluted solution was deposited onto a carbon support film on a copper grid. The excess was removed after 30 s using a piece of filter paper. A droplet of 2% potassium phosphotungstate, pH 5.5, was added for 15 s, any excess being removed

as before. Electron micrographs were made using a Philips CM 12 transmission electron microscope operating at 80 kV.

3.2.4 Conversion experiments

A series of test tubes with BSA solution at pH 2, with varying protein concentrations (0.25 – 7% (w/w)), ionic strengths (0.20 – 0.30 M), and heating times (5 min – 30 h) were heated at 60 °C. Tubes were taken out of the water bath and immediately cooled in ice water. To determine the concentration non-aggregated BSA, the heated samples were diluted in a 0.1 M citric acid/phosphate buffer at pH 4.8. After precipitation of the aggregates overnight, the supernatant was centrifuged for 10 min at 20000g. The non-aggregated BSA concentration present in the supernatant was determined by a UV spectrophotometer at a wavelength of 278 nm.

To determine the effect of dilution on the fraction non-aggregated BSA, experiments were performed in which the amount of dilution and time after dilution were varied. The heated BSA samples were diluted with pH 2 solution and after that the citric acid/phosphate buffer was added and the procedure as described above was followed.

3.2.5 Rheological measurements

A Bohlin VOR strain-controlled rheometer with a concentric cylinder geometry (C14) was used to determine the storage modulus (G') as a function of strain (frequency 1 Hz, temperature 20 °C, strain 0.000206 – 0.206). BSA samples at pH 2 with varying ionic strengths (0.20 – 0.30 M), and heating times (1 and 10 h), were heated at 60 °C, and subsequently cooled to 20 °C for 1.5 h. After this procedure a strain sweep was performed.

3.3 Results and Discussion

3.3.1 Turbidity measurements

The transmission as a function of BSA concentration was determined for various ionic strengths, at pH 2, after heating at 60 °C for 1 h and 10 h (Figure 3.1A and B). For both heating times a decreasing transmission, i.e. a decreasing transparency, with increasing ionic strength, at a fixed BSA concentration was

observed. The minimum BSA concentration needed to form a gel was higher at lower ionic strength for both heating times. Comparing Figures 3.1A and 3.1B, we see that the minimum concentration to form a gel decreases with increasing heating time. When gels were formed, the transmission did not change with increasing heating time.
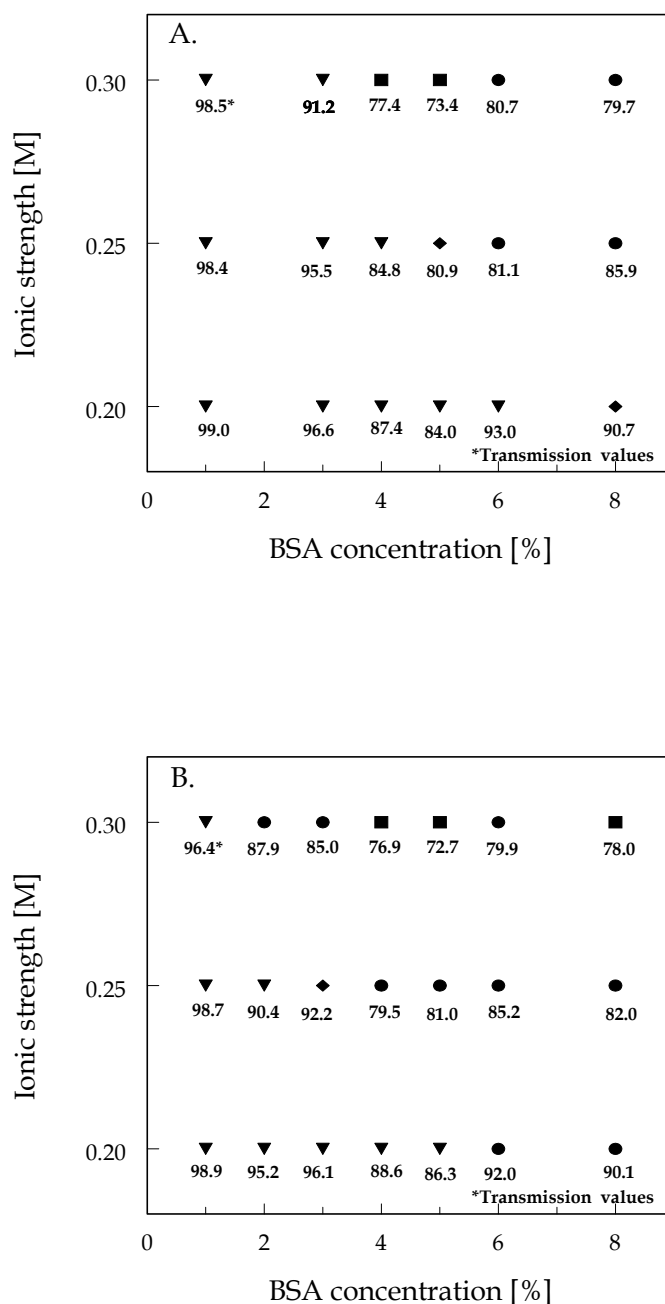
Figure 3.1 Phase diagrams of ionic strength versus protein concentration for BSA at pH 2 (A.) heated at 60 °C for 1 h; (B.) heated at 60 °C for 10 h. Symbols: transparent solution (▼); transparent viscous solution (◆); transparent gel (●); opaque gel (■).

The transmission versus heating time is shown in Figure 3.2. For high ionic strength the transparency decreases in the first hour. When gels were formed, further heating did not change the transparency significantly. At lower ionic strengths the transparency has an almost constant value as a function of heating time.

The transmission as a function of pH was determined for various ionic strengths for 6% BSA solutions, heated at 60 °C for 1 h (Figure 3.3). At low pH a higher ionic strength was required to form a gel. The transparency decreased with increasing ionic strength, at fixed pH. The transparency also decreased with increasing pH when the ionic strength was fixed. Murata et al.[10] investigated the effect of NaCl concentration on the gel formation of 6% BSA, at pH 7.5. Murata et al.[10] observed a transparent solution for BSA at pH 7 at 0.02 M NaCl or below. Transparent gels were formed at 0.025 – 0.050 M NaCl. At higher NaCl concentrations translucent or turbid gels were formed. Our results below the iso-electric point show that at least 0.10 M at pH 3.5 and 0.25 M at pH 2 was necessary to form a gel at 6% BSA, which is much higher than above the iso-electric point.
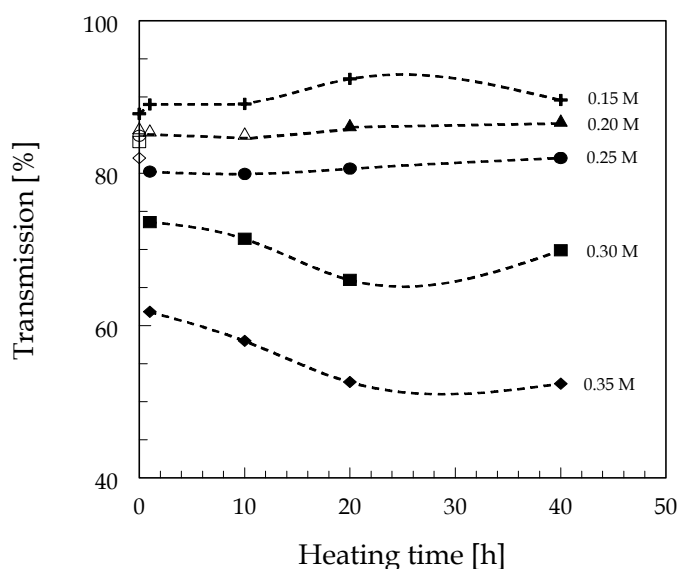
Figure 3.2 Phase diagram of transmission versus heating time for BSA, at pH 2, heated at 60 °C. The open symbols represent a solution, the closed symbols a gel.
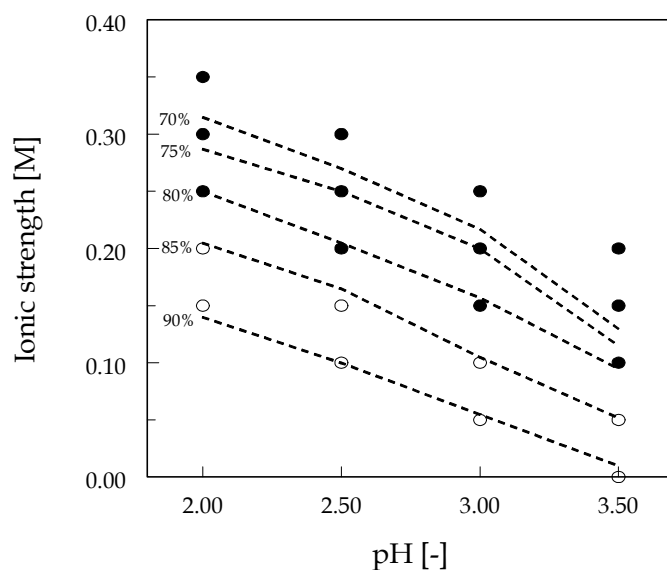
Figure 3.3 Phase diagram of ionic strength versus pH for BSA, heated at 60 °C, for 1 h. The open symbols represent a solution and the closed symbols a gel.

3.3.2 Transmission electron microscopy (TEM)

Figure 3.4A – F shows TEM micrographs for BSA, at pH 2, varying ionic strength, and heating time. Polydisperse semiflexible fibrils with an estimated contour length of about 100 – 300 nm were observed. Table 3.1 shows that the average contour length of the fibrils (based on an average of the contour length of 10 fibrils) was slightly increasing with increasing ionic strength. Increasing the heating time from 1 to 10 h also resulted in a slight increase of the average contour length of the fibrils, with fixed ionic strength. For all measured conditions, the order of magnitude of the contour length of the fibrils was the same.

Table 3.1 Average contour length of BSA fibrils.

Condition	Contour length [nm]
0.20 M heated for 1 h	115 ± 44
0.25 M heated for 1 h	121 ± 35
0.30 M heated for 1 h	264 ± 53
0.20 M heated for 10 h	203 ± 57
0.25 M heated for 10 h	331 ± 138
0.30 M heated for 10 h	230 ± 60

Murata et al.[10] found structures with a contour length of the same order of magnitude as observed in Figure 3.4, for BSA at pH 7.5, with a much lower NaCl concentration (0 – 0.02 M). Below the iso-electric point a higher ionic strength was necessary to obtain the same type of structures as above the iso-electric point.
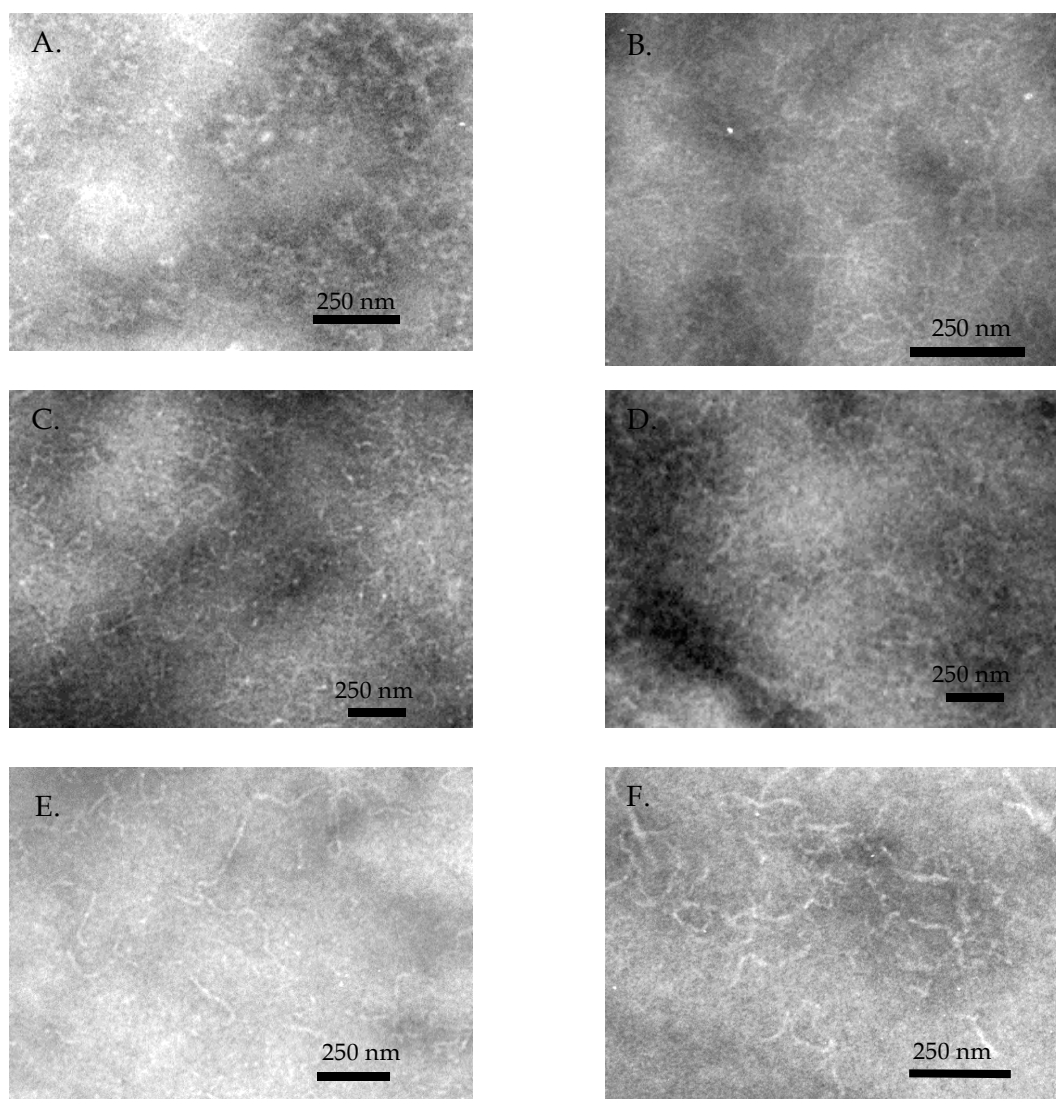
Figure 3.4 TEM micrographs of BSA, at pH 2, heated at 60 °C. (A.) 0.20 M, heated for 1 h; (B.) 0.25 M, heated for 1 h; (C.) 0.30 M, heated for 1 h; (D.) 0.20 M, heated for 10 h; (E.) 0.25 M, heated for 10 h; (F.) 0.30 M, heated for 10 h.

3.3.3 Conversion Experiments

3.3.3.1 The effect of protein concentration, ionic strength and heating time on the conversion of BSA

The conversion of BSA monomers for various protein concentrations and ionic strength was determined at pH 2, after heating at 60 °C for 1 h, 10 h (Figure 3.5) and 30 h (Figure 3.6). For each ionic strength and heating time the conversion increased with increasing BSA concentration. In addition, the conversion increases with increasing ionic strength, at a fixed BSA concentration and a fixed heating time. Finally, the conversion also increases with increasing heating time. A lower protein concentration is necessary at longer heating times, to obtain the same conversion (e.g. for 3% BSA at 0.25 M 35% was converted, while at 10 h 75% was converted).

3.3.3.2 The effect of dilution on the conversion of BSA

To obtain insight in the aggregation mechanism of BSA, we performed experiments on the effect of dilution (Figure 3.7), and the time after dilution (Table 3.2), on the conversion of BSA monomers. We determined first the conversion of BSA without dilution (as in section 3.3.3.1), and after that the conversion of BSA with increasing amount of dilution, i.e. decreasing protein concentration. Figure 3.7 shows a decrease in conversion with decreasing protein concentration for all measured conditions. This result indicates that the aggregation process of BSA is reversible and that there is a critical concentration below which no self-assembly occurs. For the BSA samples measured at 1 h, this critical concentration is between 0.04 and 0.09% for 0.20 M BSA, and between 0.01 and 0.03% for 0.30 M BSA. This result indicates that the critical concentration for assembly is decreasing with increasing ionic strength.

Table 3.2 Effect of the time after dilution on the amount of converted monomers (in %), at pH 2, heated at 60 °C, for 1 h.

Condition	Dilution factor	Time after dilution [min]				
		0	5	10	30	60
5% 0.20 M	100	69	62	57	28	95
3.2% 0.25 M	75	75	67	58	46	32
1.5% 0.30 M	30	93	92	91	90	89
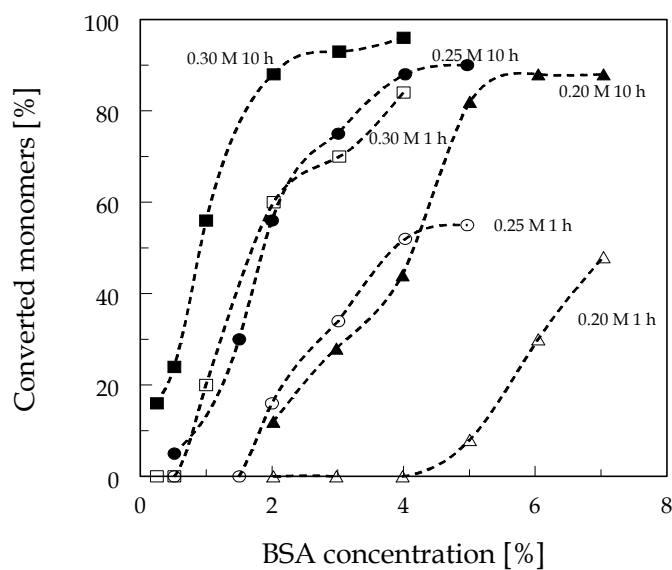
Figure 3.5 Converted monomers versus BSA concentration, at pH 2, after heating at 60 °C, for 1 h and 10 h.
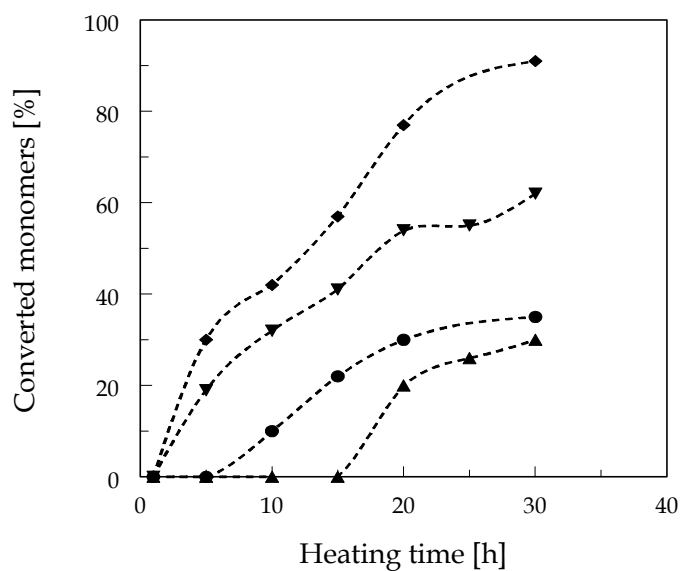
Figure 3.6 Converted monomers versus heating time for BSA at 0.20 M ionic strength and pH 2, after heating at 60 °C, during 30 h, for various BSA concentrations: 2% (▲); 3% (●); 4% (▼); 5% (◆).
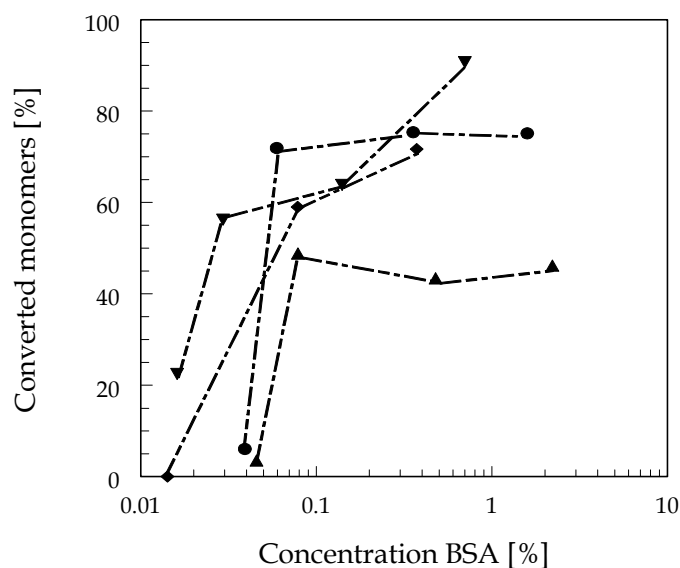
Figure 3.7 Converted monomers versus BSA concentration, at pH 2, for various ionic strength and heating times. 4.4%, at 0.20 M, heated for 1 h (▲); 3.2%, at 0.25 M, heated for 1 h (●); 1.4%, at 0.30 M, heated for 1 h (▼); 0.7%, at 0.30 M, heated for 10 h (◆).

We also investigated the effect of time after dilution on the conversion of BSA. The conversion was determined after different time periods. Table 3.2 shows that the conversion of monomers decreases with increasing time after dilution, except for 5% BSA at 0.20 M, 60 min after dilution, which is probably a measurement error. The results of these measurements also indicate that the aggregation process of BSA at pH 2 is reversible and that there is a critical concentration necessary for self-assembly.

Figure 3.8 shows TEM micrographs for 0.30 M, heated at 60 °C for 1 h, directly prepared after dilution, and 16 h after dilution. TEM micrographs, where the sample was diluted 16 h before preparation of the grids, show only the presence of structures with the length of a few monomers (Figure 3.8A). For 0.20 and 0.25 M the same result was found. Longer linear fibrils were visible when the sample was diluted, and directly used for the preparation of the grids (Figure 3.8B). All results shown indicate that the aggregation process of BSA at pH 2 is reversible, and that there is a critical concentration for the self-assembly of BSA. In the aggregation and gelation process of BSA at pH 7, covalent disulphide bond formation plays a role, indicating that there is a different aggregation mechanism below and above the iso-electric point.[2,7,18,19]
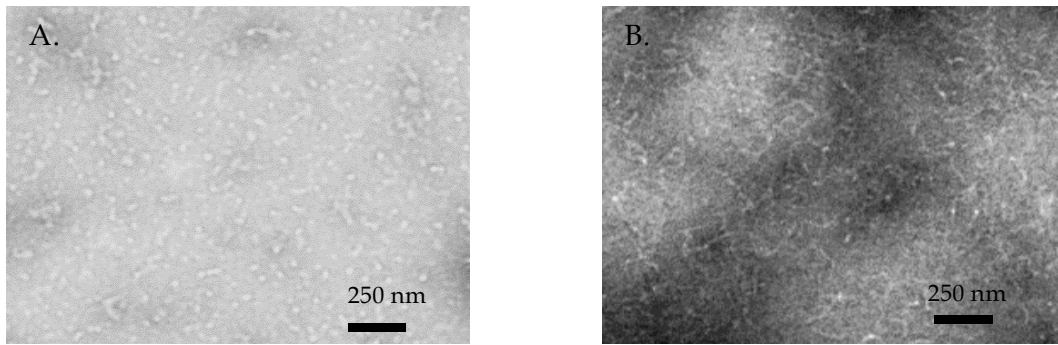
Figure 3.8 TEM micrographs of BSA at 0.30 M ionic strength, and pH 2, heated at 60 °C, for 1 h. (A.) dilution of the heated solution 16 h before preparation of the TEM sample; (B.) dilution of the heated solution 30 s before preparation of the TEM sample.

3.3.4 Rheological measurements

G' versus strain was determined for various BSA concentrations (Figure 3.9). G' was determined from the linear regime of the curve. Using these measurements the percolation concentration, c_p, can be determined, as described by van der Linden and Sagis.[14] Table 3.3 shows the values for c_p and the scaling exponent t, for various ionic strengths and heating times. The standard deviations in the data were determined according to Veerman et al.[17] c_p decreases with increasing ionic strength. For fixed ionic strength, c_p decreases with increasing heating time. For measurements performed at a heating time of 30 h, c_p could not be determined,
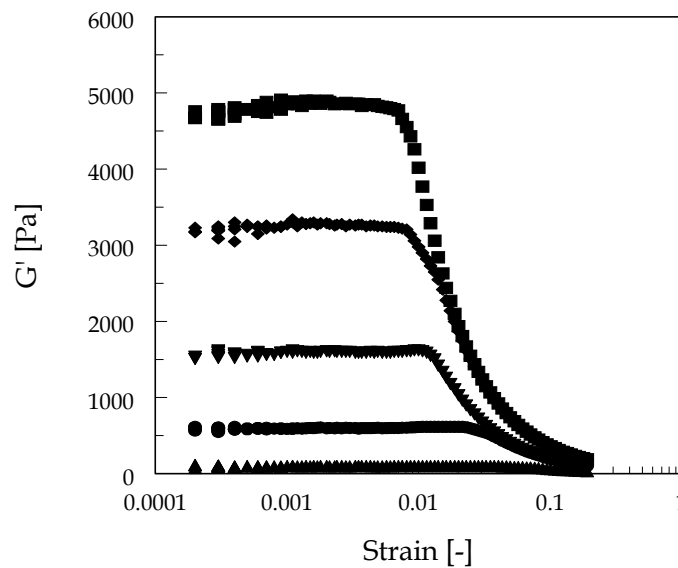
Figure 3.9 G' versus strain for various BSA concentrations, at pH 2, and 0.25 M ionic strength, heated at 60 °C, for 1 h. 6% (▲); 7% (●); 8% (▼); 9% (◆); 10% (■).

because of the large scatter in the results.

For BSA samples heated for 1 h in the ionic strength regime of 0.20 – 0.235 M, a value of 4 was found for *t*. This value indicates central force percolation.[14] Stretching forces between two entanglements are the dominant contribution to the energy of deformation.[20] For BSA samples heated for 1 h, above 0.235 M, and all samples heated for 10 h, *t* was equal to 2, indicating isotropic force percolation.[14] Here, bending of the strands between two entanglements is the dominant contribution to the deformation energy.[20] An explanation for the above observations may be that for BSA samples heated for 10 h, or heated for 1 h at 0.30 M ionic strength, more entanglements per chain will be formed, resulting in a denser network compared to the network formed after heating for 1 h, below 0.25 M. Bending forces will play a more dominant role. A transition from central to isotropic force percolation occurs, upon increasing heating time or ionic strength.

Table 3.3 Values for c_P and *t* for BSA at pH 2, heated at 60 °C, for various heating times, and ionic strengths.

Heating time [h]	Ionic strength [M]	c_P [%(w/w)]	*t*
1	0.20	7.6 ± 0.04	4.3 ± 0.10
1	0.22	6.7 ± 0.05	4.2 ± 0.11
1	0.235	5.2 ± 0.10	4.1 ± 0.13
1	0.25	5.4 ± 0.10	2.0 ± 0.13
1	0.30	3.3 ± 0.12	2.4 ± 0.14
10	0.20	6.7 ± 0.11	1.9 ± 0.14
10	0.25	4.6 ± 0.13	1.8 ± 0.11
10	0.30	1.1 ± 0.28	2.0 ± 0.16

3.3.5 Effect of ionic strength on the percolation concentration

TEM micrographs showed that the BSA fibrils formed at pH 2, in the ionic strength regime of 0.20 – 0.30 M, and heated for 1 h, have a contour length that is in the same order of magnitude (100 – 300 nm). Using the conversion experiments, we could determine that the conversion of the monomers at the percolation concentration, for BSA samples heated for 1 h, was almost equal (± 60%). Combining these results, we found for the BSA samples measured after heating for 1 h, that the same amount of fibrils with approximately equal contour length was

formed. This result indicates that we can explain the decreasing percolation concentration with increasing ionic strength in terms of electrostatic interactions between the fibrils. Qualitatively, at low ionic strength the electrostatic repulsion is high. It is difficult to form cross-links between the fibrils, which results in a high percolation concentration. At high ionic strength the electrostatic repulsion decreases, cross-links can be formed more easily, resulting in a lower critical percolation concentration.

Quantitatively, the decreasing percolation concentration with increasing ionic strength is explained as follows. TEM micrographs (Figure 3.4) show semiflexible fibrils for BSA at pH 2 heated at 60 °C for 1 h. This implies that we may use an adjusted random contact model for semiflexible charged fibrils[17]:

$$\phi_{p,m} = \alpha(D_{eff}/P) \qquad\qquad \text{for } (P/D_{eff}) \gg 1 \qquad\qquad (3.1)$$

where $\phi_{p,m}$ is the critical percolation mass fraction (equal to $0.6(c_p/100)$, where 0.6 is the conversion factor), α the average number of contacts per rod, assumed to be of order 1 at the percolation concentration[21], D_{eff} an effective diameter[22], and P the persistence length of the fibrils. Figure 3.10 shows the linear dependence of $\phi_{p,m}$ on D_{eff} for a heating time of 1 h. The vertical dashed line gives the theoretical limit of Eq 3.1. Using that $\alpha \sim O(1)$ results in a persistence length of 16 ± 4 nm. The TEM
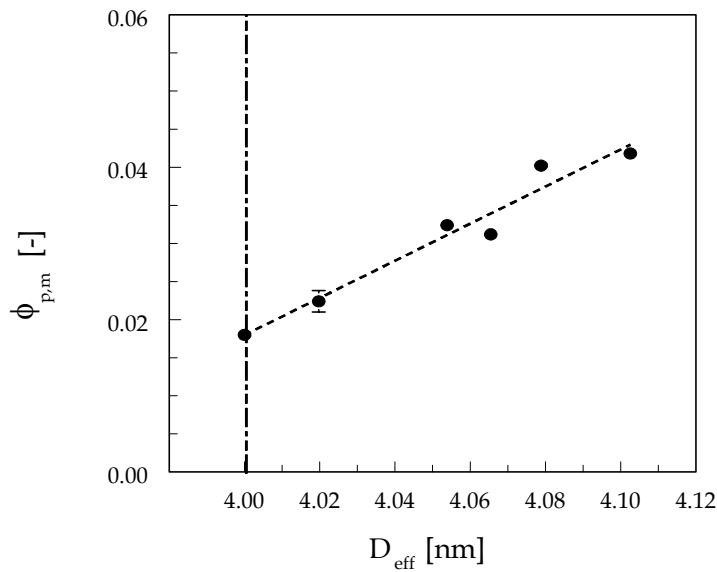
Figure 3.10 $\phi_{p,m}$ as a function of D_{eff} for BSA at pH 2, heated at 60 °C, for 1 h.

micrographs show that the contour length of the semiflexible fibrils was 100–300 nm (Figure 3.4). A factor of about 10 between contour and persistence length indicates that the BSA fibrils are indeed semiflexible. We conclude that we can use this adjusted random contact model for BSA to explain the decreasing percolation concentration with increasing ionic strength.

3.4 Conclusion

Comparing gel formation and transparency of gels formed below and above the iso-electric point, a higher ionic strength is necessary to form a gel below the iso-electric point (0.15 M below, and 0.025 M above the iso-electric point). Below the iso-electric point the transparent regime is larger than above the iso-electric point.

Experiments on the conversion of BSA as a function of dilution and as a function of time after dilution, showed that the aggregation process of BSA was reversible, and that a critical concentration exists for the self-assembly of BSA.

A decreasing percolation concentration with increasing ionic strength was found. An adjusted random contact model, which accounts for the semiflexibility and charge of the BSA fibrils, has been used to explain this result.

Acknowledgements

The authors thank Harry Baptist for his assistance with transmission electron microscopy, and Jan van Lent from the Laboratory of Virology, Wageningen University for his technical advice on transmission electron microscopy.

References

1.   Giancola, C.; De Sena, C.; Fessas, D.; Graziano, G.; Barone, G. *Int. J. Biol. Macromolecules* **1997**, *20*, 193-204.

2.   Boye, J.I.; Alli, I.; Ismail, A.A. *J. Agric. Food Chem.* **1996**, *44*, 996-1004.

3.   Relkin, P. *Crit. Rev. Food Sci. Nutr.* **1996**, *36*, 565-601.

4.   Vilker, V.L.; Colton, C. K.; Smith, K.A. *J. Coll. Interf. Sci.* **1981**, *79*, 548-565.

5.   Carter, D.C.; Ho, J.X. In *Advances in Protein Chemistry* Schumaker, V.N. (Ed.) **1994**, Academic press inc.: Los Angeles, 153-204.

6.   Lefebvre, J.; Renard, D.; Sachez-Gimeno, A.C. *Rheol. Acta* **1998**, *37*, 346-357.

7.   Yasuda, K.; Nakamura, R.; Hayakawa, S. *J. Food Sci.* **1986**, *51*, 1289-1292.

8.   Clark, A.H. In *Functional Properties of Food Macromolecules*, Hill, S.E.; Ledward, D.A.; Mitchell, J.R. (Eds.) **1998**, Aspen Publishers: Great Britain, 77-142.

9.   Tobitani, A.; Ross-Murphy, S.B. *Macromolecules* **1997**, *30*, 4845-4854.

10.   Murata, M.; Tani, F.; Higasa, T.; Kitabatake, N.; Doi, E. *Biosci. Biotech. Biochem.* **1993**, *57*, 43-46.

11.   Boye, J.I.; Kalab, M.; Alli, I.; Ma, C.Y. *Lebensm.- Wiss. Technol.* **2000**, *33*, 165-172.

12.   Clark, A.H.; Judge, F.J.; Richards, J.B.; Stubbs, J.M.; Suggett, A. *Int. J. Pept. Protein Res.* **1981**, *17*, 380-392.

13.   Tobitani, A.; Ross-Murphy, S.B. *Macromolecules* **1997**, *30*, 4855-4862.

14.   Linden van der, E.; Sagis, L.M.C. *Langmuir* **2001**, *17*, 5821-5824.

15.   Yamasaki, M.; Yano, H.; Aoki, K. *Int. J. Biol. Macromolecules* **1990**, *12*, 263-268.

16.   Alizadeh-Pasdar, N.; Li-Chan, E.C.Y. *J. Agric. Food Chem.* **2000**, *48*, 328-334.

17.   Veerman, C.; Ruis, H.; Sagis, L.M.C.; Linden van der, E.; *Biomacromolecules* **2002**, *3*, 869-873.

18.   Matsudomi, N.; Rector, D.; Kinsella, J.E. *Food Chem.* **1991**, *40*, 55-69.

19.   Gezimati, J.; Singh, H.; Creamer, L.K. *J. Agric. Food Chem.* **1996**, *44*, 804-810.

20.   Feng, S.; Sen, P.N. *Phys. Rev. Lett.* **1984**, *52*, 216-219.

21.   Philipse, A.P. *Langmuir* **1996**, *12*, 1127-1133.

22.   Stroobants, A.; Lekkerkerker, H.N.W.; Odijk, T. *Macromolecules* **1986**, *19*, 2232-2238.

4

Irreversible Self-Assembly of Ovalbumin into Fibrils and the resulting Network Rheology

Abstract

The self-assembly of ovalbumin into fibrils and resulting network properties were investigated at pH 2, as a function of ionic strength. Using transmission electron microscopy (TEM), the effect of ovalbumin concentration on the contour length was determined. The contour length was increasing with increasing ovalbumin concentration. TEM micrographs were made to investigate the effect of ionic strength on the contour length. In the measured ionic strength regime (0.01 – 0.035 M) fibrils of approximately equal length (± 200 nm) were observed. TEM micrographs showed that the contour length of the fibrils, versus time after dilution, remained constant, which indicates that the self-assembly of ovalbumin is irreversible. Using the results of rheological measurements, we observed a decreasing critical percolation concentration with increasing ionic strength. We explain this result in terms of an adjusted random contact model for charged semiflexible fibrils. Hereby, this model has now been proven to be valid for fibril networks of β-lg, BSA and, currently, for ovalbumin.

4.1 Introduction

Ovalbumin belongs to a family of more than 20 homologous proteins, the serpins, found in animals, plants and viruses.[1] Most of these proteins are serine protease inhibitors, but for ovalbumin no inhibitory activity is known.[1] Ovalbumin is a major globular protein component in egg white, and has multi functional properties, like its ability to foam and to form gels upon heating.[2-5] An ovalbumin monomer consists of 385 amino acid residues, and has a molecular weight of 45000 Da.[2,3,6] One monomer has an ellipsoidal shape with dimensions of 7 x 4.5 x 5 nm.[7] One internal S-S bridge is present in ovalbumin, and four free sulfhydryl groups.[3] Its secondary structure is composed of 30.6% α-helices and 31.4% β-sheets.[1,8] This secondary structure content is almost the same for pH 2 and pH 7. The native tertiary structure is disrupted at acidic pH, which indicates the presence of a molten globule state at acidic pH.[9]

The formation of heat-induced ovalbumin gels takes place in three steps: denaturation, aggregation and the formation of a gel network.[10] In the denaturation process, a change from the native protein conformation to a more unfolded conformation takes place, which makes the protein molecules more reactive.[11,12] Some of the hydrophobic areas that have been buried in the interior of the globular molecule are exposed on the surface, and may act as binding sites for aggregation of thermally denatured ovalbumin molecules.[2,12] The denaturation temperature of ovalbumin at pH 7 is 80 °C, whereas a denaturation temperature of 63.9 °C was found at pH 3.[13,14]

After denaturation, intermolecular bonds between heat-denatured ovalbumin monomers are formed, when the protein concentration is high enough. This aggregation process is governed by a balance between attractive hydrophobic and repulsive electrostatic interactions.[3,12,13,15] At pH values far from the iso-electric point and at low ionic strength, electrostatic repulsive forces hinder the formation of random aggregates, and linear fibrils are formed.[16-18] At high ionic strength, and a pH near the iso-electric point, random aggregates are formed because of a weaker electrostatic repulsion.[16-18]

The final step in the gelation process is the gel formation. When the protein concentration is high enough, and when there is a balance between attractive and repulsive forces between the fibrils, a well ordered tertiary network can be formed.[12,14-16,19]

The presence of fibrillar structures was observed using transmission electron microscopy (TEM).[13,20-22] Koseki et al.[13], and Doi et al.[21] performed experiments on ovalbumin at pH 7 and low ionic strength. They both observed a diameter of the fibrils of 5 nm. The contour length of fibrils was increasing with increasing heating time, and increasing protein concentration. For 0.5% ovalbumin a contour length of approximately 180 nm was found when the solution was heated at 85 °C for 20 min. A contour length of about 200 ± 50 nm was found for 1% ovalbumin heated at 75 °C for 2 h, or 0.5% ovalbumin heated at 75 °C for 24 h.[13,21] Weijers et al.[20] performed TEM experiments on 2% ovalbumin at acidic pH. For pH 2 a contour length of 25 nm was found for 0.01 M ionic strength, and a length of about 140 nm was observed for 0.025 M ionic strength.[20]

In this study we investigated the self-assembly of ovalbumin into fibrils and the resulting network rheology at conditions far below the iso-electric point. It is important to get insight in the self-assembly process and network rheology far below the iso-electric point, because these differ significantly from those at pH values above the iso-electric point. The effect of ionic strength on the critical percolation concentration of ovalbumin gels at pH 2 was investigated. TEM experiments were performed near the percolation concentration to estimate the effect of ionic strength on the contour length of the fibrils. The assembly mechanism of ovalbumin is not evident. To get more insight in the self-assembly process of ovalbumin, the effect of protein concentration, and the effect of time after dilution on the contour length was investigated, using TEM experiments. Results from rheological measurements can be used to determine the critical percolation concentration, c_p, which is the minimum concentration for gelation, as a function of ionic strength. Percolation theory assumes the following relation: $G' \sim (c - c_p)^t$, where G' is the storage modulus, c the monomer concentration, and t a scaling exponent dependent on the Hamiltonian of the system.[23] The dependence of ionic strength on c_p was explained using an adjusted random contact model for charged semiflexible fibrils.[24]

4.2 Materials and Methods

4.2.1 Sample preparation

Ovalbumin was obtained from Sigma (A5503, lotnr.120k7001) with a purity of at least 98%. The protein was dissolved in bidistilled water, of set ionic strength (between 0.01 – 0.035 M) and was stirred for 30 min. The pH was adjusted to 2, and after that stirred for 1.5 h. The ovalbumin solutions were centrifuged at 20000g for 30 min, to remove any traces of undissolved material. The supernatant was filtered through a protein filter (FP 030/2, 0.45 µm, Schleicher & Schuell). The concentration of the obtained stock solution was determined with a UV-spectrophotometer at a wavelength of 278 nm.

4.2.2 Transmission electron microscopy (TEM)

Ovalbumin solutions were heated in a water bath at 80 °C for 1 h. After cooling, the samples were diluted to 0.04%, just before the preparation of the grid. The TEM samples were prepared by negative staining. A drop of the diluted solution was deposited onto a carbon support film on a copper grid. The excess was removed after 30 s using a piece of filter paper. A droplet of 2% uranyl acetate, pH 3.8, was added for 15 s, any excess being removed as before. Electron micrographs were made using a Philips CM 12 transmission electron microscope operating at 80 kV.

4.2.3 Rheological measurements

A Bohlin VOR strain-controlled rheometer with a concentric cylinder geometry (C14) was used to determine the storage modulus (G') as a function of strain (frequency 1 Hz, temperature 20 °C, strain 0.000206 – 0.206). Ovalbumin solutions at pH 2 and various ionic strength (0.01 – 0.035 M) were heated at 80 °C for 1 h and subsequently cooled to 20 °C for 2 h. After this procedure a strain sweep was performed.

4.3 Results and Discussion

4.3.1 Transmission electron microscopy

4.3.1.1 Effect of ovalbumin concentration on the contour length

The effect of the ovalbumin concentration on the contour length was investigated for 2 – 7% ovalbumin at pH 2 and an ionic strength of 0.01 M (Figure 4.1A – F). All samples were heated at 80 °C for 1 h. An increasing contour length with increasing ovalbumin concentration was observed. Figure 4.2 shows the average value (based on the average of 10 single fibrils) of the contour length at various ovalbumin concentrations.
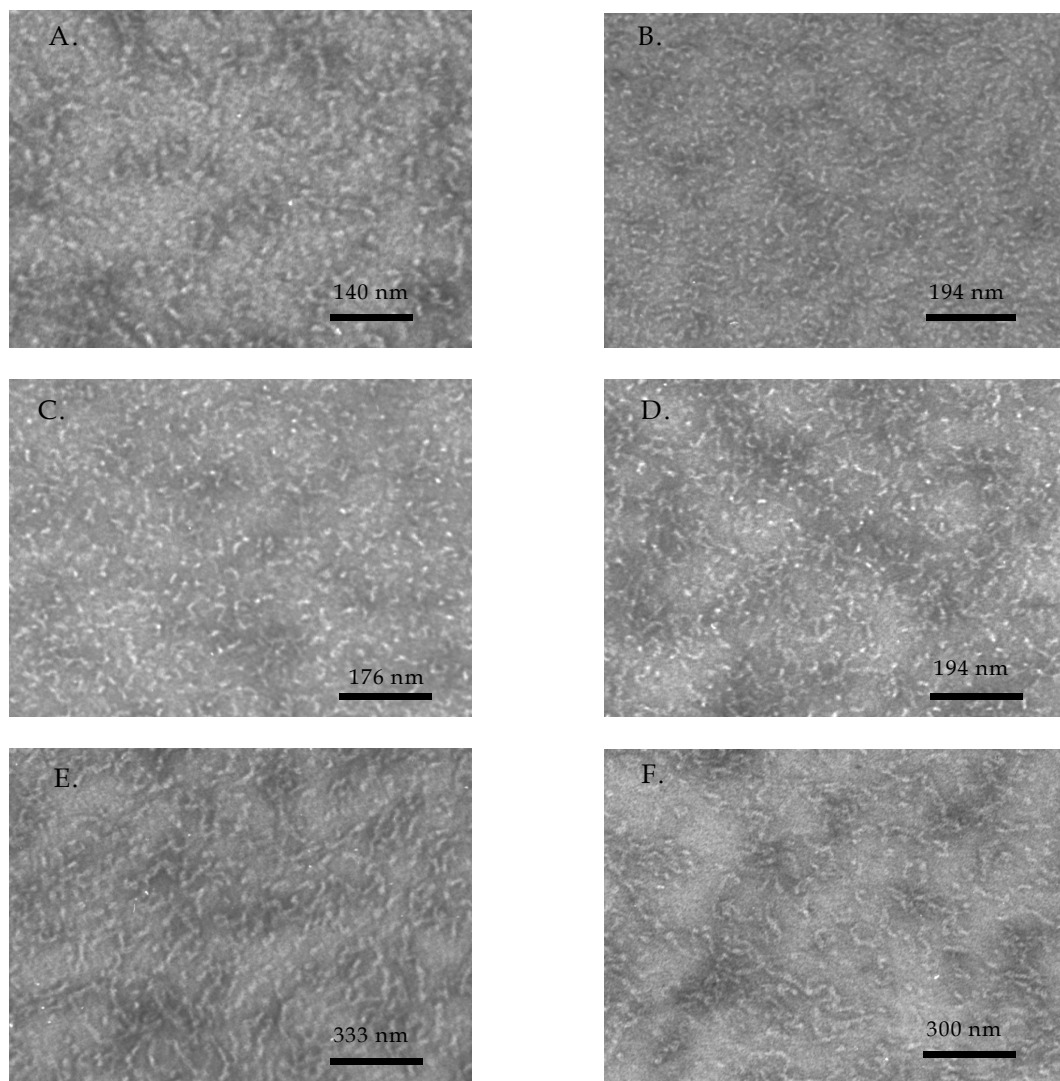
Figure 4.1 TEM micrographs of ovalbumin at pH 2, and 0.01 M ionic strength for various ovalbumin concentrations: (A.) 2%; (B.) 3%; (C.) 4%; (D.) 5%; (E.) 6%; (F.) 7%.
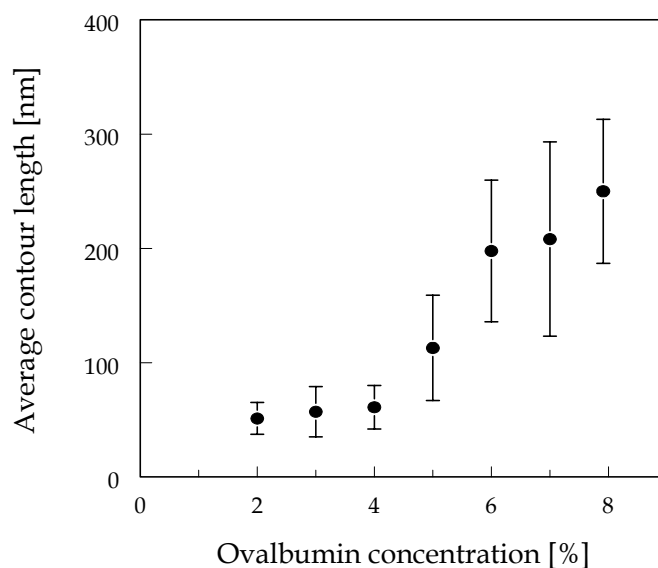
Figure 4.2 Average contour length of ovalbumin at pH 2, and 0.01 M ionic strength versus ovalbumin concentration (contour length was determined from TEM micrographs in Fig. 4.1; the contour length at 7.9% ovalbumin was determined from the TEM micrograph in Fig. 4.3A). The average contour length and the standard deviation were based on the length of 10 single fibrils visible in one TEM micrograph.

4.3.1.2 Effect of ionic strength on the contour length

Figure 4.3A – F shows the effect of ionic strength (0.01 – 0.035 M) on the contour length of ovalbumin at pH 2. The fibrils were made near the critical percolation concentration for each ionic strength (as determined in section 4.3.2). The TEM micrographs show semiflexible fibrils. The average contour length of the fibrils was determined (based on the length of 10 single fibrils), and showed that the order of magnitude of the fibrils was the same for all ionic strengths, near the critical percolation concentration (Table 4.1). Results of TEM studies of Weijers et al.[20] on ovalbumin at pH 2, showed an increasing contour length with increasing ionic strength. The difference between the results in this paper and the results of Weijers et al.[20] may be caused by a difference in experimental conditions. Weijers et al. used a fixed protein concentration of 2% at varying ionic strength. In this paper, TEM micrographs were prepared at the critical percolation concentration for each ionic strength, which is not a constant concentration. The contour length found for ovalbumin at pH 2 was of the same order of magnitude as the contour length observed at pH 7, found by Koseki et al.[13] and Doi et al.[21]
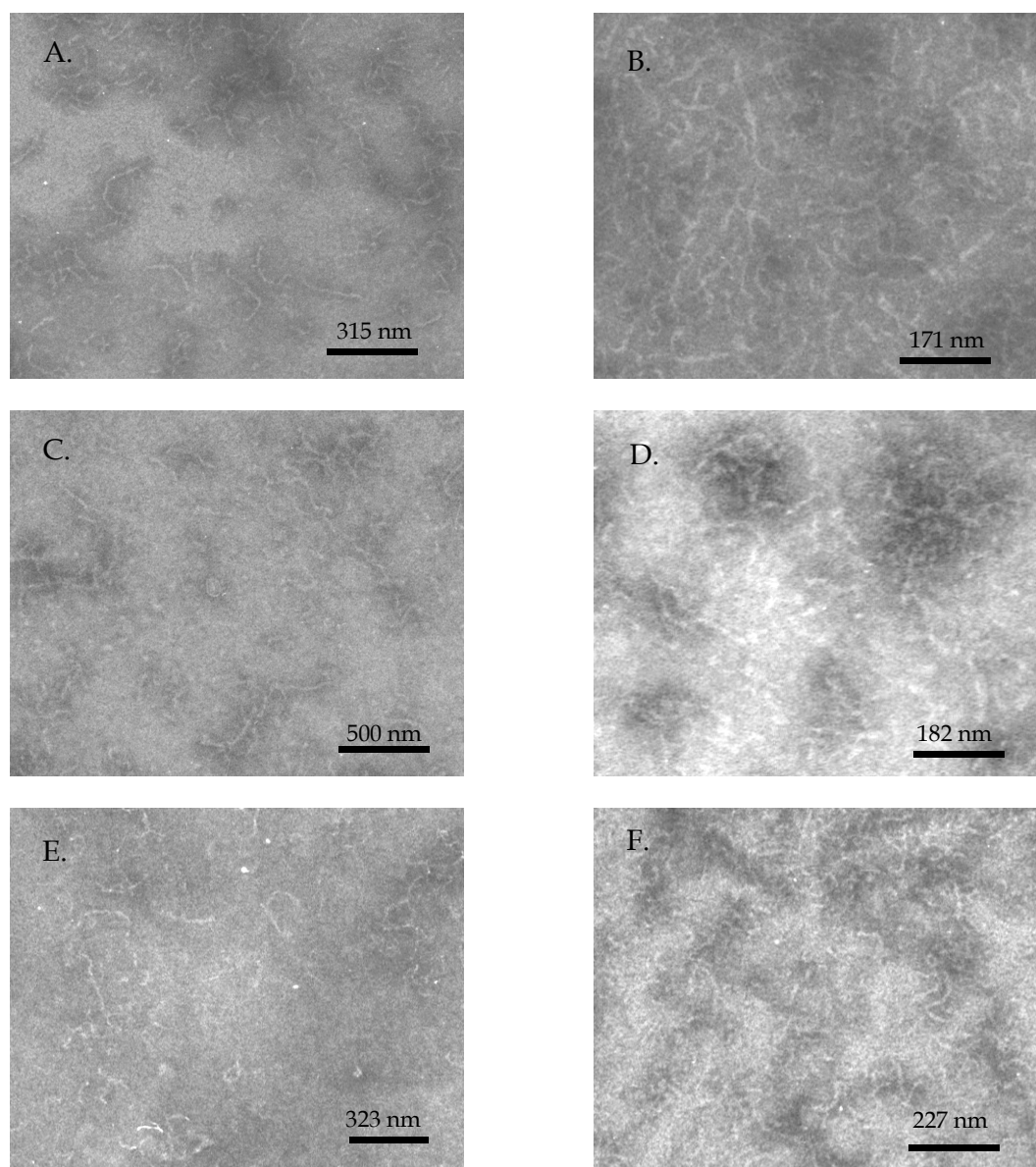
Figure 4.3 TEM micrographs of ovalbumin at pH 2, near the percolation concentration, for various ionic strengths: (A.) 0.01 M; (B.) 0.015 M; (C.) 0.02 M; (D.) 0.025 M; (E.) 0.03 M; (F.) 0.035 M.

Table 4.1 Effect of ionic strength on the average contour length, for ovalbumin at pH 2, near the critical percolation concentration. The average contour length and the standard deviation were based on the length of 10 single fibrils visible in one TEM micrograph.

Ionic strength [M]	Average contour length [nm]
0.010	250 ± 63
0.015	138 ± 33
0.020	195 ± 66
0.025	150 ± 47
0.030	263 ± 44
0.035	143 ± 30

4.3.1.3 Effect of time after dilution on the contour length

To check if the fibrils fall apart upon dilution (to 0.04%), TEM micrographs were made for 2 and 7% ovalbumin, at pH 2, and an ionic strength of 0.01 M, with a varying time after dilution. Figure 4.4A – D shows the results of 7% ovalbumin for 0 min – 24 h after dilution. The average contour length (based on the average of 10 single fibrils) was almost constant as a function of time after dilution. The same result was found for 2% ovalbumin (Table 4.2). The contour length found for 2% ovalbumin at pH 2 was in good agreement with TEM results obtained by Weijers et al. for ovalbumin at pH 2.[20] The results indicate that the self-assembly process of ovalbumin is irreversible. We do not expect the presence of covalent bonds in the form of intermolecular disulphide bridges, because these are not formed at pH 2.

Table 4.2 Effect of time after dilution on the contour length, for ovalbumin at pH 2, and 0.01 M ionic strength. The average contour length and the standard deviation were based on the length of 10 single fibrils visible in one TEM micrograph.

Ovalbumin concentration [%]	Time after dilution	Average contour length [nm]
7	0 min	208 ± 85
	10 min	171 ± 80
	105 min	152 ± 29
	24 h	219 ± 86
2	0 min	51 ± 14
	50 min	51 ± 17
	20 h	48 ± 9

A possible explanation for the irreversibility of the self-assembly process is the transition from α-helices to β-sheets, which will initiate the aggregation process.[25] It was suggested before that the formation of stable self-assembled fibrils takes place by intermolecular β-sheets between the monomers.[26,27] This type of intermolecular binding is stable upon dilution. Results on the aggregation process of another globular protein, bovine serum albumin (BSA), showed that BSA fibrils fall apart upon dilution.[28] These fibrils were probably formed only by hydrophobic interactions. This result contradicts results reported on BSA using Raman spectroscopy.[29] Based on these results, a model for denaturation, aggregation and gel formation is suggested, where intermolecular β-sheets play a role.[29] A possible explanation for this discrepancy is that the increase in β-sheets observed with Raman spectroscopy is due to the formation of intramolecular β-sheets instead of intermolecular β-sheets.
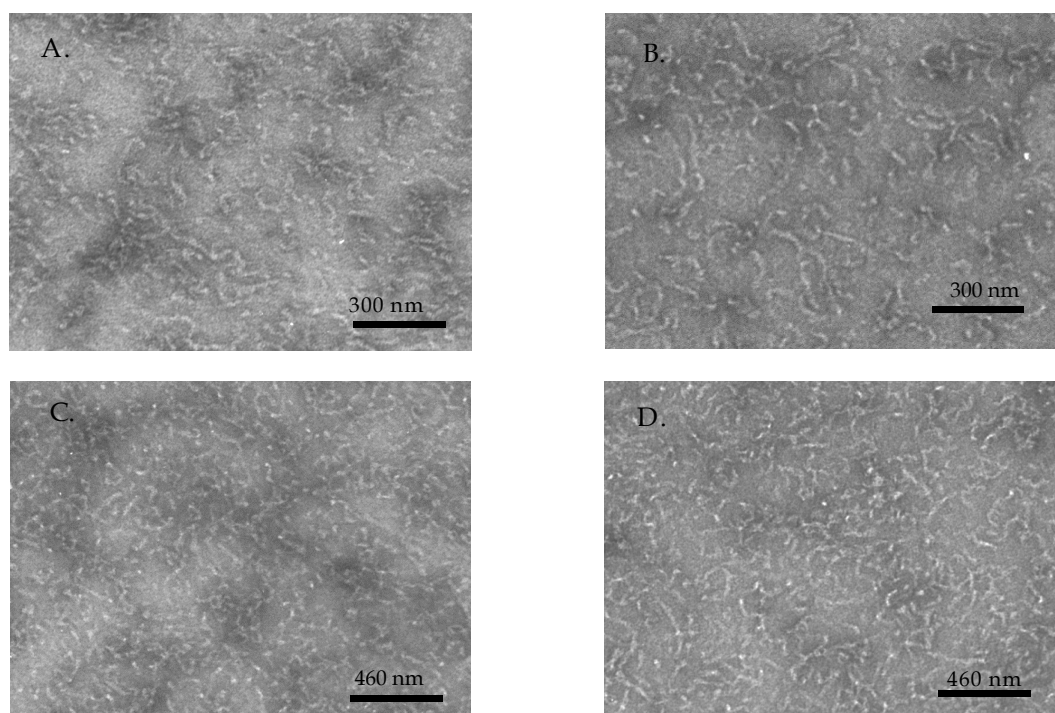
Figure 4.4 TEM micrographs of 7% ovalbumin at pH 2, and 0.01 M ionic strength, for various times after dilution: (A.) 0 min; (B.) 10 min; (C.) 105 min; (D.) 24 h.

4.3.2 Rheological measurements

Rheological measurements were performed for ovalbumin at pH 2, and an ionic strength of 0.01 – 0.035 M. Figure 4.5 shows G' versus strain for varying protein concentrations at an ionic strength of 0.03 M. G' can be determined from the linear regime of the curve. Using these results we can determine a critical percolation concentration, c_p, and the scaling exponent t using the method described by van der Linden and Sagis.[23] This method is a graphical method that uses plots of
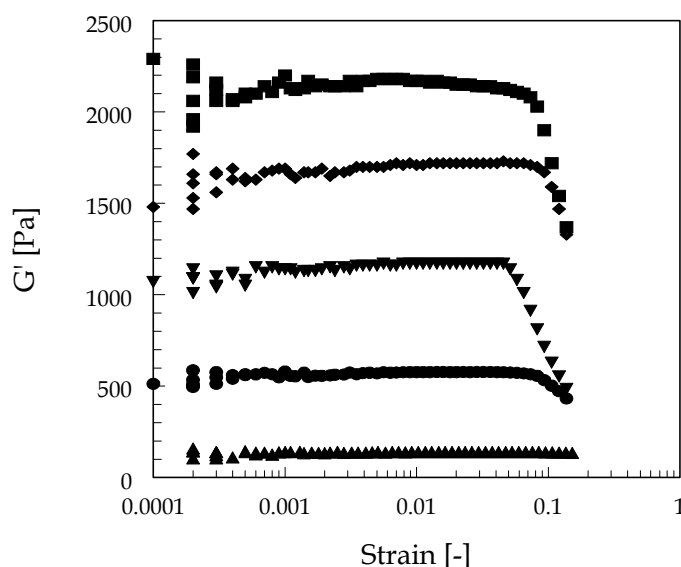
Figure 4.5 G' versus strain for various ovalbumin concentrations, at pH 2, and 0.03 M ionic strength. 6.5% (▲); 7.1% (●); 7.5% (▼); 8% (◆); 8.5% (■).

$(G')^{1/t}$ versus c and extrapolates these plots to $(G')^{1/t} = 0$. This procedure makes use of the fact that independent of the value of t the curves must all intersect the concentration axis at the same value. When the assumed value for t is close to the actual value, the plot will be linear. If t is too small or too large the lines are curved. From the plots of $(G')^{1/t}$ versus c for various t we selected those t values that give an approximately straight line. From these plots an average value of c_p was determined. We plotted log G' versus log $(c - c_p)$, using the different values for c_p obtained from the estimated t values. For each of the values for c_p we determined the t value and averaged these values. Table 4.3 shows the average values for c_p and t and the standard deviation of these values. A decreasing c_p with increasing ionic strength was observed. The value for t was about 2 for all ionic strength conditions, indicating isotropic force percolation and a homogeneous network.[23]

Table 4.3 Values for c_p and t for various ionic strengths, for ovalbumin at pH 2.

Ionic strength [M]	c_p [% (w/w)]	t [-]
0.010	7.9 ± 0.04	1.9 ± 0.24
0.015	7.3 ± 0.06	2.1 ± 0.19
0.020	6.9 ± 0.17	1.7 ± 0.17
0.025	6.2 ± 0.08	2.1 ± 0.22
0.030	5.8 ± 0.11	2.0 ± 0.18
0.035	4.8 ± 0.11	1.9 ± 0.16

4.3.3 Effect of ionic strength on the percolation concentration

TEM micrographs (Figure 4.3) showed that the fibrils formed for ovalbumin at pH 2 had a contour length, which was in the same order of magnitude for all ionic strengths. To eliminate the effect of conversion on the percolation concentration, we performed experiments on ovalbumin at 80 °C. The denaturation temperature of ovalbumin at pH 2 was 55 °C (determined with differential scanning calorimetry, unpublished result). We may safely assume that at 80 °C all monomers were converted into fibrils, since this temperature is far above the denaturation temperature. Combining these facts, approximately the same amount of ovalbumin fibrils of approximately equal length was formed for all ionic strengths. Based on these results, we can explain the decreasing percolation concentration with increasing ionic strength in terms of electrostatic interactions between the fibrils. The same trend was found for β-lactoglobulin and bovine serum albumin at pH 2.[24,28] For these proteins, an adjusted random contact model for charged semiflexible fibrils was used to explain the decreasing percolation concentration with increasing ionic strength. We also used this model to estimate a persistence length for these proteins.[24,28] The TEM micrographs for ovalbumin showed the presence of semiflexible fibrils, which implies that we may use the same model for ovalbumin.

According to the adjusted random contact model for semiflexible charged fibrils:[24]

$$\phi_{p,m} = \alpha(D_{eff}/P) \qquad \text{for } (P/D_{eff}) \gg 1 \qquad (4.1)$$

where $\phi_{p,m}$ is the critical percolation mass fraction (= $c_p/100$), α the average number of contacts per rod, assumed to be of order 1 at the percolation concentration[30], D_{eff} an effective diameter[31], and P the persistence length of the fibrils. Figure 4.6 shows the linear dependence of $\phi_{p,m}$ on D_{eff}. The vertical dashed line gives the theoretical limit of Eq. 4.1. Using that $\alpha \sim O(1)$, results in a persistence length of 296 ± 74 nm.
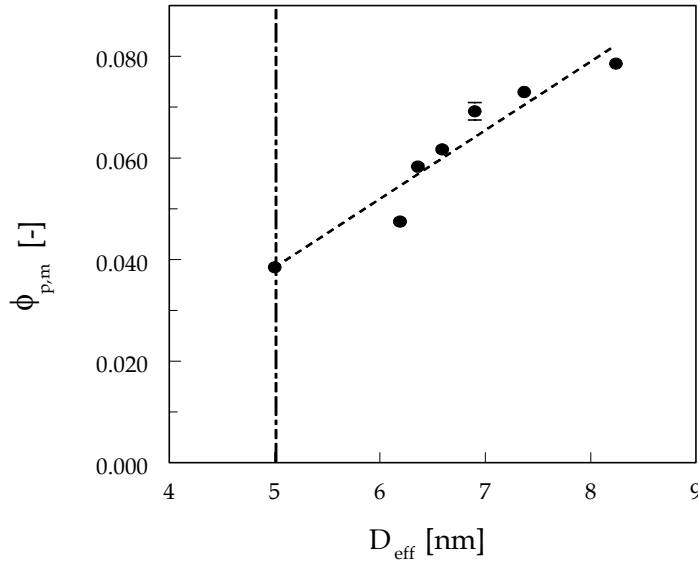
Figure 4.6 $\phi_{p,m}$ as a function of D_{eff} for ovalbumin at pH 2.

This value is in the same order of magnitude as the contour length determined with TEM micrographs (200 ± 54 nm), which indicates that the ovalbumin fibrils are indeed semiflexible. This adjusted random contact model explains the decreasing percolation concentration with increasing ionic strength for ovalbumin gels. The current established validity of the model for ovalbumin (in addition to that for β-lg and BSA) enlarges the regime of validity of the adjusted random contact model.

4.4 Conclusion

The effect of ovalbumin concentration on the contour length was investigated using TEM. An increasing contour length with increasing ovalbumin concentration was observed. Investigation of the effect of ionic strength on the contour length showed that for all measured conditions (0.01 – 0.035 M) fibrils of approximately equal length were formed. Dilution of heated ovalbumin samples showed that the

fibrils did not fall apart up to 24 h after dilution. This result indicates that the aggregation process is irreversible. This may be explained by the formation of intermolecular β-sheets.

Using the results of rheological measurements, we determined the critical percolation concentration for various ionic strengths. A decreasing c_p with increasing ionic strength was found. We can explain this result in terms of electrostatic interactions between the fibrils. An adjusted random contact model for semiflexible charged fibrils was used to explain this result quantitatively, extending the validity of this model to fibril networks of β-lg, BSA and, currently, ovalbumin.

Acknowledgements

References

1. Stein, P.E.; Leslie, A.G.W.; Finch, J.T.; Carrell, R.W. *J. Mol. Biol.* **1991**, *221*, 941-959.

2. Nemoto, N.; Koike, A.; Osaki, K.; Koseki, T.; Doi, E. *Biopolymers* **1993,** *33*, 551-559.

3. Doi, E.; Kitabatake, N. In *Food Proteins and their Applications*, Damodaran, S.; Paraf, A. Eds.) **1997**, Marcel Dekker: New York, 325-340.

4. Mine, Y. *J. Agric. Food Chem.* **1996**, *44*, 2086-2090.

5. Hagolle, N.; Relkin, P.; Dalgleish, D.G.; Launay, B. *Food Hydrocolloids* **1997**, *11*, 311-317.

6. Matsumoto, T.; Chiba, J.; Inoue, H. *Colloid Polym. Sci.* **1992**, *270*, 687-693.

7. Matsumoto, T.; Inoue, H. *J. Colloid Interf. Sci.* **1993**, *160*, 105-109.

8. Hu, H.Y.; Du, H.N.J. *Prot. Chem.* **2000**, *19*, 177-183.

9. Koseki, T.; Kitabatake, N.; Doi, E. *J. Biochem.* **1988**, *103*, 425-430.

10. Arntfield, S.D.; Murray, E.D.; Ismond, M.A.H. *J. Food Sci.* **1989**, *54*, 1624-1631.

11. Kleef van, F.S.M. *Biopolymers* **1986**, *25*, 31-59.

12. Hatta, H.; Kitabatake, N.; Doi, E. *Agric. Biol. Chem.* **1986**, *50*, 2083-2089.

13. Koseki, T.; Kitabatake, N.; Doi, E. *Food Hydrocolloids* **1989**, *3*, 123-134.

14. Arntfield, S.D.; Murray, E.D.; Ismond, M.A.H. *J. Texture Studies* **1990**, *21*, 295-322.

15.   Egelandsdal, B. *J. Food Sci.* **1980**, *45*, 570-573.

16.   Doi, E.; Kitabatake, N. *Food Hydrocolloids* **1989**, *3*, 327-337.

17.   Kitabatake, N.; Kinekawa, Y.I. *Food Chem.* **1995**, *54*, 201-203.

18.   Nakamura, R.; Sugiyama, H.; Sato, Y. *Agric. Biol. Chem.* **1978**, *42*, 819-824.

19.   Sugiyama, M.; Nakamura, A.; Hiramatsu, N.; Annaka, M.; Kuwajima, S.; Hara, K. *Biomacromolecules* **2001**, *2*, 1071-1073.

20.   Weijers, M.; Sagis, L.M.C.; Veerman, C.; Sperber, B.; Linden van der, E. *Food Hydrocolloids* **2002**, *16*, 269-276.

21.   Doi, E.; Koseki, T.; Kitabatake, N. *J. Am. Oil Chem.* **1987**, *64*, 1697-1703.

22.   Heertje, I.; Kleef van, F.S.M. *Food Microstructure* **1986**, *5*, 91-98.

23.   Linden van der, E.; Sagis, L.M.C. *Langmuir* **2001**, *17*, 5821-5824.

24.   Veerman, C.; Ruis, H.; Sagis, L.M.C.; Linden van der, E. *Biomacromolecules*, **2002**, *3*, 869-873.

25.   Mihara, H.; Takahashi, Y. *Curr. Opin. Struct. Biol.* **1997**, *7*, 501-508.

26.   Painter, P.C.; Koenig, J.L. *Biopolymers* **1976**, *15*, 2155-2166.

27.   Booth, D.R.; Sunde, M.; Bellotti, V.; Robinson, C.V.; Hutchinsion, W.L.; Fraser, P.E.; Hawkins, P.N.; Dobson, C.M.; Radford, S.E.; Blake, C.C.F.; Pepys, M.B. *Nature* **1997**, *385*, 787-793.

28.   Veerman, C.; Sagis, L.M.C.; Heck, J.; Linden van der, E. *Int. J. Biol. Macromolecules* **2003**, *31*, 139-146.

29.   Lin, V.J.C.; Koenig, J.L. *Biopolymers* **1976**, *15*, 203-218.

30.   Philipse, A.P. *Langmuir* **1996**, *12*, 1127-1133.

31.   Stroobants, A.; Lekkerkerker, H.N.W.; Odijk, T. *Macromolecules* **1986**, *19*, 2232-2238.

5

Mesoscopic Properties of Semiflexible Amyloid Fibrils

Abstract

We have determined the contour length, persistence length, bending rigidity, and critical percolation concentration for semiflexible amyloid fibrils formed from the globular proteins β-lactoglobulin, bovine serum albumin, and ovalbumin. The persistence length was estimated using an adjusted random contact model for highly charged semiflexible chains. We have found contour lengths in the range of 50 nm to 10 μm, and persistence lengths in the range of 16 nm to 1.6 μm. This wide range of contour and persistence lengths, and the ease of preparation of these amyloid fibrils, make them ideal model systems for the study of semiflexible polymers.

5.1 Introduction

The ability to form amyloid fibrils appears to be a generic property of proteins. In vivo amyloid formation is usually associated with diseases such as Creutzfeld-Jacob's disease, or bovine spongiform encephalopathy (BSE).[1] There are however many examples of fibril formation not linked to diseases. Examples are the formation of actin and tubulin fibrils, which play a role in the properties of the cytoskeleton,[2] or fibrin, an amyloid structure found in blood clots.

A lesser known fact is that many globular food proteins, commonly used as gelling agents, foaming agents or emulsifiers, also have the ability to form amyloid fibrils. Examples are the whey proteins β-lactoglobulin (β-lg),[4] α-lactalbumin,[5] and bovine serum albumin (BSA),[6] egg-white proteins such as lysozyme[7] and ovalbumin,[8] and the soy protein glycinin.[9] Amyloid formation generally occurs in a narrow pH, ionic strength, and protein concentration range, and is often induced by heating an aqueous solution of the proteins to a temperature close to the denaturation temperature of the protein.[4,6] The formation can also be induced by changing the quality of the solvent or by the addition of a surfactant. The self-assembly into fibrils is controlled by a balance between electrostatic and hydrophobic interactions between the protein molecules. It occurs only in conditions where the protein molecules are highly charged, that is, far from the iso-electric point of the protein, and at low ionic strength.

Although amyloid formation appears to be a generic property of these proteins, the mechanism of self-assembly varies, and appears to be specific for each protein. For BSA the assembly is reversible.[6] There is a critical concentration for self-assembly, and when a solution of fibrils is diluted to a concentration below this critical concentration, the amyloid fibers disassemble. The bond between the monomers is apparently of a purely physical nature. For β-lg and ovalbumin the amyloid fibrils are stable against dilution, changes of pH and ionic strength.[4] Assembly is irreversible and the fibrils appear to be stabilized by a conformational change occurring after assembly. X-ray scattering showed that β-lg molecules retain almost all of their native structure upon assembly,[10] which indicates that the structure of these fibers differs substantially from the regular stacked twisted β-sheet structures found in Alzheimer's, Huntington's and other diseases.

The mesoscopic properties of the fibrils show significant variations. Contour lengths may vary from 50 nm (ovalbumin) up to 10 µm (β-lg). Persistence lengths can vary from 16 nm (BSA) to about 1.6 µm (β-lg).[4,6] This wide range of contour and persistence lengths makes these amyloid fibrils ideal for the study of semiflexible polymers. Many of the studies on semiflexible chains have focused on actin as a model system. This protein is notoriously difficult to purify. The globular food proteins we will discuss here are commercially available in large quantities, and generally require only a single simple dialysis step to purify them.

In this paper, we will discuss the mesoscopic properties of fibrils formed from three globular food proteins: β-lg, BSA, and ovalbumin. For these systems we have determined contour lengths, persistence lengths, bending rigidities, and critical percolation concentrations. We will also briefly discuss the phase behaviour of these systems.

5.2 Contour length of the fibrils

The amyloid fibrils were prepared by heating aqueous solutions of the proteins at 60 °C (BSA) or 80 °C (β-lg and ovalbumin).[4,6,8] Heating times varied from 1 to 10 h. The pH of all solutions was equal to 2. Ionic strength was varied between 10 and 300 mM, and protein concentration was varied from 2 to 8% (w/w). The length of the fibrils was determined using transmission electron microscopy (TEM). Figure 5.1A – C shows the fibrils for β-lg, BSA, and ovalbumin.

Table 5.1 Contour lengths, L_c, of β-lg, BSA, and ovalbumin fibrils at pH 2, and near the percolation concentration, c_p, as a function of ionic strength, I, and heating time, HT.

	I [mM]	HT [h]	L_c [nm]
β-lg	10 – 80	10	4500 ± 2500
BSA	200 – 300	1	118 ± 47
BSA	200 – 300	10	255 ± 76
Ovalbumin[a]	10 – 35	1	190 ± 70
Ovalbumin[b]	10	1	113 ± 46
Ovalbumin[c]	10	1	51 ± 14

a Determined near c_p.
b Determined at a protein concentration of 5% (w/w).
c Determined at a protein concentration of 2% (w/w).

Table 5.1 summarizes the values for the contour length, L_c, determined from these micrographs. We see that ionic strength has no measurable effect on L_c in the applied ionic strength regime. For BSA there is a definite effect of heating time on L_c. The contour length doubles when heating time is increased from 1 to 10 h. For ovalbumin we observe a substantial increase in L_c with increasing protein concentration. For this system, the contour length can easily be controlled by simply adjusting the protein concentration. The polydispersity of the fibrils is significant, but this is also found in other model systems such as actin or tubulin.
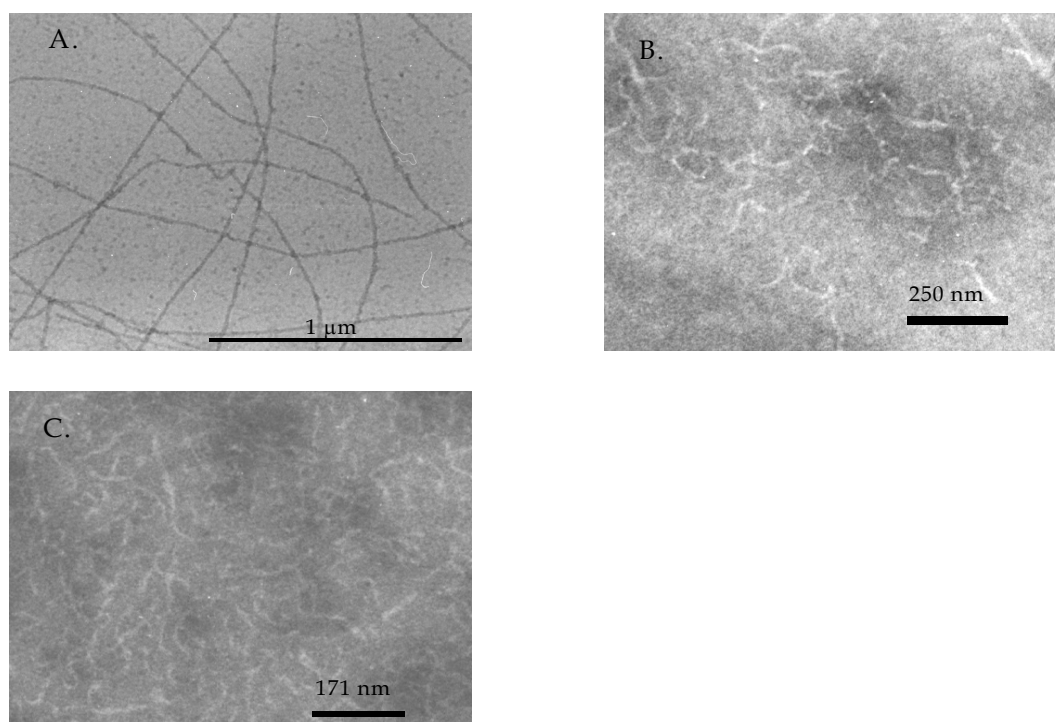
Figure 5.1 TEM micrographs of (A.) β-lg, (B.) BSA, and (C.) ovalbumin at pH 2.

5.3 Critical percolation concentration

The critical percolation concentration, c_p was determined by measuring the storage modulus, G', as a function of protein concentration. Measurements were performed using a Bohlin VOR strain-controlled rheometer, at a frequency of 1 Hz, and deformations ranging from 0.0002 to 0.2. Samples were heated in the rheometer with heating times varying from 1 to 10 h. Subsequently the samples were cooled to 25 °C, and kept at that temperature for 2 h, before measurements were started. For all concentrations we determined G' in the linear regime. The data were fitted using

a scaling relation $G' \sim (c - c_p)^t$, where c is the protein concentration, and t is a universal exponent, depending on the Hamiltonian of the system. Using a fitting procedure,[11] we determined c_p and t as a function of ionic strength. The results are summarized in Table 5.2. For almost all samples t is about 2, which indicates isotropic force percolation, and a homogeneous network. The only exceptions are the BSA samples with ionic strength of $\leq$ 235 mM and heating time of 1 h. Here t is about 4, which indicates central force percolation.[11] At pH 2, the β-lg fibrils are not cross-linked. When a gel is diluted to a concentration below c_p, the gel first shows a significant amount of swelling. It eventually dissolves completely, forming a solution of fibrils. At pH 7, the fibrils can be cross-linked using Ca^{2+}-ions, which form salt bridges between the fibrils. This attractive interaction significantly lowers the c_p of the fibrils. For β-lg we have found c_p values as low as 0.07% (w/w).[12]

Table 5.2 Critical percolation concentration, c_p, and scaling exponent t of β-lg, BSA, and ovalbumin fibrils at pH 2, as a function of ionic strength, I, and heating time, HT.

	I [mM]	HT [h]	c_p [% (w/w)]	t [-]
β-lg	10	10	2.3 ± 0.1	2.1 ± 0.2
β-lg	70	10	1.2 ± 0.1	1.9 ± 0.3
BSA	200	1	7.6 ± 0.1	4.3 ± 0.1
BSA	235	1	5.2 ± 0.1	4.1 ± 0.1
BSA	200	10	6.7 ± 0.1	1.9 ± 0.1
BSA	300	10	1.1 ± 0.3	2.0 ± 0.2
Ovalbumin	10	1	7.9 ± 0.1	1.9 ± 0.2
Ovalbumin	35	1	4.8 ± 0.1	1.9 ± 0.2

For all proteins we have found a decreasing c_p with increasing ionic strength, or decreasing Debye length κ^{-1}. This decrease can be explained quantitatively as follows. We assume that these fibrillar systems can be described with a 'mechanical equation of state' given by[13]

$$\phi_{p,m} = 2\langle\alpha\rangle V_0 / V_{ex,rod} \tag{5.1}$$

where, $\phi_{p,m}$ is the percolation mass fraction of the fibrils, α the average number of contacts per rod, assumed to be of order 1 at the percolation concentration, V_0 the

volume of the fibril, which is given by $(L_c/L_p)\frac{1}{4}\pi L_p D_{eff}^2$, and $V_{ex, rod}$ the excluded volume of charged semiflexible fibrils which is given by $(L_c/L_p)\frac{1}{2}\pi L_p^2 D_{eff}$, where L_p is the persistence length of the fibrils, and D_{eff} an effective diameter of the fibrils defined by[16]

$$D_{eff} = D_0 + \frac{1}{2}\kappa^{-1}\left(\ln A' + C_E + \ln 2 - \frac{1}{2}\right) \tag{5.2}$$

$$A' \equiv 2\pi v_{eff}^2 \kappa^{-1} Q \exp(-\kappa D_0) \tag{5.3}$$

Here D_0 is the diameter of the rods, $C_E = 0.577215\ldots$ is Euler's constant, v_{eff} is the linear charge density of the fibrils, and

$$Q = e^2/(4\pi\varepsilon_0\varepsilon_r k_B T) \tag{5.4}$$

the Bjerrum length, where e is the elementary charge, ε the dielectric permittivity, k_B the Boltzmann constant, and T the temperature. The Debye length is calculated from

$$\kappa^2 = 8\pi n e^2/\varepsilon_0\varepsilon_r k_B T \tag{5.5}$$

Using Eq. (5.1), we find for the percolation mass fraction of a charged semiflexible system:[4]

$$\phi_{p,m} = \alpha(D_{eff}/L_p) \qquad \text{for } (L_p/D_{eff}) \gg 1 \tag{5.6}$$

The plots of $\phi_{p,m}$ versus D_{eff}, for all three proteins are given in Figure 5.2. For all three proteins, $\phi_{p,m}$ depends linearly on D_{eff}, as predicted by Eq. (5.6), and the decrease of the percolation concentration with increasing ionic strength can be attributed solely to a decrease in the electrostatic repulsion between the fibrils.

If we assume that α is of order 1 in Eq. (5.6), we can use this equation to obtain an estimate for the persistence length L_p of the fibrils. We find that $L_p = 1.6 \pm 0.4$ μm for β-lg, 16 ± 4 nm for BSA, and 300 ± 75 nm for ovalbumin (Table 5.3).
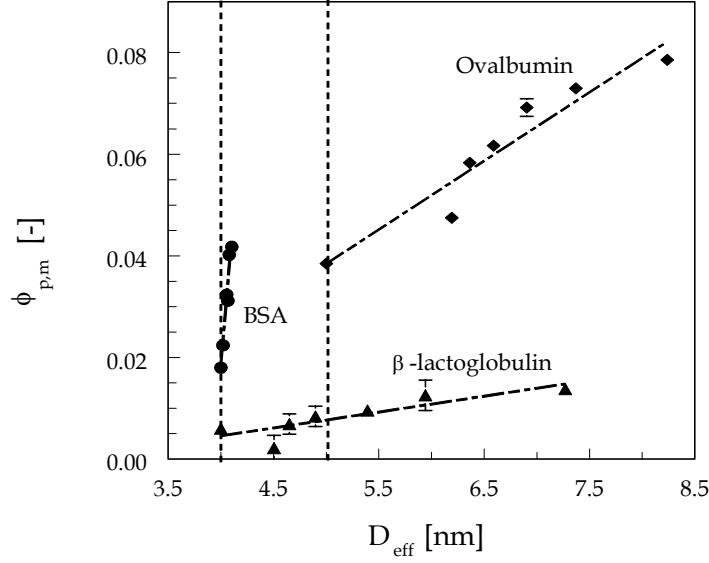
Figure 5.2 $\phi_{p,m}$ versus D_{eff} for β-lg, BSA, and ovalbumin, at pH 2.

In addition, we see that the persistence length is independent of ionic strength. This can be explained by calculating the electrostatic contribution to the persistence length,

$$L_{p,e} = \left(4Q\kappa^2\right)^{-1} \tag{5.7}$$

For all conditions tested here, $L_{p,e}$ is in the range of 0.01 to about 0.25 nm. Therefore $L_{p,e} << L_p$, and $L_p \approx L_{p,b}$ where $L_{p,b}$ is the bare bone persistence length of the fibril. In Table 5.3 we have also listed the values for L_c/L_p for all proteins. We see that these proteins cover a wide range of values for this parameter, from 0.6 up to 16.0. Table 5.3 also lists the values for the bending rigidity of the fibrils $\kappa_b = k_B T L_p$, and the number of monomers per fibril $N_m = L_c/D_0$.

Table 5.3 L_p, L_c/L_p, κ_b, and N_m for β-lg, BSA, and ovalbumin fibrils at pH 2.

	L_p [nm]	L_c/L_p [-]	κ_b [10^{-28} Nm²] [c]	N_m [-]
β-lg	1600 ± 400	2.8	65.9	1125
BSA[a]	16 ± 4	7.4	0.66	29.5[d]
BSA[b]	16 ± 4	16.0	0.66	63.8[d]
Ovalbumin	300 ± 75	0.6	12.3	38[e]

a Heating time: 1 h.
b Heating time: 10 h.
c Calculated at room temperature.
d BSA is an ellipsoidal molecule with principal axes 4 x 4 x 14 nm; here we have chosen
   D_0 = 4 nm.
e Ovalbumin is an ellipsoidal molecule with principal axes 5 x 5 x 7 nm; here we have
   chosen D_0 = 5 nm.

5.4 Phase behaviour

Solutions containing amyloid fibrils can have rich phase behaviour. BSA and ovalbumin form isotropic solutions at pH 2, up to the percolation concentration, and form transparent homogeneous isotropic gels above c_p. The phase diagram of β-lg is more complicated (Figure 5.3). At protein concentrations below approximately 0.5% (w/w), β-lg forms isotropic solutions. Above this concentration a two-phase system is formed, consisting of nematic liquid crystalline droplets, suspended in an isotropic solution. At concentrations above c_p a two-phase gel is observed, consisting of nematic droplets dispersed in an isotropic gel matrix (Figure 5.4). As the protein concentration is increased, the number and size of the droplets increase. At about 9.5% (w/w) a transition occurs from this two-phase system to what is most likely a single-phase nematic.

Onsager theory applied to charged semiflexible fibrils predicts an isotropic-to-nematic phase transition at a critical volume fraction

$$\phi_c = \mu \, (D_{\text{eff}}/L_p) \tag{5.8}$$

where μ is a constant.[15]
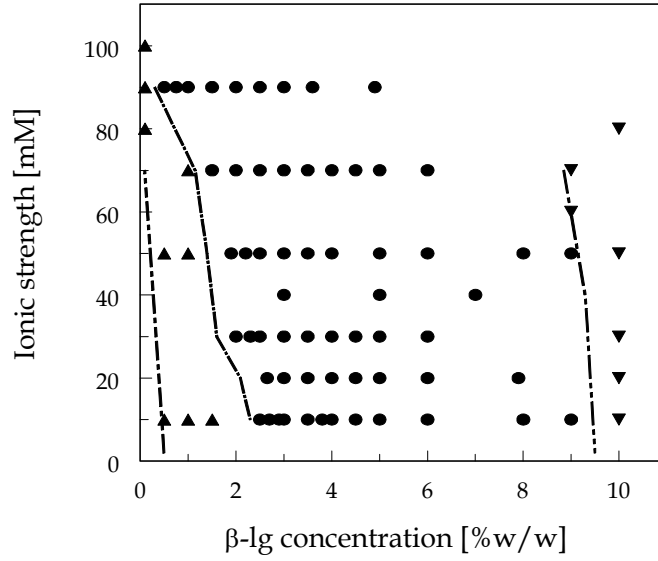
Figure 5.3 Phase diagram for β-lg at pH 2, as a function of β-lg concentration and ionic strength. (▲) denotes two-phase systems with nematic droplets dispersed in an isotropic solution. (●) denotes two-phase gels, and (▼) are most likely single-phase nematics.

For β-lg at pH 2 and 10 mM ionic strength we find that a transition from isotropic to a bi-phasic region takes place at ϕ_c = 0.025, for μ = 5.2,[15] with L_p taken from Table 5.3, and D_{eff} calculated from Eq. (5.2). This rough estimate is of the same order of magnitude as the experimental value we observed. The bi-phasic region is much wider than predicted by Onsager theory. This theory predicts a transition from a two-phase system to a single-phase nematic at μ = 5.5,[15] which corresponds to ϕ_c = 0.027. The widening of the bi-phasic region may be the result of the polydispersity of the fibrils. The transition to a single phase nematic may also be shifted to higher concentrations by gelation of the system, which occurs at concentrations just above the transition from the isotropic to the bi-phasic state. The persistence lengths of BSA and ovalbumin are much smaller than the persistence length of β-lg, which explains why we did not observe a liquid crystalline phase for amyloid fibrils of these proteins.
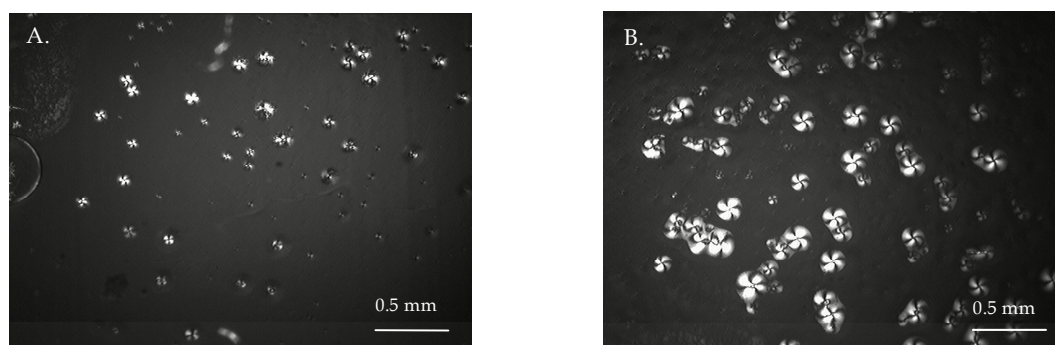
Figure 5.4 Nematic droplets dispersed in an isotropic gel matrix (A.) 4% (w/w), (B.) 8% (w/w) β-lg, at pH 2, and 0.01 M ionic strength.

5.5 Conclusion

In conclusion, we have determined the contour length, persistence length, bending rigidity, and critical percolation concentration of amyloid fibrils produced from three common food proteins: β-lactoglobulin, BSA, and ovalbumin. We have shown that these three proteins cover a wide range of contour lengths and persistence lengths. This wide range of length scales, and the ease of preparation of these amyloid fibrils, make them ideal for the study of properties of semiflexible polymers.

References

1.   Ellis, R.J.; Pinheiro, T.J.T. *Nature* **2002**, *416*, 483-484.

2.   Janmey, P.A.; Shah, J.V.; Jansen, K.P.; Schliwa, M. *Subcell. Biochem.* **1998**, *31*, 381-397.

3.   Shah, J.V.; Janmey, P.J. *Rheol. Acta* **1997**, *36*, 262-268.

4.   Veerman, C.; Ruis, H.; Sagis, L.M.C.; Linden van der, E. *Biomacromolecules* **2002**, *3*, 869-873.

5.   Goers, J.; Permyakov, S.E.; Permyakov, E.A.; Uversky, V.N.; Fink, A.L. *Biochem.* **2002**, *41*, 12546-12551.

6.   Veerman, C.; Sagis, L.M.C.; Heck, J; Linden van der, E. *Int. J. Biol. Macromolecules* **2003**, *31*, 139-146.

7.   Chamberlain, A.K.; MacPhee, C.E.; Zurdo, J.; Morozova-Roche, L.A.; Hill, H.A.O.; Dobson, C.M.; Davis, J.J. *Biophys. J.* **2000**, *79*, 3282-3293.

8.   Veerman, C.; Schiffart de, G.; Sagis, L.M.C.; Linden van der, E. *Int. J. Biol. Macromolecules* **2003**, *33*, 121-127.

9.   Hermanson, A.-M. *J. Sci. Food Agric.* **1985**, *36*, 822-832.

10.   Aymard, P.; Nicolai, T.; Durand, D.; Clark, A.H. *Macromolecules* **1999**, *32*, 2542-2552.

11.   Linden van der, E.; Sagis, L.M.C. *Langmuir* **2001**, *17*, 5821-5824.

12.   Veerman, C.; Baptist, H.; Sagis, L.M.C.; Linden van der, E. *J. Agric. Food Chem.* **2003**, *51*, 3880-3885.

13.   Philipse, A.P. *Langmuir* **1996**, *12,* 1127-1133.

14.   Onsager, L. *Ann. N.Y. Acad. Sci.* **1949**, *51*, 627-659.

15.   Vroege, G.J.; Lekkerkerker, H.N.W. *Rep. Prog. Phys.* **1992**, *55*, 1241-1309.

16.   Stroobants, A.; Lekkerkerker, H.N.W.; Odijk, T. *Macromolecules* **1986**, *19*, 2232-2238.

6

A New Multistep Ca^{2+}-Induced Cold Gelation Process for β-Lactoglobulin

Abstract

The objective of this study was to obtain β-lactoglobulin (β-lg) gels at very low protein concentrations using a new multistep Ca^{2+}-induced cold gelation process. In the conventional cold gelation process, salt free β-lg solutions were heated at neutral pH, cooled, and cross-linked by adding salts. In our new process, first long linear β-lg fibrils were formed at pH 2. Solutions of these fibrils were cooled, and subsequently the pH was adjusted to 7 or 8. Transmission electron microscopy studies showed that the long linear fibrils formed at pH 2 were stable when the pH was adjusted to 7 or 8. In the final step the fibrils were cross-linked using CaCl$_2$. Using rheological measurements, the critical percolation concentration was determined. In the new multistep cold gelation process, the critical percolation concentration was an order of magnitude lower than in the conventional cold gelation method.

6.1 Introduction

Many globular food proteins have the ability to form a gel.[1] The gel properties depend on protein concentration, ionic strength, pH, and heating procedure.[2,3] One distinguishes heat-induced gelation and cold-set gelation. The heat-induced gelation consists of heating the protein solution and subsequent cooling, during which gelation takes place.[4-10] The cold-set gelation consists of heating the protein solution, and subsequent cooling, resulting in a *solution*, from which a gel can be obtained after addition of salt.[11-14] Cold-set gelation can lead to new uses for whey proteins, in a variety of foods.[15]

To obtain cold-set gels, it is necessary to prepare a heat-denatured *solution*, with a protein concentration below the critical gelation concentration, at a temperature above the denaturation temperature. The *gelation* is induced at low temperatures by the addition of mono- or polyvalent cations.[1,3,13,16,17] In the cold-set gelation method, as is applied in many papers to salt free whey protein isolate or β-lactoglobulin (β-lg), the protein solution was heated at pH 7, cooled, and cross-linked by the addition of NaCl or $CaCl_2$.[1,3,13,16,17] In the rest of the paper, we will refer to this type of cold-set gelation as "conventional cold gelation". The cold-set gels formed using this conventional cold gelation method showed a fine-stranded structure, better water-holding capacity, and higher gel strength than gels formed by heat-induced gelation.[15,17,18]

Cold-set gels with different properties, like transparency, shear stress and strain at fracture, and water-holding capacities, were formed by varying the preheating time and/or temperature, and the amount and type of salt.[3,12,15,17-21] Monovalent and divalent salt ions both screen electrostatic interactions between charged protein molecules. Divalent cations, such as Ca^{2+}, can in addition form intermolecular ion bridges between negatively charged or carboxylic groups of β-lg.[3,12,22] This ability, combined with a larger screening effect, enables divalent cations to induce gelation at much lower salt concentrations than monovalent cations .[12,13]

Using $CaCl_2$ as a gelling agent, there is a difference in the extent of aggregation, at varying $CaCl_2$ levels, which can be due to differences in the rate of aggregation.[13] For concentrations < 0.03 M $CaCl_2$, the screening effect dominates.[14] Screening will lead to an increase in aggregation rate. At higher $CaCl_2$ concentrations, the formation of salt bridges takes place. To form a salt bridge,

molecules must be properly aligned. This effect can lead to a decrease in the aggregation rate.[13] The difference in gelation mechanism, caused by different $CaCl_2$ concentrations, could possibly be responsible for the difference in the network building process at the microscopic level.[14]

The objective of this study was to obtain β-lg gels at a very low protein concentration using a new multistep cold gelation procedure. In the new procedure long linear fibrils were formed at pH 2 and low ionic strength, after heating at 80 °C for 10 h.[23,25] Solutions of these fibrils were cooled and subsequently the pH was adjusted to 7 or 8. Transmission electron microscopy (TEM) micrographs showed that these long linear fibrils were stable against changes of pH. In the final step the fibrils were cross-linked using $CaCl_2$. Using rheological measurements, the critical percolation concentration was determined using the method described by van der Linden and Sagis.[26] The new multistep cold gelation procedure is compared with conventional cold gelation and heat-induced gelation, as defined above.

6.2 Materials and Methods

6.2.1 Sample preparation

β-lg was obtained from Sigma (L-0130) and was a mixture of the genetic variants A and B. The protein was dissolved in bidistilled water, which was adjusted to pH 2, using a 6 M HCl solution. The protein solution was subsequently adjusted to pH 2 by the addition of a 6 M HCl solution. To remove traces of calcium ions from the β-lg, and to obtain a protein solution with the same pH and ionic strength as the solvent, the protein was diluted repeatedly with HCl solvent and filtered through a 3K filter in an Omegacell™ membrane cell (Filtron; membrane consisting of polyethersulfone), at 4 °C, and a maximum pressure of 3 bar. The procedure was stopped when the pH and conductivity of the eluted solution and the solvent were the same. The β-lg solution was centrifuged at 22600g for 30 min. To remove any traces of undissolved protein, the β-lg supernatant was filtered through a protein filter (FP 030/2, 0.45 μm, Schleicher & Schuell). A UV spectrophotometer was used to determine the β-lg concentration at a wavelength of 278 nm. A molar extinction coefficient of 16.8 mM⁻¹cm⁻¹ was used. The obtained stock protein solution (10% ± 2% (w/w)) at pH 2 was used for all measurements. We checked the pH during the conduction of our experiments.

6.2.2 Transmission electron microscopy (TEM)

Five different β-lg samples were prepared for TEM experiments. A 2% (w/w) β-lg sample at pH 2 was heated at 80 °C for 10 h in a water bath, and cooled on ice, i.e. to 0 °C (I). After the sample was cooled, the pH was adjusted to 7 (II) or 8 (III) with 0.1 and 1 M NaOH. To compare the new multistep cold gelation method with the conventional cold gelation method, 3% β-lg samples at pH 7 (IV) or pH 8 (V) were heated at 80 °C for 30 min in a water bath, and cooled on ice, i.e. to 0 °C.

All samples were diluted to 0.04% β-lg. The TEM samples were prepared by negative staining. A drop of the diluted solution was deposited onto a carbon support film on a copper grid. The excess was removed after 30 s using a piece of filter paper. A droplet of 2% uranyl acetate, pH 3.8, was added for 15 s, any excess was removed as before. Electron micrographs were made using a Philips CM 12 transmission electron microscope operating at 80 kV.

6.2.3 Conversion experiments

A series of test tubes with 3% (w/w) β-lg at pH 7 or 8, without added salt, were heated at 80 °C for 30 min. The pH was adjusted from pH 2 (stock protein solution) to pH 7 or 8, by the addition of 0.1 and 1 M NaOH solution before heating. After various time periods between 0 and 30 min, tubes were taken out of the water bath and immediately cooled in ice water.

To determine the concentration of non-aggregated β-lg, the heated samples were diluted in a 0.1 M citric acid/ phosphate buffer at pH 4.8. After the aggregates precipitated overnight, the supernatant was centrifuged for 10 min at $20000g$. The non-aggregated β-lg concentration present in the supernatant was determined by a UV spectrophotometer at a wavelength of 278 nm. c_t/c_0 was determined by dividing the concentration of non-aggregated β-lg at a certain heating time (c_t) by the concentration of β-lg before heating (c_0).

6.2.4 Rheological measurements

A strain-controlled rheometer (VOR, Bohlin) with a concentric cylinder geometry (C14: cup diameter, 15.4 mm; bob diameter, 14 mm; bob height, 21 mm; depth, 6.9 mm; cone angle, 15°) was used to determine the storage modulus (G') as a function of strain (frequency, 1 Hz; temperature 25 °C; strain, 0.000206 – 0.206). A 2% β-lg sample at pH 2 was heated at 80 °C for 10 h in a water bath. After the

sample was cooled on ice, i.e. to 0 °C, the pH was adjusted to 7 or 8 with 0.1 and 1 M NaOH. Various CaCl₂ concentrations (0.005 – 0.1 M) were added very carefully on ice, and the solution was mixed well. To some samples, NaCl was added instead of CaCl₂ (0.03 or 0.15 M). After this procedure, the solution was poured into the rheometer. The rheometer was heated from 3 °C to 25 °C. After 3 h in rest, a strain sweep was performed.

To compare this new multistep cold gelation method with the conventional cold gelation method, 3% β-lg samples at pH 7 or 8 were heated at 80 °C for 30 min (this heating condition was chosen, because it was often used in papers on cold gelation).[1,13,17,19,21,27-29] After the samples were cooled on ice, i.e. to 0 °C, various CaCl₂ concentrations (0.01 or 0.05 M) were added very carefully on ice, and the solution was mixed well. After this procedure, the solution was poured in the rheometer. The rheometer was heated from 3 to 25 °C. After 3 h in rest, a strain sweep was performed.

6.3 Results and Discussion

6.3.1 Transmission electron microscopy (TEM)

TEM micrographs were made to obtain insight in the β-lg structures formed in the different steps of the cold gelation process. Figure 6.1A shows structures formed after heating 2% β-lg at pH 2, at 80 °C for 10 h, and subsequently cooled on ice to 0 °C. Long linear fibrils were formed with a contour length of about 2 – 7 µm. When the pH of this heated β-lg solution was adjusted to 7 (Figure 6.1B), or 8 (Figure 6.1C), long linear fibrils were still observed. The long linear fibrils formed at pH 2 were stable against changes of pH for at least a week.

To compare the β-lg structure formed, after it was heated, using the new multistep cold gelation method with the conventional cold gelation method, TEM micrographs were made of 3% β-lg, heated at pH 7 or 8, at 80 °C for 30 min, and subsequently cooled on ice to 0 °C (Figure 6.2A,B). The structures formed at pH 7 or 8 were more than a factor of 10 shorter as compared to the fibrils formed after heating at pH 2. For pH 8, short fibrillar-like structures were observed, whereas for pH 7 a sort of intermediate structure between fibrils and random aggregates was formed. Thus, the structures obtained using the new multistep cold gelation procedure were longer and stiffer than the conventional cold gelation procedure.
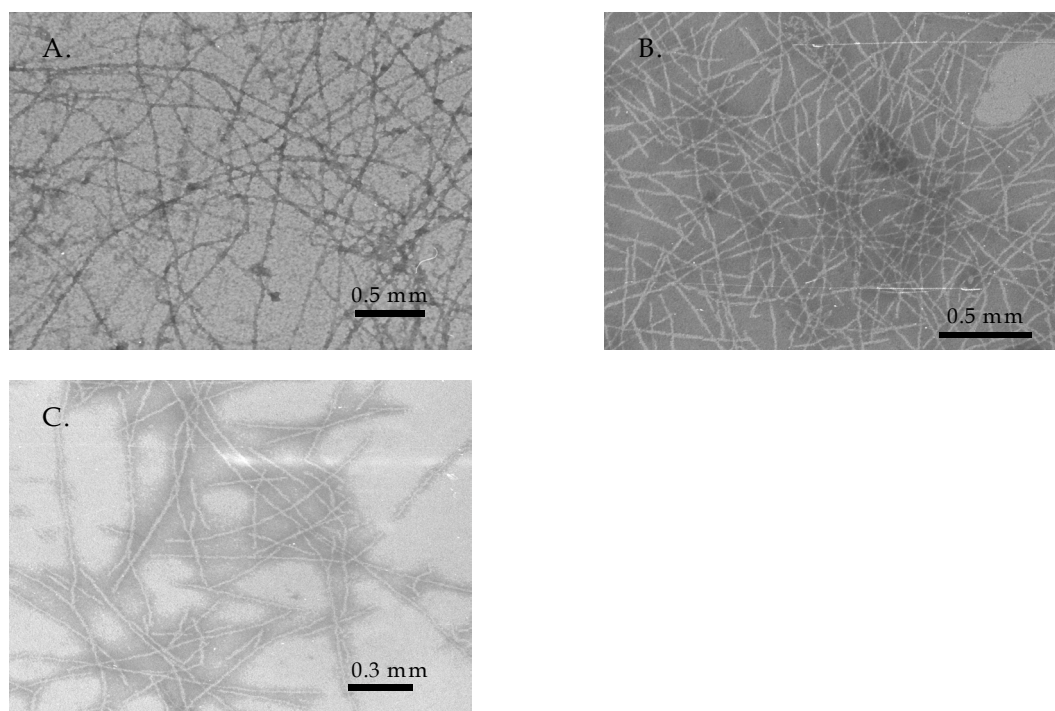
Figure 6.1 TEM micrographs of 2% β-lg, at pH 2, heated at 80 °C, for 10 h, and subsequently cooled on ice to 0 °C (A.). Afterward, the pH was adjusted to pH 7 (B.) or pH 8 (C.).
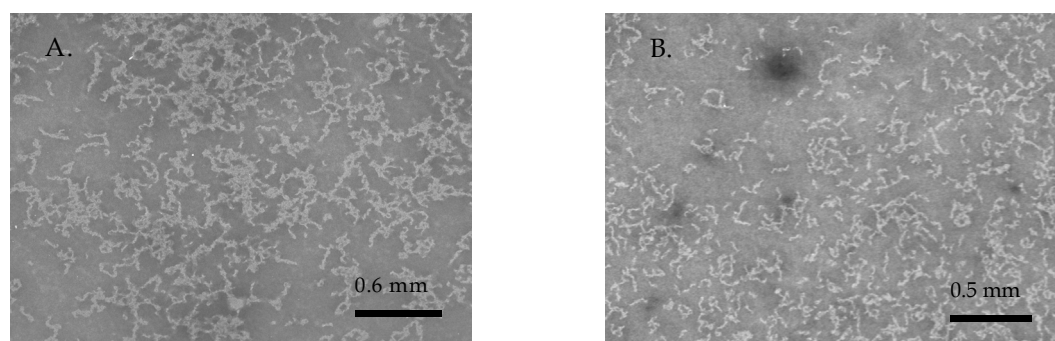
Figure 6.2 TEM micrographs of 2% β-lg at pH 7 (A.) or pH 8 (B.) heated at 80 °C for 30 min and subsequently cooled on ice to 0 °C.

6.3.2 Conversion experiments

The effect of conversion of the monomers into aggregates on the critical percolation concentration (determined in section 6.3.3) was investigated, using conversion experiments. The conversion for 3%, salt free, β-lg, at pH 7 or 8, heated at 80 °C during 30 min, was determined (Figure 6.3). For pH 7, 94% of the monomers was converted after 30 min, while for pH 8, 89% was converted.

Conversion experiments performed for β-lg at pH 2, showed that only 60% of the monomers was converted into fibrils, after heating at 80 °C for 10 h.[25]

An explanation for the difference in conversion between pH 2 and pH 7 or pH 8 can be the difference in denaturation temperature. At neutral pH the denaturation temperature for β-lg is 65 – 75 °C,[30-32] whereas the denaturation temperature for β-lg at pH 2 is about 80 °C (determined with differential scanning calorimetry, unpublished results). For the conversion experiments, all samples were heated at 80 °C. This temperature was above the denaturation temperature for β-lg at pH 7 and 8, resulting in a high conversion of the monomers into aggregates. For β-lg at pH 2, the heating temperature of 80 °C was around the denaturation temperature, resulting in a lower conversion of monomers, as compared to the conversion at pH 7 or 8.
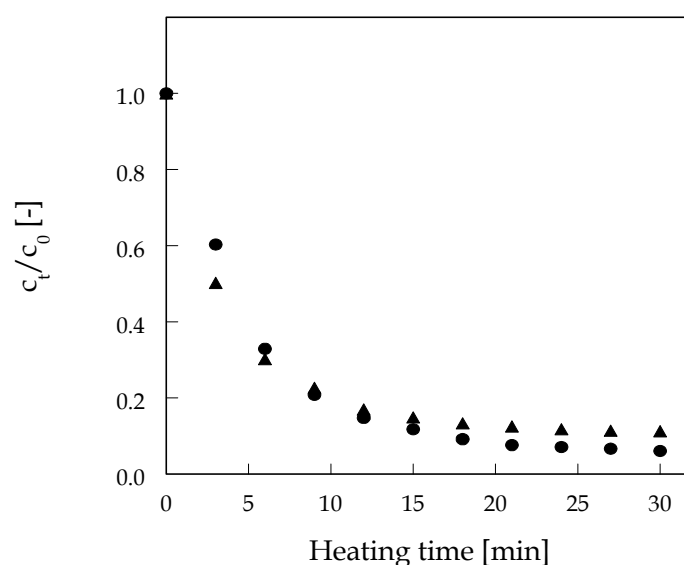
Figure 6.3 c_t/c_0 versus heating time for 3% β-lg, at pH 7 (●) or pH 8 (▲), heated at 80 °C, for 30 min, and subsequently cooled on ice to 0 °C.

6.3.3 Rheological measurements

Rheological measurements were performed for β-lg samples prepared according to the new multistep cold gelation process, and for samples prepared according to the conventional cold gelation method. Figure 6.4 shows the storage modulus, G', versus strain for 2% β-lg heated at pH 2, where after it was cooled, the pH was adjusted to pH 7, and 0.01 M $CaCl_2$ was added. We waited 3 h before

measurements were performed. We note that G' as a function of time, at low strain, after addition of $CaCl_2$, did not show a significant change after 2 h. The heated β-lg solution was diluted to various concentrations before $CaCl_2$ was added, resulting in the various concentration curves in Figure 6.4. From the linear regime of each curve (i.e. the regime where G' is independent of the strain), G' can be determined. Using G', obtained from the various concentration curves, the critical percolation concentration, c_p, and a scaling exponent, t, can be calculated. We used a scaling relation $G' \sim (c - c_p)^t$, where c is the concentration of monomers.[26] We calculated c_p and t, using the method described in van der Linden and Sagis.[26] This method is a graphical method that uses plots of $(G')^{1/t}$ versus c_p and extrapolates these plots to $(G')^{1/t} = 0$. This procedure makes use of the fact that independent of the value of t the curves must all intersect the concentration axis at the same value. When the assumed value for t is close to the actual value, the plot will be linear. If t is too small or too large, the lines are curved. From the plots of $(G')^{1/t}$ versus c_p for various t we selected those t values that give an approximately straight line. From these plots, an average value of c_p was determined. We plotted log G' versus log $(c-c_p)$, using the different values for c_p obtained from the estimated t values. For each of the values for c_p we determined the t value and averaged these values.

Figure 6.4 G' versus strain for various β-lg concentrations at pH 2, heated at 80 °C for 10 h and subsequently cool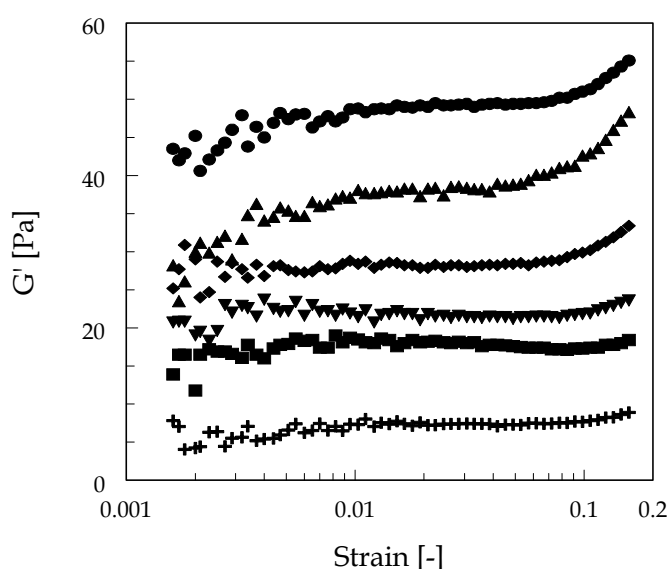ed on ice to 0 °C, after which the pH was adjusted to pH 7 and 0.01 M $CaCl_2$ was added. β-lg concentrations measured are 1% (**+**); 1.2% (■); 1.4% (▼); 1.7% (◆); 1.9% (▲); 2.2% (●).

Table 6.1 shows the calculated values for c_p, t and the value for c_p corrected for conversion. The calculated values for t were all about 2, indicating isotropic force percolation and a homogeneous network.[26]

Table 6.1 shows that the lowest value for c_p was found for a 2% β-lg solution heated at pH 2, where after it was cooled, the pH was adjusted to 7, and 0.01 M $CaCl_2$ was added. For this condition, there is an optimal interplay between the screening of electrostatic interactions between the fibrils, and the formation of intermolecular ion bridges between charged or carboxylic groups of β-lg by Ca^{2+}-ions. Using the new multistep cold gelation method, no gel was formed when $CaCl_2$ concentrations lower than 0.01 M were added. For $CaCl_2$ concentrations higher than 0.01 M, c_p increases with increasing ionic strength. This may be a result of clustering of the fibrils (bundle formation), caused by increased screening of the repulsive forces, and ion bridge formation.

Table 6.1 Calculated values for c_p, t and c_p corrected for conversion. All samples were heated at 80 °C.

Heating condition	Final pH	$CaCl_2$ [M]	c_p [%(w/w)]	Conversion [%]*	c_p corrected for conversion	t [-]
pH 2, 10 h	7	0.005	> 2	60	> 1.2	-
pH 2, 10 h	7	0.0075	> 2	60	> 1.2	-
pH 2, 10 h	7	0.01	0.12 ± 0.07	60	0.07 ± 0.04	2.0 ± 0.1
pH 2, 10 h	7	0.05	0.62 ± 0.06	60	0.37 ± 0.04	1.9 ± 0.2
pH 2, 10 h	7	0.1	0.67 ± 0.06	60	0.40 ± 0.04	1.9 ± 0.2
pH 2, 10 h	8	0.005	> 2	60	> 1.20	-
pH 2, 10 h	8	0.0075	> 2	60	> 1.20	-
pH 2, 10 h	8	0.01	0.44 ± 0.08	60	0.27 ± 0.05	1.8 ± 0.2
pH 2, 10 h	8	0.05	0.61 ± 0.06	60	0.37 ± 0.04	1.8 ± 0.2
pH 2, 10 h	8	0.1	0.89 ± 0.05	60	0.53 ± 0.03	1.9 ± 0.2
pH 7, 0.5 h	7	0.01	> 3	94	> 2.82	-
pH 7, 0.5 h	7	0.05	0.51 ± 0.07	94	0.48 ± 0.07	1.9 ± 0.2
pH 8, 0.5 h	8	0.01	> 3	89	> 2.67	-
pH 8, 0.5 h	8	0.05	0.60 ± 0.06	89	0.53 ± 0.05	2.0 ± 0.2

* The conversion of β-lg monomers into fibrils at pH 2 was determined in ref *25*. Conversion experiments were performed at pH 7 and pH 8; see section 6.3.2.

We investigated the relative importance of the screening of electrostatic interactions between the fibrils and the formation of ion bridges. Samples of 2% β-lg were heated at pH 2, and after they were cooled, the pH was adjusted to 7. NaCl was added to these samples, instead of $CaCl_2$. We added 0.03 or 0.15 M NaCl, which has an ionic strength equivalent to the ionic strength of 0.01 or 0.05 M $CaCl_2$ respectively. The ionic strength of the samples was equal to 0.03 and 0.15 M, which is equal to the ionic strength of a 0.01 and 0.05 M $CaCl_2$ sample. No gel was observed after the addition of 0.03 or 0.15 M NaCl, which indicates that for these conditions screening of electrostatic interactions between the fibrils is not the driving force to form a gel. The presence of polyvalent cations, which can form salt bridges, is necessary for the formation of a gel network.

For all conditions in Table 6.1 where a "larger than" sign is noted, no gel was formed after $CaCl_2$ was added to the heated solutions. For these conditions it is impossible to obtain a gel using the cold gelation method. To use this method it is necessary to obtain a heat-denatured solution. When we increased the β-lg concentration, a heat-denatured gel was formed immediately after heating.

The calculated values for c_P for β-lg samples heated at pH 2, where the pH afterward was adjusted to 7 or 8, all were within the same range (Table 6.1). The net negative charge of a β-lg monomer at pH 8 is slightly higher than the charge at pH 7 (-9 for pH 8; -7.8 for pH 7), resulting in a higher electrostatic repulsion between the structures formed. This effect did not result in a much different value for c_P at 0.05 and 0.1 M added $CaCl_2$. For 0.01 M added $CaCl_2$, the c_P at pH 8 was about three times higher.

We can compare the new multistep cold gelation method with the conventional cold gelation method. The c_P corrected for conversion, which indicates the effective amount of structures necessary to form a network, was a factor of 7 lower for β-lg samples prepared according to the new multistep cold gelation method (0.01 M $CaCl_2$ was added), than for β-lg samples prepared according to the conventional cold gelation method (0.05 M $CaCl_2$ was added) (Table 6.1). The new multistep cold gelation method results in a value for c_P (corrected for conversion) which is an order of magnitude lower than c_P (corrected for conversion) found using the conventional cold gelation method.

We compared samples prepared according to both cold gelation methods for the condition where 0.01 M $CaCl_2$ was added. A gel with the lowest measured c_P

was formed using the new multistep cold gelation method, whereas no gel was formed using the conventional cold gelation method. This may be explained in terms of an adjusted random contact model for semiflexible fibrils.[25] This model yields $c_p \sim 1/P$, where P denotes the persistence length of the fibrils.[25] The persistence length consists of two contributions. One contribution is the bare persistence length while the other is an electrostatic persistence length. For fibrils made at pH 2 and at ionic strength between 0.01 M – 0.08 M, the bare persistence length is much larger than the electrostatic persistence length.[25] Addition of 0.01 M CaCl₂ to fibrils made according to the new multistep cold gelation method will therefore not significantly influence P. Thus the persistence length of the fibrils in Figure 6.1 (made at pH 2) will be roughly equal to the persistence length of the fibrils made according to the new multistep cold gelation method and to which 0.01 M CaCl₂ has been added. From the above and the TEM micrographs, it follows that the persistence length P of fibrils formed according to the new multistep cold gelation method (heated at pH 2, Figure 6.1) is much larger than that of fibrils formed according to the conventional cold gelation method (heated at pH 7 or pH 8, Figure 6.2). Thus, using $c_p \sim 1/P$, one expects that using the new multistep cold gelation method would result in a much lower c_p than using the conventional cold gelation method.

Comparing the results obtained using the conventional cold gelation method with previous papers on cold gelation, previous papers showed the formation of a gel after the addition of 0.01 M CaCl₂, whereas no gel was formed when the conventional cold gelation method was used in this paper.[1,17,19,27,28] This difference may be the result of a different way of adding CaCl₂ to the heated solution. In this paper, CaCl₂ was added very carefully on ice and mixed well. Previous papers reported that CaCl₂ was added by dialysis for 24 h.[1,17,19,27,28] The combination of slowly adding CaCl₂ with a longer time to form a gel, will result in gel formation at lower CaCl₂ concentrations. For the experiments performed in this paper, it was not possible to add CaCl₂ via dialysis, because the samples needed to be poured into the VOR before a gel was formed.

When the results of the new multistep cold gelation method are compared with heat-induced gelation, a much lower c_p was found using this new multistep cold gelation method. For β-lg at pH 7 and low ionic strength, a critical gel concentration of 8% was found after heating at 100 °C for 1 h[33], and a critical gel

concentration of 10% was observed after heating at 95 °C for 1 h.[9] Also heat-induced gelation of β-lg at pH 2 resulted in a higher c_P (1.4%, at 0.01 M ionic strength) as compared with using the multistep cold gelation process.[25]

6.4 Conclusion

TEM micrographs showed that the long linear fibrils formed for β-lg at pH 2 (without added salt), after heating at 80 °C for 10 h, were stable when the pH was adjusted to 7 or 8. Short fibrils were observed when β-lg was heated at 80 °C for 30 min, at pH 8 (without added salt), and a sort of intermediate structure between fibrillar and random aggregates was found for β-lg heated at 80 °C for 30 min, at pH 7 (without added salt). Conversion experiments showed a conversion of 94% for β-lg heated at pH 7, and 89% for β-lg heated at pH 8, whereas the conversion was 60% when β-lg was heated at pH 2.[25] Using rheological measurements, c_P was calculated. The lowest value for c_P was found when a β-lg sample was heated at pH 2, and afterward the pH was adjusted to 7, and 0.01 M $CaCl_2$ was added. The lowest value for c_P obtained for β-lg samples prepared according to the new multistep cold gelation method, was an order of magnitude lower than the lowest value for c_P obtained by using the conventional cold gelation method. Using this new multistep cold gelation process, a gel network can be formed at much lower concentrations as compared to the conventional cold gelation method, or heat-induced gelation. This novel route opens possibilities for efficient use of food ingredients in general.

References

1.   Barbut, S. *Lebensm. -Wiss. Technol.* **1997**, *29*, 590-593.

2.   Doi, E. *Trends Food Sci. Technol.* **1993**, *4*, 1-5.

3.   Bryant, C.M.; McClements, D.J. *Trends Food Sci. Technol.* **1998**, *9*, 143-151.

4.   Doi, E.; Kitabatake, N. *Food Hydrocolloids* **1989**, *3*, 327-337.

5.   Koseki, T.; Kitabatake, N.; Doi, E. *Food Hydrocolloids* **1989**, *3*, 123-134.

6.   Koseki, T.; Kitabatake, N.; Doi, E. *Food Hydrocolloids* **1989**, *3*, 135-148.

7.   Matsudomi, N.; Rector, D.; Kinsella, J.E. *Food Chem.* **1991**, *40,* 55-69.

8.   Murata, M.; Tani, F.; Higasa, T.; Kitabatake, N.; Doi, E. *Biosci. Biotechnol. Biochem.* **1993**, *57*, 43-46.

9.   Stading, M.; Hermansson, A.-M. *Food Hydrocolloids* **1990**, *4*, 121-135.

10.   Langton, M.; Hermansson, A.-M. *Food Hydrocolloids* **1992**, *5*, 523-539.

11.   Bryant, C.M.; McClements, D.J. *J. Food Sci.* **2000**, *65*, 259-263.

12.   Bryant, C.M.; McClements, D.J. *J. Food Sci.* **2000**, *65*, 801-804.

13.   Hongsprabhas, P. *Lebensm. -Wiss. Technol.* **1999**, *32*, 196-202.

14.   Hongsprabhas, P.; Barbut, S. *Int. Dairy J.* **1997**, *7*, 827-834.

15.   Hongsprabhas, P.; Barbut, S. *Food Res. Int.* **1996**, *29*, 135-139.

16.   Ju, Z.Y.; Kilara, A. *J. Agric. Food Chem.* **1998**, *46*, 3604-3608.

17.   Hongsprabhas, P.; Barbut, S. *J. Food Sci.* **1997**, *62*, 382-385.

18.   Hongsprabhas, P.; Barbut, S. *Food Res. Int.* **1998**, *30*, 523-527.

19.   Roff, C.F.; Foegeding, E.A. *Food Hydrocolloids* **1996**, *10*, 193-198.

20.   Barbut, S.; Drake, D. *Food Res. Int.* **1997**, *30*, 153-157.

21.   Ju, Z.Y.; Kilara, A. *J. Food Sci.* **1998**, *63*, 288-292.

22.   Jeyarajah, S.; Allen, J.C. *J. Agric. Food Chem.* **1994**, *42*, 80-85.

23.   Aymard, P.; Nicolai, T.; Durand, D. *Macromolecules* **1999**, *32*, 2542-2552.

24.   Kavanagh, G.M.; Clark, A.H.; Ross-Murphy, S.B. *Int. J. Biol. Macromolecules* **2000**, *28*, 41-50.

25.   Veerman, C.; Ruis, H.; Sagis, L.M.C.; Linden van der, E. *Biomacromolecules* **2002**, *3*, 869-873.

26.   Linden van der, E.; Sagis, L.M.C. *Langmuir* **2001**, *17*, 5821-5824.

27.   Barbut, S. *Lebensm. -Wiss. Technol.* **1995**, *28*, 598-603.

28.   Hongsprabhas, P.; Barbut, S. *Lebensm. - Wiss. Technol.* **1997**, *30*, 45-49.

29.   Hongsprabhas, P.; Barbut, S. *Food Res. Int.* **1997**, *30*, 451-455.

30.   Kella, N.K.; Kinsella, J.E. *Biochem. J.* **1988**, *255*, 113-118.

31.   Verheul, M.; Roefs, S.P.F.M.; Kruif de, C.G. *J. Agric. Food Chem.* **1998**, *46*, 896-903.

32.   Mulvihill, D.M.; Donovan, M. *Ir. J. Food Sci. Technol.* **1987**, *11*, 43-75.

33.   Renard, D.; Lefebvre, J. *Int. J. Biol. Macromolecules* **1992**, *14*, 287-291.

7

Shear-Induced Aggregation and Break up of Fibril Clusters close to the Percolation Concentration

Abstract

To probe the behaviour of fibrillar assemblies of ovalbumin under oscillatory shear, close to the percolation concentration, c_P (7.5%), rheo-optical measurements and Fourier transform rheology were performed. Different behaviour was observed close to c_P (7.3%), compared to slightly further away from c_P (6.9 and 7.1%). For 6.9 and 7.1%, shear-thinning behaviour and a linear increase in birefringence, $\Delta n'$, with increasing strain was observed, indicating deformation and orientation of the fibril clusters. For 7.3%, a shear-thinning regime was followed by a shear-thickening regime, which coincided with a strong increase in $\Delta n'$, dichroism, $\Delta n''$, and the intensity of the normalized third harmonic (I_3/I_1). This regime was followed by a second shear-thinning regime, where $\Delta n'$, $\Delta n''$ and I_3/I_1 decreased. In the first shear-thinning regime, deformation and orientation of existing clusters takes place. At higher oscillatory shear a larger deformation occurs and larger structures are formed, which is most likely aggregation of the clusters. Finally, at even higher strains, the clusters break up again. An increase in complex viscosity, $\Delta n'$, $\Delta n''$ and I_3/I_1 was observed when a second strain sweep was performed 30 min after the first one. This indicates that the shear-induced cluster formation and break up are not completely reversible, and the initial cluster size distribution is not recovered after cessation of flow.

7.1 Introduction

Structural changes of complex fluids under steady shear flow were investigated for different type of materials, like suspensions, associating polymers and polymer solutions.[1-6] Under specific conditions, depending on the material, a shear-thickening regime is observed followed by shear-thinning behaviour.[3,4,6] Shear-thickening is often the result of shear-induced formation of intermolecular structures (clusters), leading to an increase in the effective volume fraction.[1-3,5,7] Clusters convected by shear flow may aggregate upon contact, due to attractive interactions of particles on the periphery of the clusters. Cluster-cluster collisions that occur along the streamlines of shear flow lead to the formation of larger clusters.[7] In polymer solutions the size of these clusters depends upon the concentration.[4] Shear-induced stretching of the structures can also contribute to a shear-thickening effect.[4,8,9] Increasing the shear rate increases the stress on these structures, and once a critical stress is exceeded, they break up, giving rise to shear-thinning behaviour.[3,4,6]

In a previous study, we investigated the irreversible self-assembly of ovalbumin into fibrils and the resulting linear network rheology.[10] Ovalbumin is a major globular protein component in egg white, and has multi-functional properties, like its ability to foam and to form gels upon heating.[11-14] Fibrillar structures can be formed upon heating a monomeric ovalbumin solution at pH 2 and low ionic strength at 80 °C for 1 h.[10,15] TEM micrographs showed that semiflexible ovalbumin fibrils of about 250 nm were present at low ionic strength.[10] A gel is formed above a critical ovalbumin concentration, depending on ionic strength, heating condition and pH. This critical percolation concentration was determined for ovalbumin at pH 2, heated at 80 °C for 1 h as a function of ionic strength.[10] The critical percolation concentration was decreasing with increasing ionic strength, and ranged from 7.9 to 4.8%, for ionic strengths of 0.01 to 0.035 M respectively.

Recently, we performed steady shear rheo-optical measurements on ovalbumin fibrils solutions.[16] From these results we concluded that, close to the percolation concentration, the ovalbumin fibrils are organized in flexible clusters.[16] The objective of the present study was to obtain more insight in the fibrillar ovalbumin structures under oscillatory shear, close to the percolation concentration, with the use of rheo-optical measurements and Fourier transform rheology

(FT-rheology). We measured birefringence, *Δn'*, and dichroism, *Δn''*, as a function of strain. To quantify the non-linearity of the stress deformation response of the fibrillar ovalbumin solutions, we made use of FT-rheology, allowing us to measure the intensity of higher harmonics in the stress response as a function of strain.[17-19]

7.2 Materials and Methods

7.2.1 Sample preparation

Ovalbumin was obtained from Sigma (A5503, lotnr 81K7025) with a purity of at least 99%. 8% (w/w) ovalbumin was dissolved in bidistilled water at pH 2, and stirred overnight. The pH of the protein sample was adjusted to pH 2, using a 6 M HCl solution. The ovalbumin solution was centrifuged at 26000*g* for 30 min at 4 °C, to remove any traces of undissolved material. Subsequently, the supernatant was filtered through a protein filter (FP 30/0.45 CA-S filter, Schleicher & Schuell). The pH of the solution was checked to be 2. The concentration of this stock solution was determined with a UV spectrophotometer at a wavelength of 278 nm.

Ovalbumin solutions of 6.9, 7.1 and 7.3% were prepared from the stock solution, and heated at 80 °C for 1 h in a water bath, while shaking. The solution was cooled on ice water to 4 °C, and stirred slowly at 21 °C for 1.5 h before measuring.

7.2.2 Rheo-optical measurements

Rheo-optical measurements were performed using an ARES (Rheometric Scientific Ltd) rheometer with a Couette geometry (cup diameter 33.8 mm; bob diameter 30.0 mm; bob length 20.09 mm), and an optical analysis module (OAM). The optical signal from the detector was digitized using an ADC and analysed using Labview (National Instruments). After pouring the ovalbumin sample in the Couette geometry, the sample rested for 30 min. Dynamic measurements were performed on 6.9, 7.1 and 7.3% ovalbumin (frequency 1 Hz, strain 0.1 – 400%), where each strain was measured for 60 s. To determine if shear-induced structural changes of the ovalbumin solutions were reversible, the sample was kept at rest for 30 min in the Couette cell after the first measurement (test 1), and then a second strain sweep was performed (test 2). For 7.3%, this procedure was repeated, but now with only 10 min between the first and second strain sweep (sample 2). The

rheological and optical measurements were performed simultaneously. For more detailed information about the experimental set-up see ref. 20.

7.2.3 Fourier transform rheology (FT-rheology)

FT-rheology can be used as a tool to quantify the nonlinear response to large-amplitude oscillatory shear (LAOS), by analysis of higher harmonics in the stress response.[17,19] For an oscillatory shear measurement with applied frequency ω_1, in the non-linear regime the formation of mechanical odd harmonics at 3 ω_1, 5 ω_1, 7 ω_1, and so forth appear in the torque response. The amplitudes and phases of the higher harmonics within the torque signal can be detected as spectra $I(\omega)$ in Fourier space. The torque signals were digitized using an ADC, and analysed in Fourier space using Labview (National Instruments).

7.3 Results

7.3.1 Rheological results

Results of the complex viscosity versus strain for various ovalbumin concentrations close to the percolation concentration show a shear-thinning behaviour for all concentrations (Figure 7.1). For 7.3%, this shear-thinning regime is followed by a shear-thickening behaviour, and finally at even higher strains a second shear-thinning regime was visible (Figure 7.1). This trend was different from that of 6.9 and 7.1% ovalbumin, where only shear-thinning behaviour was observed. For all concentrations, a higher complex viscosity was found for the second strain sweep (test 2), which was performed 30 min after the first measurement (test 1). For 7.3%, this effect was smaller when the second strain sweep (sample 2, test 2) was made only 10 min after the first one (sample 2, test 1).

To obtain more insight in the elasticity of the ovalbumin fibrils solution, tan δ versus strain was plotted in Figure 7.2. For 6.9 and 7.1%, tan δ was increasing with increasing strain, indicating that the sample was more viscous at higher strains. For almost all strains, tan δ was higher than 1, which indicates a fluid-like behaviour. For 7.3% ovalbumin, tan δ was first increasing, then decreasing, and finally increasing again as a function of strain. This trend indicated that at lower strains the sample became more viscous, but was still gel-like because tan δ was smaller than 1.

Figure 7.1 Complex viscosity versus strain for three different ovalbumin concentrations close to the percolation concentration. 6.9% test 1 (▲); 6.9% test 2 (△); 7.1% test 1 (●); 7.1% test 2 (○); 7.3% sample 1, test 1 (◆); 7.3% sample 1, test 2 (◇); 7.3% sample 2, test 1 (■); 7.3% sample 2, test 2 (□).

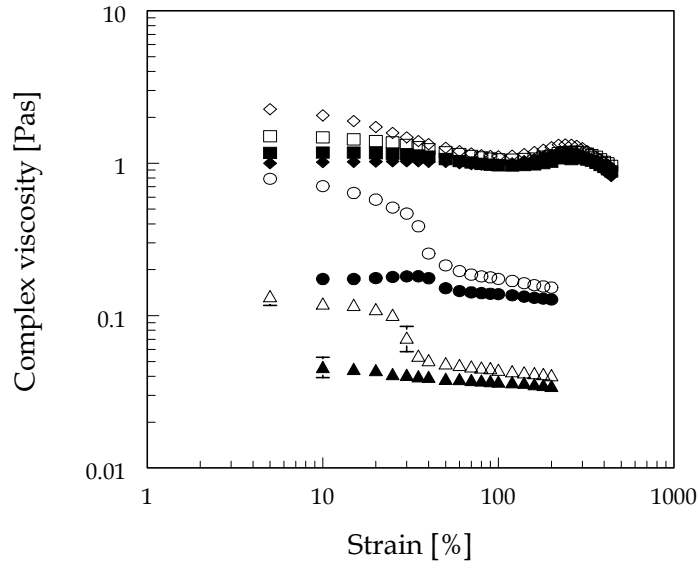**Figure 7.2** Tan δ versus strain for three different ovalbumin concentrations close to the percolation concentration. 6.9% test 1 (▲); 6.9% test 2 (△); 7.1% test 1 (●); 7.1% test 2 (○); 7.3% sample 1, test 1 (◆); 7.3% sample 1, test 2 (◇); 7.3% sample 2, test 1 (■); 7.3% sample 2, test 2 (□).
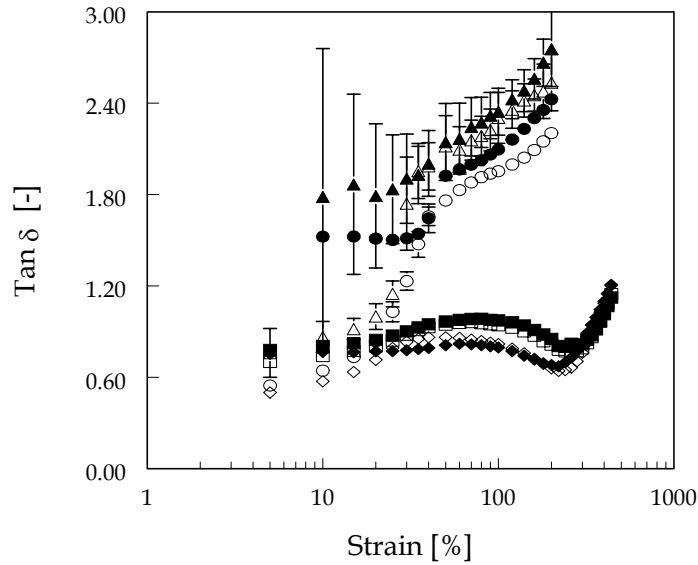
At strains higher than 100%, the sample became more elastic. Above a strain of about 250%, a strong increase in tan δ was observed indicating a more viscous sample. At very high strains, tan δ was larger than 1, indicating a more fluid-like behaviour.

7.3.2 Fourier transform rheology

To probe the non-linearity of the stress response of the ovalbumin samples, we used Fourier transform rheology (FT-rheology). For 6.9 and 7.1%, no clear higher harmonics could be detected in the Fourier spectrum, in the range of strains we applied. For ovalbumin fibrils solutions made at 7.3%, third harmonics were present. Harmonics higher than the third were not found. Figure 7.3 shows the intensity of the third harmonic normalised by the intensity of the first harmonic (I_3/I_1) for both samples at 7.3%. Up to a strain of about 100% I_3/I_1 is slightly increasing. Above 100%, a strong increase in non-linearity was observed. At strains higher than 250% a decrease in I_3/I_1 was found. The time between the first and the second strain sweep seems to have influence on the increase in I_3/I_1 observed in the second sweep compared to the first one. This increase is higher when the time between sweeps is larger.
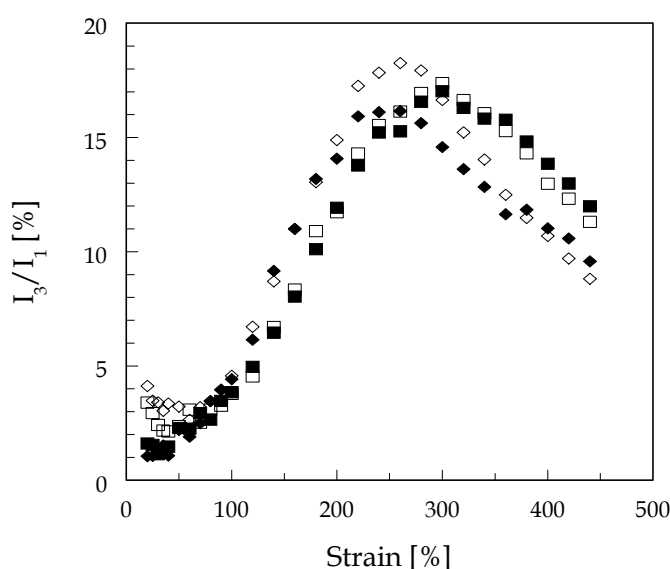

Figure 7.3 I_3/I_1 versus strain for 7.3% ovalbumin. Sample 1, test 1 (◆); sample 1, test 2 (◇); sample 2, test 1 (■); sample 2, test 2 (□).

7.3.3 Optical results

Figure 7.4 shows the results of birefringence, $\Delta n'$, measurements versus strain for ovalbumin fibrils solutions at 6.9, 7.1 and 7.3%. For 6.9 and 7.1%, a linear increase of $\Delta n'$ with increasing strain was found, where for 7.1% $\Delta n'$ was higher at equal strain compared to 6.9%. For 7.3%, a higher value for $\Delta n'$ at equal strain was observed than for 6.9 and 7.1%. Above a strain of about 100%, $\Delta n'$ was strongly increasing. At strains higher than 200%, a decrease in $\Delta n'$ was observed. This trend was found for both samples of 7.3%. The order of magnitude of $\Delta n'$ was 10^{-6} – 10^{-5}. For all samples the values for $\Delta n'$ of the second sweep (tests 2) were slightly higher compared to the first one (tests 1).
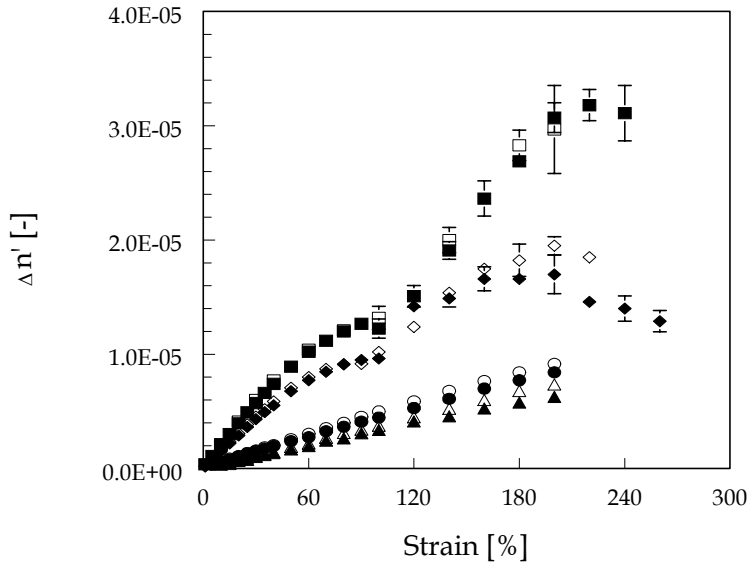
Figure 7.4 $\Delta n'$ versus strain for three different ovalbumin concentrations close to the percolation concentration. 6.9% test 1 (▲); 6.9% test 2 (△); 7.1% test 1 (●); 7.1% test 2 (○); 7.3% sample 1, test 1 (◆); 7.3% sample 1, test 2 (◇); 7.3% sample 2, test 1 (■); 7.3% sample 2, test 2 (□).

Dichroism, $\Delta n''$, measurements were performed for a 7.3% fibrillar ovalbumin solution (Figure 7.5). The order of magnitude of $\Delta n''$ was 10^{-9} – 10^{-8}, indicating that the value of $\Delta n''$ is negligible compared to $\Delta n'$ values. At low strains, $\Delta n''$ was very small and nearly independent of strain. Above strains of 100% an increase in $\Delta n''$ was observed, followed by a decrease in $\Delta n''$ at strains higher than 220%. For both tests the same trend was found.
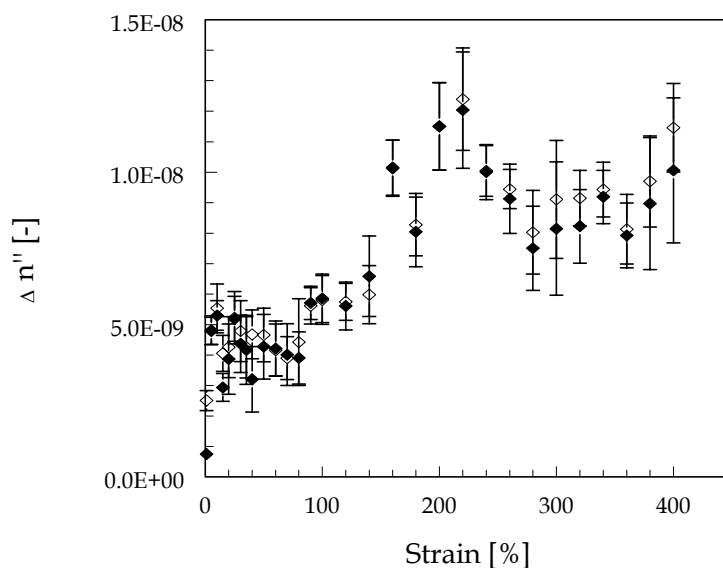
Figure 7.5 $\Delta n''$ versus strain for 7.3% ovalbumin. Test 1 ($\blacklozenge$); test 2 ($\lozenge$).

7.4 Discussion

We investigated the behaviour of fibrillar assemblies of ovalbumin under oscillatory shear, close to the percolation concentration, c_p (which is 7.5%). At 7.3% the behaviour was different from the behaviour at 6.9 and 7.1%. The difference may be explained in terms of a difference in cluster size. Percolation theory assumes the presence of clusters, whose size depends on $c_p - c$, where c is the monomer concentration.[21,22] For ovalbumin, fibrillar structures were formed after heating, which form isotropic clusters. These clusters can be thought of as finite size or 'local' network structures. Closer to c_p, these clusters are larger, and become infinite at c_p.[21,22] The radius of a cluster signifies the correlation length, or spatial extent of the connectivity function, equal to the probability that two fibrils at distance r belong to the same cluster.[21] The difference in cluster size influences the rheological and optical behaviour under oscillatory shear, as we will discuss now. For 6.9 and 7.1% ovalbumin, shear-thinning behaviour, and increase in tan δ, and a linear increase in $\Delta n'$ with increasing strain was observed, indicating deformation and alignment of the clusters, without much hindrance between neighbouring clusters.

Normalized values for the measured parameters, $\Delta n'$, $\Delta n''$, complex viscosity, tan δ, and I_3/I_1 at 7.3% ovalbumin are given in Figure 7.6. This figure can

be divided in three strain regions. The first region (I), up to a strain of 100%, shows a decrease in complex viscosity, which indicates small deformation of the ovalbumin clusters. Tan δ was slightly increasing, corresponding to a slightly more viscous system, but still gel-like because tan δ is smaller than 1. The results of FT-rheology show a gradual increase in I_3/I_1, indicating slightly non-linear behaviour. In the same region a linear increase in $\Delta n'$ was observed, so more alignment and or deformation of the clusters takes place. The values for $\Delta n''$ were very small and hard to distinguish from the background noise, which indicates that the clusters present were smaller than the wavelength of the laser light, which is 670 nm. All results indicate that the clusters deform and align slightly in region I.
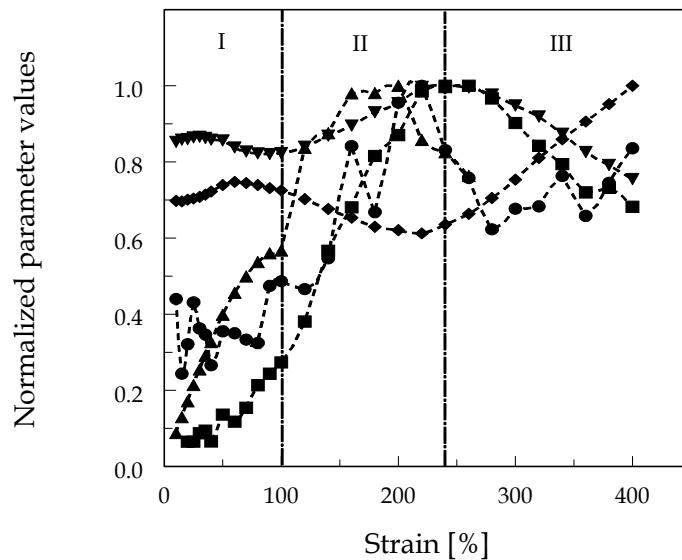
Figure 7.6 Normalized values for measured parameters for 7.3% ovalbumin. All values are divided by the maximum value of the measurement, for each parameter. $\Delta n'$ (▲); $\Delta n''$ (●); complex viscosity (▼); tan δ (◆); I_3/I_1 (■).

In the second region (II), ranging from 100% to about 240% strain, the complex viscosity was increasing. A larger deformation may cause hindrance between the clusters, resulting in a shear-thickening behaviour. Also growth of the clusters can contribute to a shear-thickening effect. Tan δ was decreasing, corresponding to a more elastic gel-like behaviour. An increase in $\Delta n''$ measurements was found, indicating that part of the laser light entering the material is absorbed. This can be explained by the presence of more deformed or larger structures, with a size larger than the wavelength of the laser light (670 nm). Also a

strong increase in *Δn′* was observed in this regime, which can be explained by a strong alignment of the clusters, due to a large deformation. The non-linearity increased strongly in this region, which may be due to the more deformed or larger clusters. The trends found in region II can be summarised as a combined effect of large deformation and the formation of larger structures, which is most likely aggregation of the fibril clusters.

Finally, in region III, from about 240% to 400% strain, the complex viscosity was decreasing again. Tan *δ* increases to above 1, indication a more viscous fluid-like behaviour. The decrease in I_3/I_1 indicates less non-linearity of the sample. Also the values for *Δn′* and *Δn′′* were decreasing. Both optical and rheological results indicate the break up of clusters at high oscillatory shear.

Another trend observed in all measurements, were the higher values for the complex viscosity, tan *δ*, I_3/I_1, *Δn′* and *Δn′′* for the second strain sweep (tests 2) performed 30 min after the first one (tests 1). For all concentrations these results indicate rearrangements during rest resulting in a different initial cluster size distribution when the second measurement was started. For 7.3%, this effect was smaller with only 10 min rest between the first and second strain sweep, indicating that the resting time between two measurements is an important factor, which influences the cluster size distribution when starting the second measurement. For 7.3% ovalbumin, another effect may also play a role. At high oscillatory shear the clusters break up, but the size of the clusters may still be larger than the size when the first measurement was started, which will also contribute to a different cluster size distribution at the start of the second measurement.

7.5 Conclusion

We investigated the behaviour of fibrillar assemblies of ovalbumin under oscillatory shear, close to the percolation concentration, c_p (which is 7.5%). Near c_p (7.3%) different behaviour was observed compared to slightly further away from c_p (6.9 and 7.1%). This can be explained with the use of percolation theory, which assumes the presence of clusters, with a size that depends on the distance to c_p. For 6.9 and 7.1%, the clusters present after heating will deform and align when oscillatory shear is applied. For 7.3%, we propose, based on the results of rheo-optics and FT-rheology, that the strain regime can be divided in three regions.

In region I deformation and orientation of the clusters occur up to a strain of about 100%. At higher oscillatory shear (region II) a larger deformation occurs and larger structures are formed, which is most likely aggregation of the clusters. Finally, at strains higher than 240% (region III), the clusters break up. Both rheo-optical and FT-rheology results showed rearrangements of the clusters in time, which indicates that the initial cluster size distribution is not recovered after cessation of flow. All results give more insight in the behaviour of ovalbumin fibrils under oscillatory shear close to the percolation concentration.

Acknowledgments

References

1. Egmond van, J.W. *Curr. Opin. Coll. Interf. Sci.* **1998**, *3*, 385-390.

2. Raghavan, S.R.; Khan, S.A. *J. Colloid Interf. Sci.* **1997**, *185*, 57-67.

3. Verduin, H.; Gans van, B.J.; Dhont, J.K.G. *Langmuir* **1996**, *12*, 2947-2955.

4. Yekta, A.; Xu, B.; Duhamel, J.; Adiwidjaja, H.; Winnik, M.A. *Macromolecules* **1995**, *28*, 956-966.

5. Kishbaugh, A.J.; McHugh, A.J. *Rheol. Acta* **1993**, *32*, 9-24.

6. Bergenholtz, J.; Wagner, N.J. *Langmuir* **1996**, *12,* 3122-3126.

7. Varadan, P.; Solomon, M.J. *Langmuir* **2001**, *17,* 2918-2929.

8. Marrucci, G.; Bhargava, S.; Cooper, S.L. *Macromolecules* **1993**, *26,* 6483-6488.

9. Groisman, A.; Steinberg, V. *Phys. Rev. Lett.* **2001**, *86,* 934-937.

10. Veerman, C.; Schiffart de, G.; Sagis, L.M.C.; Linden van der, E. *Int. J. Biol. Macromolecules* **2003**, *33,* 121-127.

11. Nemoto, N.; Koike, A.; Osaki, K.; Koseki, T.; Doi, E. *Biopolymers* **1993**, *33,* 551-559.

12. Doi, E.; Kitabatake, N. In *Food Proteins and their Applications.* Damodaran, S.; Paraf, A. (Eds.) **1997**, Marcel Dekker: New York, 325-340.

13. Mine, Y. *J. Agric. Food Chem.* **1996**, *44*, 2086-2090.

14. Hagolle, N.; Relkin, P.; Dalgleish, D.G.; Launay, B. *Food Hydrocolloids* **1997**, *11,* 311-317.

15. Weijers, M.; Sagis, L.M.C.; Veerman, C.; Sperber, B.; Linden van der, E. *Food Hydrocolloids* **2002**, *16,* 269-276.

16. Veerman, C.; Sagis, L.M.C., Venema, P.; Linden van der, E. S*ubmitted for publication*.

17. Wilhelm, M.; Maring, D.; Spiess, H.-W. *Rheol. Acta* **1998**, *37,* 399-405.

18. Wilhelm, M.; Reinheimer, P.; Ortseifer, M. *Rheol. Acta* **1999**, *38*, 349-356.

19. Wilhelm, M. *Macromol. Mat. Eng.* **2002**, *287,* 83-105.

20. Klein, C. et al. *In Preparation*.

21. Stauffer, D. *Physics Rep.* **1979**, *54,* 1-74.

22. Stauffer, D.; Coniglio, A.; Adam, M. *Adv. Polym. Sci.* **1982**, *44,* 103-158.

8

The Effect of Shear Flow on the Percolation Concentration of Fibrillar Protein Assemblies

Abstract

The objective of this study was to investigate the effect of shear flow on the percolation concentration (c_P) for solutions of fibrillar protein assemblies. The results of viscosity measurements were analysed using percolation theory, taking into account the effect of shear flow. We found c_P to increase with increasing shear rate. Results of birefringence measurements were used to obtain the rotational diffusion coefficient at c_P, which enables us to express c_P, from viscosity measurements, as a function of Peclet number. We compared our experimental data with theoretical calculations on c_P versus Peclet number, based on a random contact model for rodlike particles, making use of a shear dependent excluded volume per fibril. The experimental and theoretical results are in good agreement, considering the fact that polydispersity of the ovalbumin fibrils has been neglected and that the fibrils are semiflexible.

8.1 Introduction

The effect of shear flow on the arrangement of fibrillar structures in solution is of interest in many applications.[1-3] A better understanding of the dynamics of sheared solutions of fibrils allows a more accurate prediction of the behaviour of fibrillar structures in for example processing in industrial applications.[1-3] Although rheo-optics is a useful and established method to investigate the arrangement of fibrils under shear[1,3-12], there are few investigations on the effect of shear flow on fibrillar protein structures, which is the subject of this paper.[8,9,13]

The ability to form fibrils appears to be a generic property of proteins. Many biological molecules can assemble into fibrillar structures. Fibrinogen assembles into fibrin, a component found in blood clots.[14] Fibrils of actin and microtubules formed by tubulin determine the mechanical properties of the cytoskeleton.[15] Several neurodegenerative disorders such as Alzheimer's and Creutzfeldt-Jacob disease, are associated with the formation of amyloid fibrils.[16] Many globular food proteins, commonly used as gelling agents, foaming agents or emulsifiers, also have the ability to form fibrils. Examples are the whey proteins β-lactoglobulin (β-lg)[17], α-lactalbumin[18], and bovine serum albumin (BSA)[19], egg-white proteins like lysozyme[20] and ovalbumin[21], and the soy protein glycinin[22]. The formation of fibrils generally occurs in a narrow pH, ionic strength, and protein concentration range, and is often induced by heating an aqueous solution of the proteins to a temperature close to the denaturation temperature of the protein.[17,19]

The protein used in this study is ovalbumin, which is a major globular protein component in egg white.[23-26] Fibrillar structures were observed after heating a monomeric ovalbumin solution at pH 2, and low ionic strength, at 80 °C for 1 h.[21,27] TEM micrographs showed the presence of semiflexible fibrils of about 250 nm.[21] A critical percolation mass fraction, c_p, was determined from the gel region ($c > c_p$), using percolation theory: $G' \sim (c - c_p)^t$.[21] Here G' is the storage modulus, c the monomer concentration, and t a universal scaling exponent, dependent on the Hamiltonian of the system.[28,29] We found c_p to decrease with increasing ionic strength (0.079 – 0.048, from 0.01 to 0.035 M ionic strength respectively), and the value for t was found to be 2, indicating isotropic force percolation.[21,28] The dependence of c_p on ionic strength was explained using an adjusted random contact model, where c_p is related to the average number of contacts per particle, and the excluded volume of the rod.[21]

So far the determination of c_p was performed using G' data in the limit of zero shear. The objective of this study is to obtain c_p under shear, as suggested by van der Linden and Sagis.[28] This approach is inspired by results for microemulsions where the effect of an external electric field on c_p was described,[30,31] and by results on silica spheres, where the effect of temperature on c_p was investigated.[32] In the work presented here, we investigated the effect of an external shear field on c_p, for solutions of fibrillar protein assemblies, using viscosity measurements and a relation for viscosity near the percolation threshold. With the use of rheo-optical measurements, we obtained values for c_p as a function of Peclet number (Pe). We compared c_p (Pe) as obtained from experimental data with c_p (Pe) as obtained from a theoretical analysis. This analysis is based on a random contact model for rodlike particles, now making use of an excluded volume per fibril as a function of shear, instead of in the limit of zero shear.

The outline of this paper is as follows. The theoretical behaviour of viscosity near the percolation threshold is outlined in section 8.2.1. The random contact model, with the excluded volume per fibril as a function of shear is treated in section 8.2.2. The behaviour of the viscosity near the threshold is used to analyse the results of viscosity measurements to obtain c_p as a function of shear rate (sections 8.4.1.1 and 8.4.1.2). In section 8.4.1.3 results of birefringence measurements were used to obtain a rotational diffusion coefficient at c_p, which enables one to express the experimentally obtained c_p versus shear rate as c_p (Pe). The analysis that leads to the theoretical values of c_p as a function of Peclet number is given in section 8.4.2. Our experimental data and the theoretically values are compared in section 8.4.3.

8.2 Theory

8.2.1 Percolation theory

Percolation theory predicts the following relation, when the percolation mass fraction, c_p, is approached from the sol-side ($c < c_p$):[33]

$$\eta_0 \sim \left(c_p - c\right)^{-k}$$

(8.1)

where η_0 is the zero-shear viscosity, c the mass fraction, and k a universal scaling exponent, which can have values between 0 and 1.35.[33,34] Since the scaling exponent k is a universal exponent, it will not change when shear is applied. This in contrast to c_p, which will change as a function of shear. When shear is applied, Eq. (8.1) takes the form

$$\eta = A\left(c_p(\dot{\gamma}) - c\right)^{-k} \tag{8.2}$$

where A is a proportionality constant, and $\dot{\gamma}$ the shear rate. Using a Taylor series expansion, $c_p(\dot{\gamma})$ can be written as

$$c_p(\dot{\gamma}) = c_p(\dot{\gamma} = 0) + \left(\frac{\partial c_p}{\partial \dot{\gamma}}\right)_{\dot{\gamma}=0} \dot{\gamma} + \frac{1}{2}\left(\frac{\partial^2 c_p}{\partial^2 \dot{\gamma}}\right)_{\dot{\gamma}=0} \dot{\gamma}^2 + ... \tag{8.3}$$

Using relation (8.2) and (8.3), $c_p(\dot{\gamma})$, $c_p(\dot{\gamma} = 0)$, and A can be determined from viscosity measurements at various mass fractions close to c_p.

8.2.2 Random contact model

8.2.2.1 Random contact model without shear flow

A random contact model for rigid hard rods, with a high aspect ratio, has been derived by Philipse.[35] This model assumes that for sufficiently thin rods mechanical contacts are effectively uncorrelated.[35] This model gives the following relation for c_p:[35]

$$c_p = \rho V_0 \tag{8.4}$$

with V_0 the volume of one rod ($V_0 = \frac{1}{4}\pi L D^2$, where D is the diameter of the rod, and L the length of the rod), and ρ the number density of the particles, which is assumed to obey a mechanical equation of state according to:[35]

$$\rho = 2\alpha / V_{ex} \tag{8.5}$$

with α the average number of contacts per particle, assumed to be of O(1) at c_p, and V_{ex} the excluded volume for a pair of randomly oriented particles.[36,37]

Combining Eq. (8.4) and (8.5) yields:

$$c_{\mathrm{p}} = 2\alpha \frac{V_0}{V_{\mathrm{ex}}}$$

(8.6)

where V_{ex} is given by:[36,37]

$$V_{\mathrm{ex}} = -\iint \beta_1(\mathbf{u}, \mathbf{u}') f(\mathbf{u}) f(\mathbf{u}') d^2\mathbf{u} \, d^2\mathbf{u}'$$

(8.7)

with $\mathbf{u}$ the orientation vector of a test rod, $\mathbf{u}'$ the orientation vector of a neighbouring rod, $d^2\mathbf{u}$ an integration over all possible orientations of $\mathbf{u}$, and β_1, the cluster integral, which can be expressed as:

$$-\beta_1(\mathbf{u}, \mathbf{u}') \approx 2DL^2 \sin(\varphi(\mathbf{u}\mathbf{u}'))$$

(8.8)

where $\varphi(\mathbf{u}\mathbf{u}')$ is the angle between the test rod and a neighbouring rod. Without an external field, all particles are randomly oriented and the normalized orientational distribution function $f(\mathbf{u})$ reduces to

$$f_{\mathrm{iso}}(\mathbf{u}) = \frac{1}{4\pi}$$

(8.9)

Integration of Eq. (8.7) leads to a relation for V_{ex} for isotropically oriented rigid hard rods, $V_{\mathrm{ex}}^{\mathrm{iso}}$:[36,37]

$$V_{\mathrm{ex}}^{\mathrm{iso}} = \frac{\pi}{2} DL^2$$

(8.10)

Combining relation (8.6) and (8.10) results in an expression for c_{p} for rigid hard rods without an external field:[35]

$$c_{\mathrm{p}} = \alpha \frac{D}{L}$$

(8.11)

8.2.2.2 Random contact model adjusted for shear flow

To extend the random contact model for rigid hard rods, described above, in order to include the effect of shear flow, the expression for V_{ex} (Eq. (8.7)) needs to become shear dependent. The orientation distribution function for isotropic particles (Eq. (8.9)) has to be replaced by an orientation distribution function dependent on shear rate, or as a function of Peclet number (Pe = $\dot{\gamma}/D_r$, where D_r is the rotational diffusion coefficient). The shear dependent distribution function is calculated using the Doi-Edwards model.[38]

This is a model for monodisperse, rigid rods in the semidilute concentration regime:[38]

$$\frac{1}{L^3} << c << \frac{1}{DL^2} \tag{8.12}$$

This model calculates the particle orientation distribution function, and takes into account the effects of shear and hindered rotational diffusion.[2,38] When a test rod is assigned an orientation vector $\mathbf{u}(t)$, the diffusion equation governing the orientation probability distribution function, $f(\mathbf{u},t)$, is given by[2]

$$\frac{\partial f(\mathbf{u},t)}{\partial t} + div\left(f\dot{\mathbf{u}}(t) - \tilde{D}_r \nabla f\right) = 0 \tag{8.13}$$

where

$$\dot{\mathbf{u}}(t) = \mathbf{G}(t) \cdot \mathbf{u}(t) - (\mathbf{u} \cdot \mathbf{G} \cdot \mathbf{u})\mathbf{u} \tag{8.14}$$

G(t) is the velocity gradient tensor of the applied shear field, and $\tilde{D}_r$ the orientation-dependent rotational diffusion constant of a rod. The expression for $\tilde{D}_r$ can be simplified by approximating $\tilde{D}_r$ by an effective diffusion constant $\overline{D}_r$ that only depends on the shear rate:[38]

$$\overline{D}_r = \left\langle \tilde{D}_r \right\rangle = D_r Q^{-2} \tag{8.15}$$

where

$$D_r = \beta\left(cL^3\right)^{-2} D_{r0} \tag{8.16}$$

with β an undetermined numerical constant ranging from 10^3 – 10^4,[39-41] and D_{r0} the rotational diffusion coefficient for a single isolated rod[42]

$$D_{r0} = \frac{3k_B T \ln(L/D)}{\pi \eta_s L^3}$$

(8.17)

where k_B is the Boltzmann constant, T the temperature, and η_s the viscosity of the solvent. Q is given by:

$$Q = \frac{4}{\pi} \iint d^2\mathbf{u} d^2\mathbf{u}' f(\mathbf{u}) f(\mathbf{u}') \sin(\varphi(\mathbf{uu'}))$$

(8.18)

Comparing Eq. (8.7) with Eq. (8.18) leads to:

$$V_{ex} = V_{ex}^{iso} Q$$

(8.19)

To determine Q, one may expand the shear dependent orientational distribution function in terms of an infinite series of spherical harmonics, Y_{lm}, as

$$f(\mathbf{u}) = \sum_{l=0}^{\infty} \sum_{m=0}^{l} b_{lm} Y_{lm}(\theta, \Phi)$$

(8.20)

where b_{lm} is a coefficient, which can be determined from the following set of linear equations in the steady state:

$$-\overline{D}_r l(l+1) b_{lm} - \dot{\gamma} \sum_{l'=0}^{\infty} \sum_{m'=0}^{l'} (lm|\Gamma|l'm') b_{l'm'} = 0$$

(8.21)

where

$$\overline{D}_r = D_r \left(1 - 8\pi \sum_{l=2}^{\infty} \sum_{m=0}^{l} \left(\frac{l-1}{l+2}\right) \left[\frac{(l-3)!!}{l!!}\right]^2 |b_{lm}|^2 \right)^{-2}$$

(8.22)

The matrix element $(lm|\Gamma|l'm')$ is defined in ref. 38. With the use of Eq. (8.21) and (8.22), $\overline{D}_r$ can be obtained as a function of Peclet number ($= \dot{\gamma}/D_r$). The term between brackets in Eq. (8.22) corresponds to Q, which can be inserted in Eq. (8.19)

to determine V_{ex}. This V_{ex} is now a function of Peclet number and can be used in the random contact model to yield

$$c_p(Pe) = 2\alpha \frac{V_0}{V_{ex}(Pe)}$$

(8.23)

8.3 Materials and Methods

8.3.1 Sample preparation

Ovalbumin was obtained from Sigma (A5503, lotnr 81K7025) with a purity of at least 99%. Ovalbumin with a mass fraction of 0.08 was dissolved in bidistilled water at pH 2, and stirred for 2 h. The pH of the protein sample was adjusted to 2, using a 6 M HCl solution, and stirred for another 2 h. The ovalbumin solution was centrifuged at $26000g$ for 30 min at 4 °C, to remove any traces of undissolved material. Subsequently, the supernatant was filtered through a protein filter (FP 30/0.45 CA-S filter, Schleicher & Schuell). The pH of the solution was checked to be 2. The concentration of this stock solution was determined with a UV spectrophotometer at a wavelength of 278 nm.

An ovalbumin solution with a mass fraction of 0.072 was prepared from the stock solution, and heated at 80 °C for 1 h in a water bath, while shaking. The solution was cooled to 4 °C on ice-water. This 0.072 heated ovalbumin solution was stored at 7 °C. Before the measurement, the solution was diluted to the required concentration, and stirred slowly at 21 °C for 2 h.

8.3.2 Rheo-optical measurements

Rheo-optical measurements were performed using an ARES (Rheometric Scientific Ltd) rheometer with a Couette geometry (cup diameter 33.8 mm; bob diameter 30.0 mm; bob length 20.09 mm), and an optical analysis module (OAM). The optical signal from the detector was digitized using an ADC and analysed using Labview (National Instruments). After pouring the ovalbumin sample in the Couette geometry, the sample rested for 20 min. Then steady-shear measurements were performed up to a shear rate of 140 s^{-1}, where each shear rate was measured for 60 s. The measurements were performed in duplicate. The rheological and optical measurements were performed simultaneously. For more detailed information about the experimental set-up see ref. 43.

8.4 Results and Discussion

8.4.1 Percolation theory

8.4.1.1 Determination of the scaling exponent k and $c_p(\dot{\gamma}=0)$ from viscosity measurements

Results of viscosity measurements of a heated ovalbumin solution with a concentration, or mass fraction, of 0.072, which was diluted to various concentrations, showed shear-thinning behaviour, and a lower viscosity at lower ovalbumin concentration at equal shear rate (Figure 8.1). The zero-shear viscosity, η_0, was determined using the Carreau model, according to which[44]

$$\eta = \eta_0 \left[1 + \left(\frac{\dot{\gamma}}{\dot{\gamma}_{\text{crit}}} \right)^2 \right]^{-\frac{a}{2}} \tag{8.24}$$

with η the apparent viscosity, $\dot{\gamma}$ the shear rate, $\dot{\gamma}_{\text{crit}}$ a so called critical shear rate, which indicates the transition from Newtonian to Non-Newtonian behaviour[45], and a the negative of the power-law slope.[45] For the highest ovalbumin concentration, 0.072, more reliable datapoints were available than at lower ovalbumin concentrations. At 0.072 ovalbumin, data measured at shear rates down to 1 s^{-1} gave reliable results, in contrast to the lower concentrations where reliable results were obtained only above shear rates of 10 s^{-1}. The viscosity data for 0.072 were fitted first to obtain values for η_0, a, and $\dot{\gamma}_{\text{crit}}$. We assumed that $\dot{\gamma}_{\text{crit}}$ did not significantly depend on the measured ovalbumin concentrations. The value for $\dot{\gamma}_{\text{crit}}$ obtained for 0.072 (0.91 s^{-1}) was used in the fits for all ovalbumin concentrations. The fitted values for η_0 and a are shown in Table 8.1. All fits, using the Carreau model, are drawn in Figure 8.1.

The universal scaling exponent k and c_p can be determined using Eq. (8.1). A method described by van der Linden and Sagis[28] for determination of c_p and t from the gel-side of c_p, can be used also to determine c_p and k from the sol-side of c_p. This method is a graphical method that uses plots of $(\eta_0)^{-1/k}$ versus c and extrapolates these plots to $(\eta_0)^{-1/k} = 0$. This procedure makes use of the fact that independent of

Table 8.1 Values for η_0 and a, obtained using the Carreau model.

Mass fraction [-]	η_0 [Pas]	a [-]
0.048	0.056	0.21
0.053	0.067	0.19
0.058	0.065	0.17
0.062	0.166	0.24
0.066	0.313	0.31
0.072	0.407	0.32

the value of k the curves must all intersect the concentration axis at the same value. When the assumed value for k is close to the actual value, the plot will be linear. If k is too small or too large the line is curved. From the plot of $(\eta_0)^{-1/k}$ versus c for various k we selected the k value that gave an approximately straight line. For the viscosity results, a value for $k = 1.35$ resulted in a straight line. From the plot $(\eta_0)^{-1/k}$ versus c, c_p was determined to be 0.077. Rheological measurements on ovalbumin fibrils, performed at the gel-side of c_p ($c > c_p$), resulted in a value for c_p of 0.075 (corrected value from ref. 21, because c was determined differently), and a universal exponent t equal to 2.[21] We can conclude that c_p as obtained via elasticity
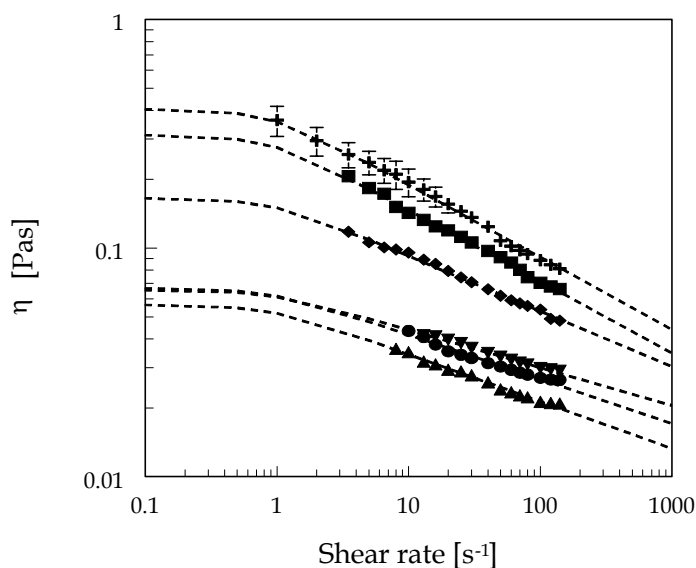

Figure 8.1 Apparent viscosity versus shear rate for a 0.072 heated ovalbumin solution, which was diluted to various concentrations: 0.048 (▲); 0.053 (●); 0.058 (▼); 0.062 (◆); 0.066 (■); 0.072 (+). The dotted lines indicate the fits obtained from the Carreau model.

measurements is in good agreement with c_p as determined from viscosity measurements. The value for k of 1.35 found for our viscosity measurements corresponds to a Rouse approximation.[33,34,46] Results from ovalbumin fibrils determined at the gel-side of c_p, showed a value for $t = 2$, indicating isotropic force percolation.[21] Based on isotropic force percolation, a value for $k = 0.7$ was expected.[33,47,48] An explanation for the value of $k = 1.35$ found for our results, may be the fact that the ovalbumin fibrils may self-organize in flexible clusters at the sol-gel transition.

8.4.1.2 Determination of c_p as a function of shear rate from viscosity measurements

In the previous section, we determined $k = 1.35$ and $c_p(\dot{\gamma}=0) = 0.077$ using Eq. (8.1). With the use of Eq. (8.2) and (8.3), we can calculate $c_p(\dot{\gamma})$, $c_p(\dot{\gamma}=0)$, and the proportionality constant A from viscosity measurements. Figure 8.2 shows $(\eta)^{(-1/1.35)}$ versus shear rate, with a trendline added, up to the second order. Plotting $\lim_{\dot{\gamma}\downarrow 0}(\eta)^{(-1/1.35)}$ versus concentration gives the proportionality factor A, which is the slope of the curve, and $c_p(\dot{\gamma}=0)$ is the intercept (Figure 8.3). These values were –305.24 and 0.077 respectively. $c_p(\dot{\gamma}=0) = 0.077$ is in good agreement with the values obtained from η_0 calculated using the Carreau model ($c_p = 0.077$), and from G' measurements on ovalbumin ($c_p = 0.075$).[21]

To obtain more insight in how c_p depends on shear rate close to c_p, we can determine $\partial c_p / \partial \dot{\gamma}$ and $\partial^2 c_p / 2\partial^2 \dot{\gamma}$. For the second order equations of the trendlines in Figure 8.2, the coefficient before the first order term in the trendline corresponds to $A\partial c_p / \partial \dot{\gamma}$, and the coefficient before the second order term corresponds to $A\partial^2 c_p / 2\partial^2 \dot{\gamma}$. Using the calculated value for A results in values for $\partial c_p / \partial \dot{\gamma} = 5.1 \times 10^{-4}$ and $\partial^2 c_p / 2\partial^2 \dot{\gamma} = -9.1 \times 10^{-6}$. These values were inserted in Eq. (8.3) and plotted in Figure 8.4. Figure 8.4 shows an increase in c_p with increasing shear rate. Note that this curve is valid only for low shear rates (up to about 25 s^{-1}). At higher shear rates, the value of the second order term of the Taylor series expansion is too large in comparison to $c_p(\dot{\gamma}=0)$, and the Taylor series expansion becomes less accurate. The increase in c_p with increasing shear rate is in agreement with the shear-thinning behaviour observed from the viscosity measurements. Shear-thinning behaviour indicates disentanglements of the fibrils with increasing shear rate, which makes it

Figure 8.2 $(\eta)^{(-1/1.35)}$ versus shear rate for a 0.072 heated ovalbumin solution, which was diluted to various concentrations: 0.048 (▲); 0.053 (●); 0.058 (▼); 0.062 (◆); 0.066 (■); 0.072 (+). The added trendlines are second-order polynomials.

Figure 8.3 $\lim_{\dot{\gamma}\downarrow 0}(\eta)^{(-1/1.35)}$ versus ovalbumin concentration. (▼) denotes the value for 0.058, which was not taken into account in the fitting procedure.

Figure 8.4 c_p versus shear rate.

more difficult to form a gel network. This results in a higher c_p with increasing shear rate. Birefringence measurements confirm this trend. Birefringence, *$\Delta n'$*, versus shear rate was measured for a 0.072 heated ovalbumin concentration, which was diluted to various concentrations (Figure 8.5). An increasing *$\Delta n'$* with increasing shear rate was observed, which indicates that orientation of the fibrils takes place. When fibrils orient, fewer contact points are present, so a higher c_p is expected at higher shear rates.

8.4.1.3 Determination c_p versus Peclet number

In the previous section we obtained a relation for c_p as a function of $\dot{\gamma}$. It is more convenient to express c_p as a function of Peclet number (Pe = $\dot{\gamma} / D_r$), because the theoretical dependence of c_p as a function of shear flow, obtained from the random contact model, will also be expressed as a function of Peclet number (see Eq. (8.21) and (8.22)). This will allow easy comparison between experiment and theory. *$\Delta n'$* measurements for various concentrations (Figure 8.5), which are measured simultaneously with the viscosity measurements, can be used to obtain D_r, from which the Peclet numbers can be calculated for each concentration.
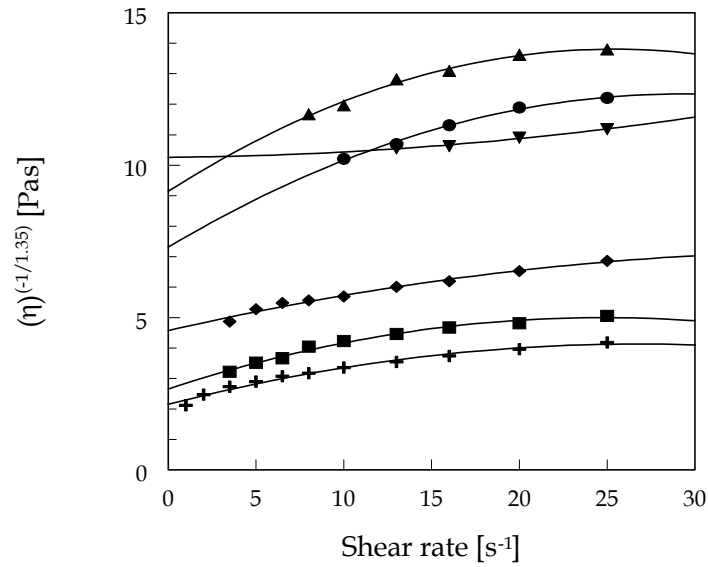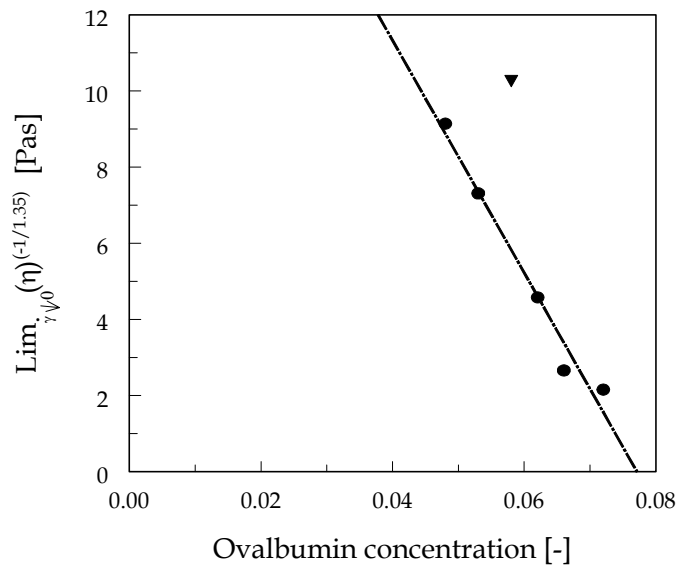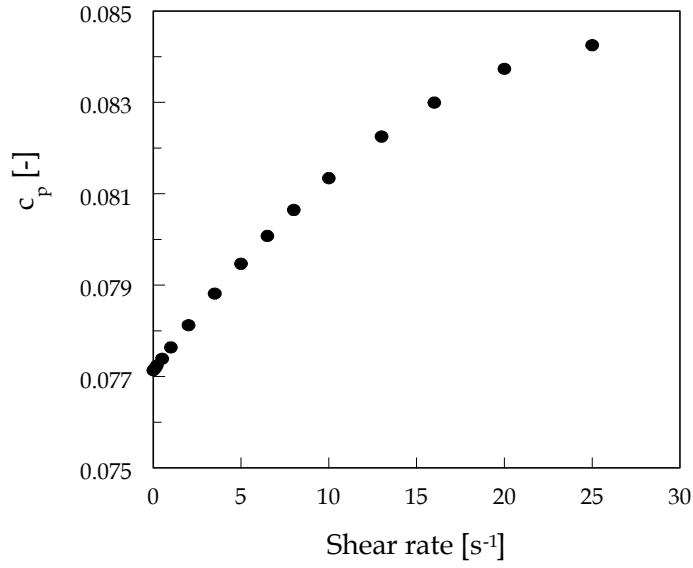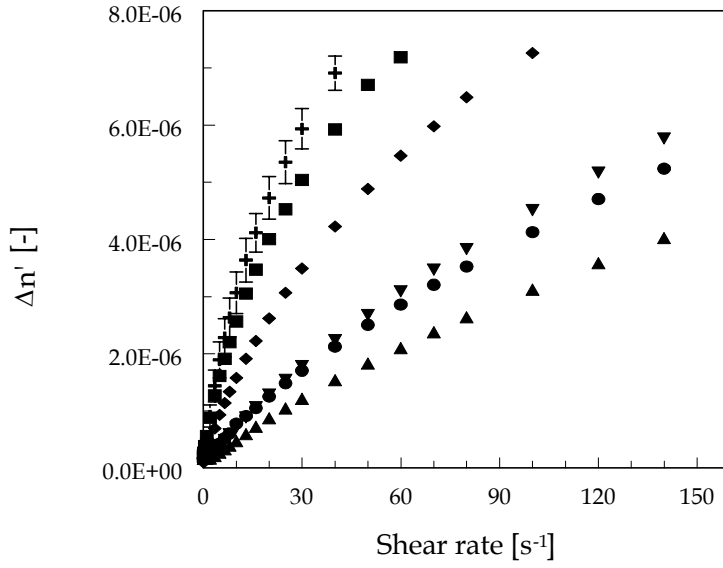
Figure 8.5 $\Delta n'$ versus shear rate for a 0.072 heated ovalbumin solution, which was diluted to various concentrations: 0.048 (▲); 0.053 (●); 0.058 (▼); 0.062 (◆); 0.066 (■); 0.072 (+).

c_p was compared with the valid concentration regime of the Doi-Edwards model. We found that cL^3 was about 300, which is clearly >>1, indicating that our measured concentrations are above the dilute regime. cDL^2 was about 6, which is not <<1, as required for semidilute solutions, indicating that our concentrations are higher than valid for the semidilute regime. Because we are still far away from the isotropic-nematic transition, we may assume that the Doi-Edwards model is still applicable at concentrations around c_p. This is also demonstrated by the fact that the scaling of D_r with concentration still follows $D_r \sim c^{-2}$ (Figure 8.7), as predicted for the semidilute regime. The results of $\Delta n'$ measurements have been fitted with the use of the Doi-Edwards model for monodispers rods. The Lorentz-Lorenz rule, which expresses the components of the refractive index tensor in terms of the polarizability tensor, was used to obtain the following expression for $\Delta n'$:[2,4]

$$\frac{\Delta n'}{\Delta n'_{max}} \approx \left[\left\langle u_x^2 - u_y^2 \right\rangle^2 + 4 \left\langle u_x u_y \right\rangle^2 \right]^{1/2} = \quad (8.25a)$$

$$\left[\frac{4\pi}{15} \left(b_{22} - 3^{1/2} b_{20} \right)^2 - \frac{16\pi}{15} b_{21}^2 \right]^{1/2} \quad (8.25b)$$

where $\Delta n'_{max}$ is the birefringence at infinite shear rate. The coefficients b_{lm} are obtained by numerically solving Eq. (8.21).[2] An approximate result, written in the form of tensor components, which can be used conveniently to fit with the measured $\Delta n'$ data, is given by:[38]

$$\langle u_x u_y \rangle = \frac{Pe}{30}\left(1+0.0710 Pe^2\right)^{-0.525} \tag{8.26}$$

$$\langle u_x^2 - u_y^2 \rangle = \frac{Pe^2}{90}\left(1+0.0558 Pe^2\right)^{-0.874} \tag{8.27}$$

Fitting our results by inserting Eq. (8.26) and (8.27) in Eq. (8.25a) gives a value for D_r and $\Delta n'_{max}$ for each measured concentration. The values for D_r varied from 28.3 s^{-1} to 4.2 s^{-1} and $\Delta n'_{max}$ from 1.7×10^{-5} to 2.2×10^{-5} for 0.048 to 0.072 ovalbumin solutions respectively. Figure 8.6 shows the fitted experimental data and a comparison with the theoretical solution for $\Delta n'/\Delta n'_{max}$ versus Peclet number from the Doi-Edwards model (Eq. (8.25)). The fitted data show a good agreement with the theoretical solution.

D_r values at various concentrations obtained from the fitted $\Delta n'$ data, can be used to find a D_r value at $c_p(\dot\gamma=0)$ using Eq. (8.16) which assumes $D_r \sim c^{-2}$ (Figure 8.7). D_r at $c_p(\dot\gamma=0)$ can be determined by extrapolating the curve in Figure 8.7 to a concentration of 0.077, i.e. $c_p(\dot\gamma=0)$. D_r was found to be 0.96 s^{-1}, and this value is used to plot the measured c_p as a function of Peclet number (Pe = $\dot\gamma/D_r$). We have used one D_r value at $c_p(\dot\gamma=0)$ to calculate the Peclet numbers for the whole curve, because this approach was also used in the theoretical analysis. Figure 8.8 shows c_p versus Peclet number.

With the use of Eq. (8.16) we could now also estimate a value for β. First $D_{r,0}$ was calculated with Eq. (8.17) and found to be 983 s^{-1}. A value for β was found of about 100, which is an order of magnitude lower than found previously in literature.[39-41]
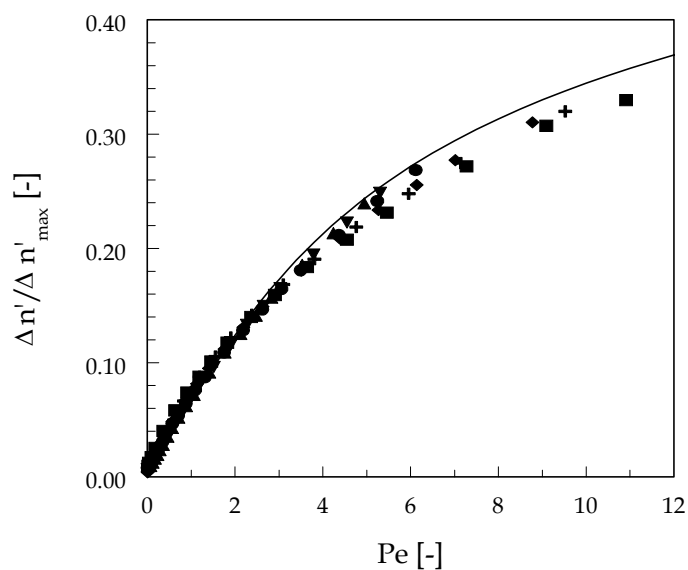
Figure 8.6 Fitted curves for $\Delta n' / \Delta n'_{max}$ versus Peclet number for a 0.072 heated ovalbumin solution, which was diluted to various concentrations: 0.048 (▲); 0.053 (●); 0.058 (▼); 0.062 (◆); 0.066 (■); 0.072 (+) (curves were fitted by inserting Eq. (8.26) and (8.27) in Eq. (8.25a)). The drawn line gives the theoretical solution for $\Delta n' / \Delta n'_{max}$ versus Peclet number (Eq. (8.25)).

Figure 8.7 D_r versus c^{-2}. The equation of the trendline is given by $D_r = 0.1072 \, c^{-2} - 17.13$.

8.4.2 Random contact model

To investigate the change in c_p as a function of shear flow for the shear dependent random contact model, we need the solution of Eq. (8.21), which can be obtained numerically. With the use of Eq. (8.19) V_{ex} as a function of Pe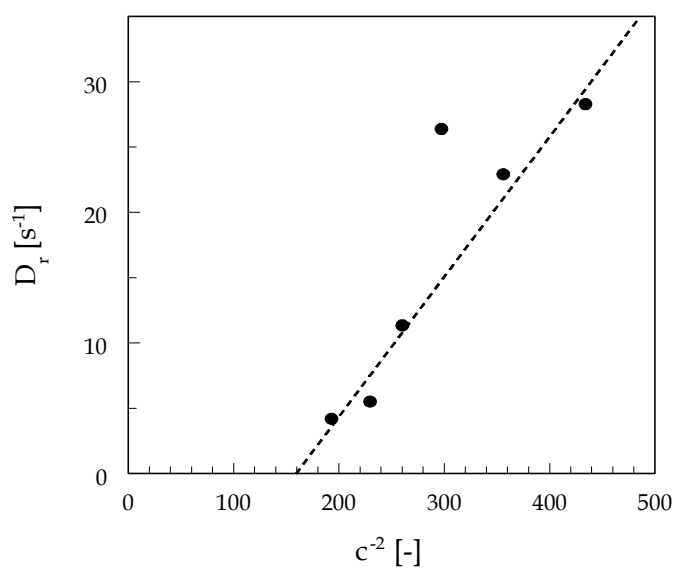clet number was inserted in the random contact model as outlined in section 8.2.2.2. For α, the average number of contacts per particle, we choose such a value that the theoretical value of c_p at a Peclet number of 0.1 corresponds to the experimental value for c_p at the same Peclet number. Then, α was found to be 3.9, which is in agreement with the assumption that α is O(1) at c_p in the random contact model. The theoretical values for c_p versus Peclet number are also plotted in Figure 8.8.
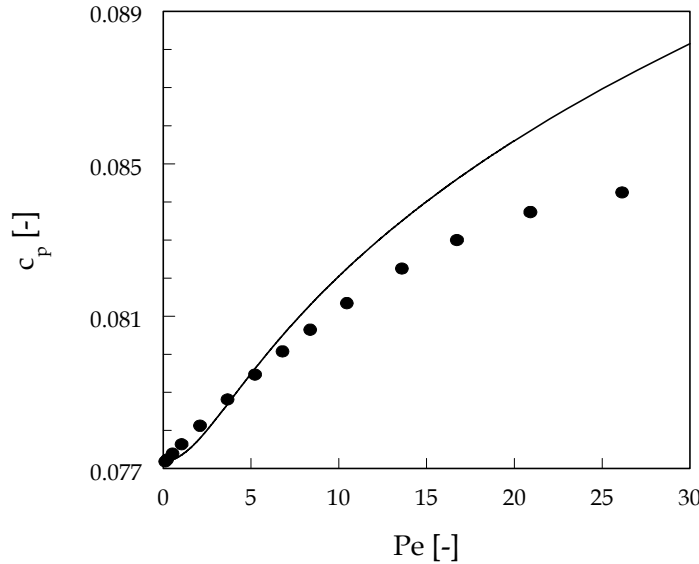
Figure 8.8 c_p versus Peclet number. (●) indicates the results of the experimental data, and the drawn line indicates the results from the theoretical analysis.

8.4.3 Comparison of experimental data and theory

In Figure 8.8, we compare experimental data with our theoretical calculations for c_p versus Peclet number. The theoretical curve shows a higher value for c_p as a function of Peclet number than the experimental curve. This difference may be explained by the polydispersity of the ovalbumin fibrils. TEM micrographs showed that the ovalbumin fibrils are polydisperse.[21] For a polydisperse system near c_p, the length of the rods, which play a dominant role in the network formation, will have an average length larger than the overall average length of the rods. This effectively decreases D_r, resulting in a higher Peclet number, at equal c_p. Thus, the points on the

theoretical curve for c_p versus Peclet number will shift in the direction of the experimental curve. The theoretical curve coincides with the experimental curve for a D_r about 1.3 times smaller than the value obtained from our experiments. Because of the very strong dependence of D_r on the average rod length, $O(L^{-9})$, this factor 1.3 in D_r would require an adjustment to the average rod length of only 3%. This 3% is within our current accuracy of the average rod length. Reversely, the discrepancy of a factor 1.3 in Peclet number is well within the regime of experimental accessibility. The influence of the average rod length on c_p is of $O(1)$, i.e. negligible compared to the influence of D_r on the average rod length. Another effect that might explain the difference between the two curves is the semiflexibility of the ovalbumin fibrils.[21] The Doi-Edwards model is strictly speaking only applicable to rigid and infinitely thin rodlike particles. For a more accurate comparison with ovalbumin fibrils, i.e. finite and semiflexible fibrils, the Doi-Edwards model may have to be modified to incorporate the semiflexible nature of the fibrils.

8.5 Conclusion

The effect of shear flow on c_p was investigated for fibrillar protein assemblies. The results of viscosity measurements were analysed near the percolation threshold, c_p, to yield c_p as function of shear rate. The percolation threshold increases with increasing shear rate. Flow birefringence data were used to determine the rotational diffusion coefficient, D_r, at various concentrations. D_r at $c_p(\dot{\gamma}=0)$ was determined via extrapolation, and found to be 0.96 s^{-1}. This value was used to obtain c_p, determined from experiments, as a function of Peclet number. c_p versus Peclet number was also calculated theoretically, based on a random contact model for rodlike particles, making use of a shear dependent excluded volume per fibril. The experimental and theoretical results are in good agreement, considering the fact that polydispersity of the ovalbumin fibrils has been neglected and that the fibrils are semiflexible.

References

1.   Meyer, E.L.; Fuller, G.G. *Macromolecules* **1993,** *26,* 504-511.

2.   Chow, A.W.; Fuller, G.G. *Macromolecules* **1985,** *18,* 786-793.

3.   Hilliou, L.; Vlassopoulos, D.; Rehahn, M. *Macromolecules* **2001,** *34,* 1742-1750.

4.   Fuller, G.G. *Ann. Rev. Fluid Mech.* **1990,** *22,* 387-417.

5.   Chow, A.W.; Fuller, G.G. *J. Rheol.* **1984,** *28,* 23-43.

6.   Yevlampieva, N.P.; Pavlov, G.M.; Rjumtsev, E.I. *Int. J. Biol. Macromolecules* **1999,** *26,* 295-301.

7.   Clasen, C.; Kulicke, W.-M. *Progress in Polymer Sci.* **2001,** *26,* 1839-1919.

8.   Joly, M.; Barbu, E. *Bull. Ste. Chim. Biol.* **1949,** *31,* 1642-1655.

9.   Chow, A.W.; Fuller, G.G.; Wallace, D.G.; Madri, J.A. *Macromolecules* **1985,** *18,* 805-810.

10.   Immaneni, A.; McHugh, A.J. *J. Polymer Sci. B: Polymer Phys.* **1998,** *36,* 181-190.

11.   Mead, D.W.; Larson, R.G. *Macromolecules* **1990,** *23,* 2524-2533.

12.   Gatzonis, Y.; Siddiquee, S.K.; Egmond van, J.W. *Macromolecules* **1997,** *30,* 7253-7262.

13.   Chow, A.W.; Fuller, G.G.; Wallace, D.G.; Madri, J.A. *Macromolecules* **1985,** *18,* 793-804.

14.   Shah, J.V.; Janmey, P.A. *Rheol. Acta* **1997,** *36,* 262-268.

15.   Janmey, P.A.; Shah, J.V.; Janssen, K.P.; Schliwa, M. *Subcell. Biochem.* **1998,** *31,* 381-97.

16.   Ellis, R.J.; Pinheiro, T.J.T. *Nature* **2002,** *416,* 483-484.

17.   Veerman, C.; Ruis, H.; Sagis, L.M.C.; Linden van der, E. *Biomacromolecules* **2002,** *3,* 869-873.

18.   Goers, J.; Permyakov, S.E.; Permyakov, E.A.; Uversky, V.N.; Fink, A.L. *Biochem.* **2002,** *41,* 12546-12551.

19.   Veerman, C.; Sagis, L.M.C.; Heck, J. Linden van der, E. *Int. J. Biol. Macromolecules* **2003,** *31,* 139-146.

20.   Chamberlain, A.K.; MacPhee, C.E.; Zurdo, J.; Morozova-Roche, L.A.; Allen, H.; Hill, O.; Dobson, C.M.; Davis, J.J. *Biophys. J.* **2000,** *79,* 3282-3293.

21.   Veerman, C.; Schiffart de, G.; Sagis, L.M.C.; Linden van der, E. *Int. J. Biol. Macromolecules* **2003,** *33,* 121-127.

22.   Hermansson, A.-M. *J. Sci. Food Agric.* **1985,** *36,* 822-832.

23.   Nemoto, N.; Koike, A.; Osaki, K.; Koseki, T.; Doi, E. *Biopolymers* **1993,** *33,* 551-559.

24.   Doi, E.; Kitabatake, N. In *Food proteins and their applications* Damodaran, S.; Paraf, A. (Eds.) **1997**, Marcel Dekker: New York, 325-340.

25.   Mine, Y. *J. Agric. Food Chem.* **1996,** *44,* 2086-2090.

26.   Hagolle, N.; Relkin, P.; Dalgleish, D.G.; Launay, B. *Food Hydrocolloids* **1997,** *11,* 311-317.

27.   Weijers, M.; Sagis, L.M.C.; Veerman, C.; Sperber, B.; Linden van der, E. *Food Hydrocolloids* **2002,** *16,* 269-276.

28.   Linden van der, E.; Sagis, L.M.C. *Langmuir* **2001,** *17,* 5821-5824.

29.   Stauffer, D. *Physics Reports* **1979,** *54,* 1-74.

30.   Eicke, H.F.; Hilfiker, R.; Thomas, H. *Chem. Phys. Lett.* **1985,** *120,* 272-275.

31.   Eicke, H.F.; Hilfiker, R.; Thomas, H. *Chem. Phys. Lett.* **1986,** *125,* 295-298.

32.   Grant, M.C.; Russel, W.B. *Phys. Rev. E* **1993,** *47,* 2606-2614.

33.   Stauffer, D.; Coniglio, A.; Adam, M. *Adv. Polym. Sci.* **1982,** *44,* 103-158.

34.   Martin, J.E.; Adolf, D.; Wilcoxon, J.P. *Phys. Rev. Lett.* **1988,** *61,* 2620-2623.

35.   Philipse, A.P. *Langmuir* **1996,** *12,* 1127-1133.

36.   Onsager, L. *Ann. N.Y. Ac. Sci.* **1949,** *51,* 627-659.

37.   Vroege, G.J.; Lekkerkerker, H.N.W. *Rep. Prog. Phys.* **1992,** *55,* 1241-1309.

38.   Doi, M.; Edwards, S.F. *J. Chem. Soc. Faraday Trans. 2* **1978,** *74,* 918-932.

39.   Doi, M.; Edwards, S.F. *The theory of polymer dynamics* **1986**, Oxford: Oxford university Press.

40.   Jain, S.; Cohen, C. *Macromolecules* **1981,** *14,* 759-765.

41.   Odell, J.A.; Atkins, E.D.T.; Keller, A. *J. Polymer Sci.: Polymer Lett.* **1983,** *21,* 289-300.

42.   Kirkwood, J.G.; Plock, R.J. *J. Chem. Phys.* **1956,** *24,* 665-669.

43.   Klein, C. et al. *In Preparation.*

44.   Bird, R.B.; Armstrong, R.C.; Hassager, O. *Dynamics of polymeric liquids.* second ed. Vol. 1. **1987**: Wiley-Interscience. 171.

45.   Yasuda, K.; Armstrong, R.C.; Cohen, R.E. *Rheol. Acta* **1981,** *20,* 163-178.

46.   Martin, J.E.; Adolf, D.; Wilcoxon, J.P. *Phys. Rev. A* **1989,** *39,* 1325-1332.

47.   Axelos, M.A.V.; Kolb, M. *Phys. Rev. Lett.* **1990,** *64,* 1457-1460.

48.   Adam, M.; Delsanti, M.; Durand, D.; Hild, G.; Munch, J.P. *Pure and Applied Chem.* **1981,** *53,* 1489-1494.

Summary

Samenvatting

Summary

The relation between macroscopic properties of complex systems and molecular properties of their ingredients has received considerable attention in recent years. To bridge the gap between properties at these two length scales, it is important to focus on the intermediate mesoscopic level (10 – 1000 nm). The description of complex systems at this intermediate length scale offers challenges from a fundamental and applied point of view.

The objective of this thesis was to explore the assembly of food proteins into fibrils, and to describe the resulting percolating systems at rest and under shear flow, in terms of mesoscopic fibril properties.

In chapter 2 the effect of electrostatic interactions on the critical percolation concentration (c_p) of fibrillar β-lactoglobulin (β-lg) gels at pH 2 was investigated, using rheological measurements, transmission electron microscopy (TEM), and performing conversion experiments. A decreasing c_p with increasing ionic strength was found. The fraction non-aggregated β-lg was independent of ionic strength in the regime of 0.01 – 0.08 M. TEM experiments showed long fibrils (2 – 7 μm) for ionic strengths between 0.01 and 0.08 M. Since both the conversion of monomers and the contour length of the fibrils were independent of ionic strength (0.01 – 0.08 M), the linear increase of c_p with the Debye length can be attributed purely to an increase of electrostatic repulsion between the fibrils. This increase is explained in terms of an adjusted random contact model which takes into account the charge and semiflexibility of the fibrils.

The mesostructure of bovine serum albumin (BSA) at low pH was investigated in chapter 3. Rheological measurements were performed to determine c_p. A decreasing c_p with increasing ionic strength was found. Fibrils with a contour length of about 100 – 300 nm were found using TEM. The measured conversion of monomers into fibrils was independent of ionic strength (0.20 – 0.30 M). Dilution of BSA samples showed that the aggregation process is reversible and that there exists a critical concentration for the self-assembly of BSA. The decrease in c_p with increasing ionic strength is again described well by the adjusted random contact model derived in chapter 2.

In chapter 4 the self-assembly of ovalbumin into fibrils and resulting network properties were studied at pH 2, as a function of ionic strength. Using TEM, the effect of ovalbumin concentration on the contour length was determined. The

contour length increased with increasing ovalbumin concentration. TEM micrographs were made to investigate the effect of ionic strength on the contour length. In the measured ionic strength regime (0.01 – 0.035 M) fibrils of approximately equal length (± 200 nm) were observed. TEM micrographs showed that the contour length of the fibrils, versus time after dilution, remained constant, which indicates that the self-assembly of ovalbumin is irreversible. Using the results of rheological measurements, we observed a decreasing c_p with increasing ionic strength. Just like for β-lg and BSA, the ionic strength dependence of c_p of ovalbumin fibrils is described by the adjusted random contact model, indicating that the behaviour of these three fibril networks may be generic for a wide range of fibrillar protein systems.

Chapter 5 summarizes the results obtained in chapters 2 to 4, and gives a further characterization of the fibrillar properties of the three protein assemblies. We have determined the contour length, persistence length, bending rigidity, and c_p for semiflexible amyloid fibrils formed from the globular proteins β-lg, BSA, and ovalbumin. Also the phase behaviour of β-lg at low pH was discussed. The persistence length was estimated from the adjusted random contact model for highly charged semiflexible chains. We have found contour lengths in the range of 50 nm to 10 μm, and persistence lengths in the range of 16 nm to 1.6 μm. This wide range of contour and persistence lengths, and the ease of preparation of these amyloid fibrils, makes them ideal model systems for the study of semiflexible polymers.

The objective of the study described in chapter 6 was to obtain β-lg gels at very low protein concentrations using a new multistep Ca^{2+}-induced cold gelation process. In the conventional cold gelation process, salt free β-lg solutions were heated at neutral pH, cooled, and cross-linked by adding salts. In our new process, first long linear β-lg fibrils were formed at pH 2. Solutions of these fibrils were cooled, and subsequently the pH was adjusted to 7 or 8. TEM studies showed that the long linear fibrils formed at pH 2 were stable when the pH was adjusted to 7 or 8. In the final step the fibrils were cross-linked using $CaCl_2$. Using rheological measurements, the c_p was determined. In the new multistep cold gelation process, c_p was an order of magnitude lower than in the conventional cold gelation method. This proves that these fibrillar protein assemblies are indeed ideal systems for structuring at extremely low weight fractions.

In chapter 7 the behaviour of fibrillar assemblies of ovalbumin under oscillatory shear, close to c_p (= 7.5%), was probed with the use of rheo-optical measurements and Fourier transform rheology. Different behaviour was observed close to c_p (7.3%), compared to slightly further away from c_p (7.1% and 6.9%). For 7.1 and 6.9%, shear-thinning behaviour and a linear increase in birefringence, $\Delta n'$, with increasing strain was observed, indicating deformation and orientation of the fibril structures. For 7.3%, a shear-thinning regime was followed by a shear-thickening regime, which coincided with a strong increase in $\Delta n'$, dichroism, $\Delta n''$, and the intensity of the normalized third harmonic (I_3/I_1) as obtained from Fourier transform rheology. This regime was followed by a second shear-thinning regime, where $\Delta n'$, $\Delta n''$ and I_3/I_1 decreased. In the first shear-thinning regime, deformation and orientation of existing clusters takes place. At higher oscillatory shear a larger deformation occurs and larger structures are formed, which is most likely aggregation of the clusters. Finally, at even higher strains, the clusters break up again. An increase in complex viscosity, $\Delta n'$, $\Delta n''$ and I_3/I_1 was observed when a second strain sweep was performed 30 min after the first one. This indicates that the shear-induced cluster formation and break up are not completely reversible, and the initial cluster size distribution is not recovered after cessation of flow.

The objective of the study described in chapter 8 was to investigate the effect of shear flow on c_p for solutions of fibrillar protein assemblies. The results of viscosity measurements were analysed using percolation theory, taking into account the effect of shear flow. We found c_p to increase with increasing shear rate. Results of birefringence measurements were used to obtain the rotational diffusion coefficient at c_p, which enables us to express c_p, from viscosity measurements, as a function of Peclet number. We compared our experimental data with theoretical calculations on c_p versus Peclet number, based on a random contact model for rodlike particles, making use of a shear dependent excluded volume per fibril. The experimental and theoretical results are in good agreement, considering the fact that polydispersity of the ovalbumin fibrils has been neglected and that the fibrils are semiflexible.

In conclusion, chapters 2 to 6 all discuss conditions leading to gel formation, and critical percolation concentrations in terms of mesoscopic fibril properties, under static, i.e. non-flow conditions. The critical percolation concentration was determined using the results of elasticity measurements, and explained in terms of

an excluded volume per fibril (at zero shear). In chapters **7** and **8** the influence of shear flow on the critical percolation concentration is described. Here, the critical percolation concentration versus shear flow could again be expressed in terms of an excluded volume per fibril, in this case as a function of shear.

Samenvatting

De relatie tussen macroscopische eigenschappen van complexe systemen en de moleculaire eigenschappen van hun ingrediënten staat al geruime tijd in de belangstelling. Om de kloof tussen eigenschappen op deze twee lengteschalen te dichten is het belangrijk om het tussenliggende mesoscopische lengteschaalniveau (10 – 1000 nm) in ogenschouw te nemen. De bestudering van complexe systemen op deze tussenliggende lengteschaal opent nieuwe perspectieven vanuit een fundamenteel en toegepast oogpunt.

Het doel van dit promotieonderzoek was om meer inzicht te verkrijgen in de aggregatie van eiwitten, die voorkomen in levensmiddelen, in fibrillen, en om de resulterende gelerende systemen te beschrijven, zowel in rust als onder invloed van afschuifstroming, in termen van de mesoscopische fibrileigenschappen.

In hoofdstuk 2 is het effect van elektrostatische interacties op de kritische geleringsconcentratie of percolatieconcentratie (c_p) van fibrillaire β-lactoglobuline (β-lg) gelen bij pH 2 onderzocht, waarbij gebruik is gemaakt van reologische metingen, transmissie electronen microscopie (TEM), en conversie-experimenten. Er werd gevonden dat c_p afnam bij een toenemende ionsterkte. De fractie niet geaggregeerd β-lg was onafhankelijk van de ionsterkte tussen 0.01 – 0.08 M. TEM foto's lieten lange fibrillen (2 – 7 μm) zien voor ionsterktes variërend van 0.01 – 0.08 M. Zowel de conversie van monomeren als de contourlengte van de fibrillen waren onafhankelijk van de ionsterkte (0.01 – 0.08 M). De lineaire toename van c_p met de Debyelengte kon hiermee alleen worden toegeschreven aan een toename van de elektrostatische repulsie tussen de fibrillen. Deze toename kon worden uitgelegd in termen van een aangepast "random contact model", waar rekening gehouden wordt met zowel de lading als semi-flexibiliteit van de fibrillen.

De mesostructuur van bovine serum albumine (BSA) bij lage pH werd onderzocht in hoofdstuk 3. Reologische metingen zijn uitgevoerd om c_p te bepalen. Hier werd gevonden dat c_p afnam met een toenemende ionsterkte, evenals het geval was voor β-lg. Uit TEM experimenten bleek dat de fibrillen een contourlengte van 100 – 300 nm hebben. De gemeten conversie van monomeren in fibrillen was onafhankelijk van de ionsterkte (0.20 M – 0.30 M). Door de BSA monsters te verdunnen, werd duidelijk dat het aggregatieproces reversibel is. Er is dus een kritische concentratie voor aggregatie van BSA. De afname van c_p met toenemende

ionsterkte kan ook voor BSA goed worden beschreven met het aangepaste "random contact model", zoals ontwikkeld in hoofdstuk 2.

In hoofdstuk 4 zijn de aggregatie van ovalbumine in fibrillen en de resulterende netwerkeigenschappen bestudeerd bij pH 2, als een functie van ionsterkte. Door gebruik te maken van TEM is het effect van de ovalbumineconcentratie op de contourlengte bepaald. De contourlengte nam toe bij een toenemende ovalbumineconcentratie. TEM foto's zijn gemaakt om het effect van ionsterkte op de contourlengte te bestuderen. In het gemeten ionsterktebereik (0.01 – 0.035 M), zijn fibrillen met een ongeveer gelijke lengte ($\pm$ 200 nm) waargenomen. Uit TEM foto's bleek ook dat de contourlengte van de fibrillen, als een functie van de tijd na het verdunnen, constant bleef, wat er op duidt dat de aggregatie van ovalbumine irreversibel is. Gebruik makend van de resultaten van reologische metingen, werd vastgesteld dat c_p afnam bij toenemende ionsterkte. Net als voor β-lg en BSA, kan deze afhankelijkheid van de ionsterkte op c_p worden beschreven met een aangepast "random contact model". Dit in hoofdstuk 2 beschreven model is hiermee toepasbaar voor fibrilnetwerken van drie verschillende eiwitten. Dit suggereert sterk dat het gebruikte model generiek is.

Hoofdstuk 5 vat de resultaten die verkregen zijn in de hoofdstukken 2 tot 4 samen, en geeft een verdere karakterisering van de fibrileigenschappen van de drie eiwitten. De karakterisering betreft contourlengte, persistentielengte, buigingsrigiditeit en c_p voor de semi-flexibele amyloïde fibrillen gevormd uit de globulaire eiwitten β-lg, BSA en ovalbumine. Het fasegedrag van β-lg bij een lage pH is ook bestudeerd. De persistentielengte is geschat met behulp van het aangepaste "random contact model" voor geladen semi-flexibele ketens. De contourlengtes varieerden van 50 nm tot 10 µm, en de persistentielengtes varieerden van 16 nm tot 1.6 µm. Dit grote bereik van contour- en persistentielengtes, en het gemak van bereiding van deze amyloïde fibrillen, maken ze tot ideale modelsystemen voor het bestuderen van semi-flexibele polymeren.

Het doel van de studie zoals beschreven in hoofdstuk 6 was om β-lg gelen te verkrijgen bij een heel lage eiwitconcentratie, waarbij gebruik is gemaakt van een nieuw meerstaps Ca^{2+}- geïnduceerd koud geleringsproces. In het conventionele koudegeleringsproces zijn zoutvrije β-lg oplossingen verhit bij neutrale pH, gekoeld, en gecross-linkt door de toevoeging van zouten. In dit nieuwe proces worden eerst lange lineaire β-lg fibrillen gevormd bij pH 2. Oplossingen van deze

fibrillen werden gekoeld, en daarna werd de pH langzaam aangepast tot 7 of 8. Uit TEM-studies volgde dat de lange lineaire fibrillen die gevormd zijn bij pH 2, stabiel blijven nadat de pH is aangepast naar 7 of 8. In de volgende stap werden de fibrillen gecross-linkt door toevoeging van $CaCl_2$. Met behulp van reologische metingen werd de c_p bepaald. In het nieuwe meerstaps koudegeleringsproces, was de c_p een ordegrootte lager dan in de conventionele koudegeleringsmethode. Uit bovengenoemde resultaten blijkt dat deze fibrillaire eiwitaggregaten ideale systemen zijn om structuren te maken bij extreem lage gewichtsfracties (0.07%).

In hoofdstuk 7 is het gedrag van fibrillaire aggregaten van ovalbumine onder invloed van een afschuifveld, dichtbij c_p (= 7.5%), bestudeerd waarbij gebruik is gemaakt van reo-optische metingen en Fourier-transform reologie. Het gedrag vlakbij c_p (7.3%) was anders dan het gedrag iets verder van c_p (7.1 en 6.9%). Bij 7.1 en 6.9%, werd een shear-thinning gedrag en een lineaire toename van de birefringence, $\Delta n'$, met een toename in vervorming waargenomen, wat duidt op deformatie en oriëntatie van de fibrilstructuren. Voor 7.3% werd dit shear-thinning gebied gevolgd door een shear-thickening gebied, dat samenviel met een sterke toename in $\Delta n'$, dichroïsme, $\Delta n''$, en de intensiteit van de genormaliseerde derde harmonische (I_3/I_1) zoals verkregen uit Fourier-transform reologie. Dit gebied werd gevolgd door een tweede shear-thinning gebied, waar $\Delta n'$, $\Delta n''$, en I_3/I_1 afnamen. In het eerste shear-thinning gebied vindt deformatie en oriëntatie van bestaande clusters plaats. Bij hogere oscillatorische afschuiving vindt meer deformatie plaats en worden grotere structuren gevormd. Deze structuren zijn hoogstwaarschijnlijk aggregaten van clusters. Uiteindelijk, bij nog hogere vervormingen, vallen de clusters weer uit elkaar. Een toename in complexe viscositeit, $\Delta n'$, $\Delta n''$, en I_3/I_1 vond plaats indien een tweede strain-sweep werd uitgevoerd, 30 min na de eerste. Dit laat zien dat de afschuiving-geïnduceerde vorming en afbraak van clusters niet compleet reversibel is, en dat de initiële clustergrootteverdeling niet hersteld wordt nadat het afschuifveld opgeheven is.

Het doel van de studie beschreven in hoofdstuk 8 was om het effect van een afschuifveld op c_p te bestuderen voor oplossingen van fibrillaire eiwitaggregaten. De resultaten van viscositeitsmetingen werden geanalyseerd met behulp van percolatietheorie, waarbij rekening is gehouden met het effect van een afschuifveld. c_p nam toe met een toenemende afschuifsnelheid. Resultaten van dubbele-brekingsmetingen zijn gebruikt om c_p uit te drukken als een functie van het

Pecletgetal. We hebben onze experimentele data vergeleken met theoretische berekeningen bij c_P versus het Pecletgetal. Deze berekeningen zijn gebaseerd op een "random contact model" voor staafvormige deeltjes, waarbij gebruik is gemaakt van een uitgesloten volume per fibril, afhankelijk van het afschuifveld. De experimentele en theoretische resultaten komen goed overeen, in het bijzonder als rekening wordt gehouden met het feit dat polydispersiteit- en semi-flexibiliteit van de ovalbumine fibrillen werd verwaarloosd in de berekening.

Concluderend beschrijven hoofdstukken 2 tot en met 6 de condities die leiden tot gelformatie, en kritische percolatieconcentraties in termen van mesoscopische fibrileigenschappen, zonder afschuifveld. De kritische percolatieconcentratie werd bepaald door gebruik te maken van elasticiteitsmetingen, en uitgelegd in termen van een uitgesloten volume per fibril (zonder afschuiving). In de hoofdstukken 7 en 8 wordt de invloed van een afschuifveld op de kritische percolatieconcentratie beschreven. In dit geval kan de kritische percolatieconcentratie als een functie van een afschuifveld wederom worden uitgedrukt in termen van een uitgesloten volume per fibril, nu als een functie van de afschuiving.

Dankwoord

Het is af! Na vier jaar met heel veel plezier aan mijn promotieonderzoek te hebben gewerkt, is ook voor mij het moment aangebroken om de meest gelezen bladzijden van mijn proefschrift te schrijven. Als ik terugkijk op de afgelopen vier jaar zijn er een aantal personen die in de werksfeer of op het persoonlijke vlak hebben bijgedragen aan het boekje zoals het nu is.

Ten eerste Erik, ik wil je bedanken voor jouw enthousiasme en betrokkenheid bij mijn project. De vele discussies en jouw kritische blik hebben zeker bijgedragen aan de artikelen zoals ze nu zijn. Ik waardeer heel erg jouw interesse in mijn persoonlijke ontwikkeling, en heb onze samenwerking als zeer prettig ervaren. Leonard, jou wil ik graag bedanken voor de goede begeleiding en het vertrouwen dat je altijd in mij hebt gehad. Ik heb heel veel geleerd van jouw uitleg over voor mij moeilijke wiskundig problemen, bedankt hiervoor. Paul, dank voor alle hulp met de reo-optica zowel op het experimentele als op het theoretische vlak. Harry, ik vond het heel leuk om met je samen te werken, en heb het erg gewaardeerd dat je altijd klaar stond om te helpen als het nodig was. De dropjes op het lab waren ook heel lekker! Jan van Lent, bedankt voor het gebruik van de electronenmicroscoop en jouw technische assistentie hierbij.

Zonder Tom, Hilde, Jeroen, Geertje en Maartje, die hun afstudeervak bij mij hebben uitgevoerd, was dit boekje zeker niet geworden tot wat het nu is. Bedankt!

Henny, Elke, en Suzanne met jullie was het vaak iets te gezellig op kamer 306, soms vloog de tijd voorbij zonder iets nuttigs te doen, maar plezier hebben we zeker gehad. Elke, ik vind het heel leuk dat je mijn paranimf wilt zijn. Alle andere collega's van Food Physics wil ik bij deze bedanken voor de gezellige sfeer, de maandelijkse borrels, en andere leuke uitjes. Ook collega's van PDQ, bedankt voor de goede sfeer in de wandelgangen en tijdens de koffiepauzes.

Kontiki, de jaarclubuitjes zijn altijd een welkome ontspanning geweest en ik hoop dat er nog veel leuke activiteiten mogen volgen. Ik weet dat onderscheid maken gevaarlijk is, maar ik doe het toch. Ten eerste, Zwannet, ondanks dat we de laatste jaren wat minder contact hebben gehad dan in onze studententijd, wil ik jou graag aan mijn zijde hebben bij mijn promotie. Ik vind het heel leuk dat jij mijn paranimf wilt zijn. Ook Marjan wil ik graag bij naam noemen. Marjan, bedankt voor jouw vriendschap. Bij jou kan ik altijd terecht om samen te sporten, eten, een serieus

gesprek te voeren of om te kletsen over het wel en wee van het AIO zijn. In september jouw feestje?

Salien, bedankt voor alle relax weekendjes, het is altijd fijn om even op adem te komen in het zuiden. Lieve pappie en mammie, bedankt voor jullie nooit aflatende interesse, altijd een luisterend (telefoon)oor, en het vertrouwen dat jullie steeds in mij hebben gehad! Het is elke keer heel gezellig om bij jullie, en bij Frederic en José, "thuis" te komen.

Lieve Theo, dank je wel voor je relativeringsvermogen, dat je mij af kan remmen als het nodig is, maar vooral voor het altijd "er zijn" en je onvoorwaardelijke liefde. Dit draagt er in grote mate aan bij dat ik optimaal kan functioneren, wat voor mij heel belangrijk is geweest tijdens mijn promotieonderzoek, en ook hierna heel belangrijk zal zijn. Nu we in dezelfde periode onze AIO tijd afsluiten, kunnen we vooruit kijken naar alle nieuwe uitdagingen die we samen aan zullen gaan!

Cecile

List of publications

K.P. Plucknett, S.J. Pomfret, V. Normand, D. Ferdinando, **C. Veerman**, W.J. Frith, I.T. Norton. Dynamic experimentation on the confocal laser scanning microscope: application to soft-solid composite food materials. *J. Microscopy* **2001,** *201,* 279 – 290.

L.M.C. Sagis, **C. Veerman**, R. Ganzevles, M. Ramaekers, S.G. Bolder, E. van der Linden. Mesoscopic structure and viscoelastic properties of β-lactoglobulin gels at low pH and low ionic strength. *Food Hydrocolloids* **2002,** *16,* 207-213.

M. Weijers, L.M.C. Sagis, **C. Veerman**, B. Sperber, E. van der Linden. Rheology and structure of ovalbumin gels at low pH and low ionic strength. *Food Hydrocolloids* **2002**, *16,* 269-276.

C. Veerman, H. Ruis, L.M.C. Sagis, E. van der Linden. Effect of electrostatic interactions on the percolation concentration of β-lactoglobulin gels. *Biomacromolecules* **2002**, *3,* 869-873.

C. Veerman, J. Heck, L.M.C. Sagis, E. van der Linden. Mesostructure of fibrillar bovine serum albumin gels. *Int. J. Biol. Macromolecules* **2003**, *31,* 139-146.

C. Veerman, L.M.C. Sagis, E. van der Linden. Gels at extremely low weight fractions formed by irreversible self-assembly of proteins. *Macromol. Biosci.* **2003**, *3,* 243-247.

C. Veerman, H. Baptist, L.M.C. Sagis, E. van der Linden. A new multi-step Ca^{2+}-induced cold gelation process for β-lactoglobulin. *J. Agric. Food Chem.* **2003**, *51,* 3880-3885.

C. Veerman, G. de Schiffart, L.M.C. Sagis, E. van der Linden. Irreversible self-assembly of ovalbumin into fibrils and the resulting network rheology. *Int. J. Biol. Macromolecules* **2003**, *33,* 121-127.

L.M.C. Sagis, **C. Veerman**, E. van der Linden. Mesoscopic properties of semiflexible amyloid fibrils. **2004**. *Accepted for publication in Langmuir.*

C. Veerman, L.M.C. Sagis, P. Venema, E. van der Linden. Shear-induced aggregation and break up of fibril clusters close to the percolation concentration. **2004.** *Submitted for publication.*

C. Veerman, L.M.C. Sagis, P. Venema, E. van der Linden. The effect of shear flow on the percolation concentration of fibrillar protein assemblies. **2004**. *Submitted for publication.*

T.B.J. Blijdenstein, **C. Veerman**, E. van der Linden. Depletion-flocculation in oil-in-water emulsions using fibrillar protein assemblies**. 2004**. *Submitted for publication.*

Conference proceedings

C. Veerman, L.M.C. Sagis, E. van der Linden. Fibril based mesostructures and their rheological response. In *Food Colloids, Biopolymers and Materials* **2002** Eds. E. Dickinson and T. van Vliet, Royal Society of Chemistry: Cambridge. 58-67.

C. Veerman, H. Ruis, L.M.C. Sagis, E. van der Linden. Rheology and mesostructure of β-lactoglobulin gels at pH 2. *Proceedings 6th European conference on rheology* **2002**, *Erlangen, Germany*, 321-322.

C. Veerman, L.M.C. Sagis, E. van der Linden. Mesostructure of fibrillar protein gels. *Proceedings of the 3rd International Symposium on Food Rheology and Structure* **2003**, *Zurich, Switserland*, 385-388.

C. Veerman, H. Baptist, L.M.C. Sagis, Erik van der Linden. Fibrillar β-lactoglobulin gels at neutral pH. 2003. *Proceedings of the 3rd International Symposium on Food Rheology and Structure* **2003**, *Zurich, Switserland,* 605-606.

Curriculum Vitae

Cecile Veerman werd geboren op 5 november 1975 in Rotterdam. In 1994 behaalde zij het VWO-diploma aan de C.S.G. Willem van Oranje te Oud-Beijerland, waarna zij in datzelfde jaar begon met de studie Levensmiddelentechnologie aan de toenmalige Landbouwuniversiteit te Wageningen. Tijdens haar studie deed zij afstudeervakken bij de sectie Levensmiddelennatuurkunde en bij Fysische- en Kolloïdchemie, waarbij het laatstgenoemde afstudeervak werd uitgevoerd bij NIZO food research te Ede. Haar stage voerde zijn uit bij Unilever Research Colworth House in Groot-Brittannië. Zij studeerde af in januari 2000. Vanaf februari 2000 tot en met februari 2004 is zij aangesteld als assistent in opleiding bij de leerstoelgroep Fysica en fysische chemie van levensmiddelen, bij Wageningen Universiteit. De resultaten van het verrichte promotieonderzoek staan beschreven in dit proefschrift. Vanaf 1 juni 2004 zal zij met een verkregen NWO-TALENT-beurs voor een jaar onderzoek gaan verrichten getiteld "microstructural properties of novel self-assembled hydrogels for tissue engineering" bij het departement Chemische Technologie aan de Universiteit van Delaware in de Verenigde Staten.